

# **MODELLING THE EFFECTS OF SOIL VARIABILITY ON STABILITY ANALYSIS OF NATURAL SLOPES IN DURBAN**

Presented by

**KHADIJA MOHSIN ARBEE**

211504075



**UNIVERSITY OF  
KWAZULU-NATAL**  

---

**INYUVESI  
YAKWAZULU-NATALI**

PRESENTED TO THE COLLEGE OF AGRICULTURE, ENGINEERING AND SCIENCE,  
HOWARD COLLEGE CAMPUS, DISCIPLINE OF CIVIL ENGINEERING UNIVERSITY  
OF KWAZULU-NATAL

IN FULFILMENT OF THE REQUIREMENTS FOR THE DEGREE OF MASTER OF  
SCIENCE IN ENGINEERING (MSc. ENG)

SUPERVISOR: DR F I ANEKE

CO-SUPERVISOR: PROF M M H MOSTAFA

JUNE 2021

## DECLARATION - PLAGIARISM

As the candidate's Supervisor I agree to the submission of this thesis.

-----  
Supervisor: Dr F.I. Aneke

I, **Khadija Mohsin Arbee** declare that:

1. The research reported in this thesis, except where otherwise indicated, is my original research.
2. This thesis has not been submitted for any degree or examination at any other university.
3. This thesis does not contain other persons' data, pictures, graphs or other information, unless specifically acknowledged as being sourced from other persons.
4. This thesis does not contain other persons' writing, unless specifically acknowledged as being sourced from other researchers. Where other written sources have been quoted, then:
  - a. Their words have been re-written, but the general information attributed to them has been referenced.
  - b. Where their exact words have been used, then their writing has been placed in italics and inside quotation marks and referenced.
5. This thesis does not contain text, graphics or tables copied and pasted from the Internet, unless specifically acknowledged, and the source being detailed in the thesis and in the References sections.

Signed

.....

## **ACKNOWLEDGEMENTS**

Thanks are due to my supervisor Dr. Frank Aneke for his role in this research project. Great thanks to my co-supervisor Professor Mohamed Mostafa, for his support and assurance during this trying year and a half. I would like to acknowledge the immense help and guidance provided by Mr. Ishaan Ramlakhan, who consistently went out of his way to help me complete all technical aspects of this project under the constrained circumstances caused by the COVID-19 outbreak. Greatest thanks are due to my family, for without their support and motivation I would not have been able to even imagine, let alone undertake the completion of my MSc. Finally, thanks be to God Almighty, for granting me the strength and perseverance to complete this task.

## ABSTRACT

Slope failure occurs due to various factors, one of the most significant being that of soil variability in a slope and associated geological threats such as unconsolidated soils, settlement, groundwater seepage and infiltration. The analysis of slope stability should incorporate and analyse the interactions between slope configuration, shear strength resistance, pore-water pressure and water conditions of a slope. This study focuses on the causal effects and slope stability of two natural slopes in Durban, KwaZulu-Natal. Large parts of the study area are underlain to great and varying depths by problem soils, namely the Berea Red Sands. These are dune soils, deposited by ancient wind activity, that are found parallel to the east coast of Durban. The Berea Red “sands” vary greatly in soil type ranging from fine grained sands to silts and clays. Those of looser consistency are known to undergo significant settlement under loading, and also with water interaction. The clay and silt varieties are known to exhibit heave under the same circumstances. In some cases, liquefaction of Berea sands may occur due to the loss of soil structure upon water introduction into the soil mass. The aim of this research is to formulate and compare the stability of the two slopes under different water conditions in the form of Factors of Safety and Probabilities of Failure, using RocScience© software. Site investigations were conducted to classify and collect soils, which were then put through rigorous laboratory testing. The results from testing were applied where possible to the modelling software and a host of important findings were made. The liquefaction potential of poorly graded, uniform Berea sands was observed first-hand on site, in the laboratory and again during slope stability analyses. As anticipated, the slope stability of both sites proved to increase reaching “optimum” conditions due to the positive effects of matric suction. Upon increasing water conditions further or saturating the slope, increasing incidences of failure and instability occurred due to the loss of matric suction and cohesion. This instability can also be attributed to the proven decrease in shear strength properties of the soil, cohesion and internal friction, leading to loss of shear strength in the slope. The positive effects of matric suction were further proven when the slope of Site A that considered matric suction (in the form of an air entry value), exhibited a slightly higher FOS and improved slope stability than the one without. The results and conclusions of this research project prove the importance of investigating a soils variability and the subsequent slope reaction under varying moisture conditions. These are key factors to consider prior to civil construction on problem soils, so as to mitigate major failures and the consequences thereof.

**Keywords:** slope stability; soil variability; slope stability analysis; kinematic analysis; Factor of Safety; Probability of Failure; geotechnical design; applied geology; matric suction; soil shear strength; liquefaction potential; Berea Red sands.

# TABLE OF CONTENTS

<b>DECLARATION - PLAGIARISM .....</b>	<b>ii</b>
<b>ACKNOWLEDGEMENTS .....</b>	<b>iii</b>
<b>ABSTRACT.....</b>	<b>iv</b>
<b>TABLE OF CONTENTS .....</b>	<b>v</b>
<b>LIST OF FIGURES .....</b>	<b>viii</b>
<b>LIST OF TABLES .....</b>	<b>xii</b>
<b>LIST OF ABBREVIATIONS .....</b>	<b>xiii</b>
<b>CHAPTER ONE INTRODUCTION .....</b>	<b>1</b>
1.1 General Background.....	1
1.2 Problem Statement .....	3
1.3 Research Objectives .....	4
1.4 Hypothesis.....	4
1.5 Research Significance .....	5
1.6 Research Limitations .....	5
1.7 Research Organisation .....	6
<b>CHAPTER TWO LITERATURE REVIEW .....</b>	<b>7</b>
2.1 Background into Slope Stability .....	7
2.2 Rainfall Induced Slope Failure .....	10
2.3 Soil Variability Induced Slope Failure .....	12
2.4 Methods of Slope Stability Analysis .....	14
2.4.1 Limit Equilibrium Methods (LEM) .....	14
2.4.2 Limitations of conventional slope stability methods.....	17
2.4.3 Numerical Simulation Method.....	18
2.4.4 Probabilistic Slope Stability Analysis: Reliability analysis and Probability of Failure	19
2.5 Comparison of stability analysis methods .....	25
2.5.1 Finite Element Method vs Limit Equilibrium Method .....	26
2.5.2 Finite Element Method vs Random Finite Element Method .....	27
2.6 Summary .....	29
<b>CHAPTER THREE METHODOLOGY.....</b>	<b>31</b>
3.1 Introduction.....	31
3.1.1 Fieldwork.....	31

3.1.2	Laboratory Testing .....	32
3.1.3	Slope Stability Analysis / Numerical Modelling .....	32
3.2	Fieldwork: Observations and Information obtained.....	32
3.2.1	Site A Description.....	32
3.2.2	Site B Description.....	34
3.3	Geological Background.....	36
3.3.1	Site A Local Geology.....	37
3.3.2	Site B Local Geology.....	38
3.4	Laboratory test methods and standards.....	40
3.4.1	Moisture content .....	42
3.4.2	Particle Size Analysis .....	42
3.4.3	Specific Gravity of Soil Solids .....	47
3.4.4	Atterberg Limits .....	49
3.4.5	Free Swell test.....	55
3.4.6	Compaction testing.....	56
3.4.7	Soil-Suction testing .....	58
3.4.8	Consolidation testing / Oedometer test.....	62
3.4.9	Direct Shearbox test .....	65
3.4.10	Triaxial test - Consolidated Undrained .....	68
<b>CHAPTER FOUR LABORATORY RESULTS AND INTERPRETATION.....</b>		<b>72</b>
4.1	Introduction.....	72
4.2	Natural Moisture Content of Soils .....	72
4.3	Particle Size Analysis .....	73
4.4	Specific Gravity.....	76
4.5	Free Swell .....	77
4.6	Atterberg Limits.....	78
4.7	Compaction .....	80
4.8	Soil Suction .....	83
4.9	Consolidation .....	86
4.10	Direct Shear Box tests .....	93
4.11	Triaxial tests - Consolidated Undrained .....	103
4.12	Summary of laboratory results for Site A.....	107
4.13	Summary of laboratory results for Site B.....	107
<b>CHAPTER FIVE SLOPE STABILITY ANALYSES .....</b>		<b>109</b>
5.1	Introduction.....	109
5.2	Site A Slope Stability Analysis.....	113

5.2.1	Site A FEA Groundwater Seepage Analysis and subsequent slope stability analysis	117
5.3	Site B Slope Stability Analysis.....	119
5.4	Summary of slope stability analyses .....	123
<b>CHAPTER SIX DISCUSSION.....</b>		<b>124</b>
6.1	Introduction.....	124
6.2	Discussion on Site A slope stability .....	124
6.3	Discussion on Site B slope stability .....	125
<b>CHAPTER SEVEN CONCLUSION AND RECOMMENDATIONS.....</b>		<b>128</b>
7.1	Conclusions.....	128
7.2	Recommendations .....	129
7.2.1	Site A recommendations.....	129
7.2.2	Site B recommendations.....	129
<b>REFERENCES.....</b>		<b>132</b>

## LIST OF FIGURES

<b>Figure 1.1:</b> Landslide susceptibility map of South Africa (Chiliza and Richardson, 2008).....	2
<b>Figure 2. 1:</b> The two general types of sliding slope failures that occur, dependent on soil properties (Niroumand et al, 2012).....	7
<b>Figure 2. 2:</b> “Fall” type of landslide failure .....	8
<b>Figure 2. 3:</b> “Toppling” slope failure .....	8
<b>Figure 2. 4:</b> “Spreading” slope failure .....	8
<b>Figure 2. 5:</b> “Flowing” slope failure .....	8
<b>Figure 2. 6:</b> Types of wedge failures (Kumsar et al, 2000) .....	9
<b>Figure 2. 7:</b> The two main failure mechanisms in soil slopes a) shallow slide b) deep slide (Li et al, 2019a). .....	9
<b>Figure 2. 8a and b:</b> Showing a few of the failures that occurred during April 2019 rainfall. (Floodlist, 2019).....	11
<b>Figure 2. 9:</b> Illustration of the multi-scale nature of soil (Huber, 2013).....	13
<b>Figure 2. 10:</b> Illustration of LEM and theory of FOS (Abramson et al., 2002).....	15
<b>Figure 2. 11:</b> General Monte Carol simulation approach (Krahn, 2004).....	21
<b>Figure 2. 12:</b> Showing the application of the Finite Element Method (FEM) of slope stability analysis (adapted from Baba et al., 2012).....	22
<b>Figure 2. 13a, b and c:</b> Stress distribution of 3D soil slope in a FEM stability analysis (Yang et al, 2016) .....	23
<b>Figure 2. 14:</b> Probability of failure versus coefficient of variation for various normalised scales of fluctuation (Griffiths and Fenton, 2004).....	28
<b>Figure 2. 15:</b> Comparison of the probability of failure for various coefficients of variation of normalised undrained strength predicted by RFEM (curves with points) and by probabilistic analyses accounting for spatial averaging (Griffiths and Fenton, 2004) .....	29
<b>Figure 3. 1a, b and c:</b> Northerly views of Site A showing stream in the distance, vegetation on site and first initial drop. ....	33
<b>Figure 3. 2:</b> Site map showing location of Site A in relation to road and stream (Adapted from Google Earth).....	33
<b>Figure 3. 3:</b> Westerly view of Site A showing slope face (adapted from Google Earth) .....	34

<b>Figure 3. 4a and b:</b> showing Site B and close up of failure on top of slope .....	35
<b>Figure 3. 5:</b> Site map showing location of Site B in relation to roads (adapted from Google Earth).....	35
<b>Figure 3. 6:</b> Close-up view of Site B, showing slope face. (Adapted from Google Earth).....	36
<b>Figure 3. 7a and b:</b> showing TP1 dug on Site A and exposed bedrock within 0.1 mbegl. ....	37
<b>Figure 3. 8:</b> Map showing local geology underlying Site A, indicated by the green X (Source: Council for Geoscience, 2008. Adapted from Durban map, area 2930).....	38
<b>Figure 3. 9a and b:</b> Showing TP2 dug on Site B, with evidence of water table at base of pit. ....	39
<b>Figure 3. 10:</b> Map showing local geology underlying Site B, indicated by the green dot (Source: Council for Geoscience, 2008. Adapted from Durban map, area 2930).....	39
<b>Figure 3. 11a and b:</b> Images of samples collected from the two sites. ....	40
<b>Figure 3.12:</b> Showing samples after oven-drying. ....	42
<b>Figure 3. 13:</b> Showing mechanical sieve shaker as sample is being separated. ....	44
<b>Figure 3. 14:</b> Samples 1 and 2 after being weighed out and mixed with the dispersing agents. ....	45
<b>Figure 3. 15:</b> Sample 3 being stirred with an automatic whisk for 5 minutes. ....	45
<b>Figure 3. 16a and b:</b> Showing Samples 1 through 4 during hydrometer analysis; a) Sample 1 and 2, b) Sample 3 and 4.....	46
<b>Figure 3. 17:</b> Sample under vacuum to remove air bubbles, during specific gravity test.....	48
<b>Figure 3. 18a, b, c, d and e:</b> a) Casagrande cup once calibrated; b) sample once arranged into a pat, c) groove created before start of test; d) Sample after completion of one liquid limit test; with groove closure evident; e) removal of sample at the source of closure for moisture content testing.....	51
<b>Figure 3. 19:</b> Sample crumbling at 3mm diameter .....	52
<b>Figure 3. 20a and b:</b> Sample before (a.) and after (b.) oven drying.....	54
<b>Figure 3. 21a and b:</b> Sample before (a.) and after (b.) addition of water and kerosene (water is the murkier solution). ....	55
<b>Figure 3. 22:</b> Showing free swell of samples after 24 hours. In this case, it is evident that the sample had not increased in volume, i.e., there was no swelling. ....	56
<b>Figure 3. 23:</b> Showing apparatus used for compaction testing. ....	57
<b>Figure 3. 24:</b> Sample 3 after compaction <b>Figure 3. 25:</b> Extrusion of Sample 1.....	58
<b>Figure 3. 26a and b:</b> a) Compacted samples being preserved prior to soil suction test; b) apparatus used in soil suction testing.....	59

<b>Figure 3. 27a, b and c:</b> a) Sample trimmed and cut in half; b) filter paper placed between the two halves of the sample (within 2 other buffer filter papers); c) plastic spacer used to separate top filter paper from top of sample. ....	60
<b>Figure 3. 28a and b:</b> a) Sealed sample in airtight container; b) kept in contained environment for 5 to 10 days with temperature regulation. ....	61
<b>Figure 3. 29:</b> Showing oedometer apparatus. ....	63
<b>Figure 3. 30:</b> Showing loading of oedometer <b>Figure 3. 31:</b> 3 Saturated specimens (Sample 1) after test in preparation for final moisture content determination. ....	64
<b>Figure 3. 32:</b> Direct shearbox apparatus .....	66
<b>Figure 3. 33:</b> DSB tests under active loading <b>Figure 3. 34:</b> Showing failure of a specimen after shearing.....	67
<b>Figure 3. 35:</b> Showing basic triaxial testing apparatus (in UKZN soils laboratory). ....	69
<b>Figure 3. 36:</b> Showing the failure of Sample 3 at an effective constant stress of 200kPa.....	70
<b>Figure 4. 1a, b, c and d:</b> Particle size distribution curves for samples 1, 2, 3 and 4, respectively. ....	75
<b>Figure 4. 2a, b, c and d:</b> Flow curves to determine LL for samples 1, 2, 3 and 4, respectively. ....	79
<b>Figure 4. 3a, b, c and d:</b> Compaction curves to determine MDD and OMC for samples 1 , 2, 3 and 4, respectively. Samples 1, 3 & 4 as provided by Soilco laboratory.....	82
<b>Figure 4. 4a and b:</b> Total and Matric soil suction curves for samples 1 and 2, respectively. ....	84
<b>Figure 4. 5:</b> Typical Soil-Water Characteristic Curve (SWCC) and zones (Hong <i>et al</i> , 2016). ....	85
<b>Figure 4. 6a and b:</b> Soil-water Retention curves for a. Sample 1 and b. Sample 2 (Created on: SWRC Fit ( <a href="http://purl.org/net/swrc/">http://purl.org/net/swrc/</a> ); Seki, 2007). ....	86
<b>Figure 4. 7a and b:</b> Consolidation curves for Sample 1 at 12 % MC .....	87
<b>Figure 4. 8a and b:</b> Consolidation curves for Sample 1 at 19.56% MC .....	88
<b>Figure 4. 9a and b:</b> Consolidation curves for Sample 1 at 25.76% MC .....	88
<b>Figure 4. 10a and b:</b> Consolidation curves for Sample 2 at 12% MC .....	90
<b>Figure 4. 11a and b:</b> Consolidation curves for Sample 2 at 17.79% MC. ....	91
<b>Figure 4. 12a and b:</b> Consolidation curves for Sample 2 at 21.80% MC .....	92
<b>Figure 4. 13a and b:</b> Shear stress curves for Sample 1 at 12% MC.....	94
<b>Figure 4. 14a and b:</b> Shear stress curves for Sample 1 at 19.56% MC.....	95
<b>Figure 4. 15a and b:</b> Shear stress curves for Sample 1 at 22.34% MC.....	96

<b>Figure 4. 16a and b:</b> Shear stress curves for Sample 3 at 9% MC.....	97
<b>Figure 4. 17a and b:</b> Shear stress curves for Sample 3 at 12% MC.....	98
<b>Figure 4. 18a and b:</b> Shear stress curves for Sample 3 at 14% MC.....	99
<b>Figure 4. 19a and b:</b> Shear stress curves for Sample 4 at 8% MC.....	100
<b>Figure 4. 20a and b:</b> Shear stress curves for Sample 4 at 12% MC.....	101
<b>Figure 4. 21a and b:</b> Shear stress curves for Sample 4 at 13.41% MC.....	102
<b>Figure 4. 22:</b> Mohr-Coulomb circles and failure envelope for Sample 1.....	104
<b>Figure 4. 23:</b> Mohr-Coulomb circles and failure envelope for Sample 3.....	105
<b>Figure 4. 24:</b> Mohr-Coulomb circles and failure envelope for Sample 4.....	106
<b>Figure 5. 1a and b:</b> Showing close up model of Site A as drawn on RocScience Slide; a) uppermost, left hand side of the model close to the road, b) bottommost right hand side of model close to the stream.....	112
<b>Figure 5. 2:</b> Showing close up model of Site B as drawn on Rocscience Slide.....	112
<b>Figure 5. 3:</b> Slope stability analysis of site A in “dry” water conditions (< 8.7 %).....	113
<b>Figure 5. 4:</b> Slope stability analysis of site A in “optimum” water conditions (8.7 %).....	114
<b>Figure 5. 5:</b> Slope stability analysis of site A in “wet” water conditions (12%).....	115
<b>Figure 5. 6a, b and c:</b> Histogram/bar graphs of Site A showing FOS for the slope of Site A in a) dry water conditions, b) optimum water conditions and c) wet conditions.....	116
<b>Figure 5. 7:</b> FEA and Groundwater Seepage Analysis of Site A in Optimum conditions....	117
<b>Figure 5. 8:</b> Slope stability analysis of Site A (OMC) with matric suction parameters .....	118
<b>Figure 5. 9:</b> Slope stability analysis of site B in “dry” water conditions (~8.5 %)......	119
<b>Figure 5. 10:</b> Slope stability analysis of site B in “optimum” water conditions (~ 10%).....	120
<b>Figure 5. 11:</b> Slope stability analysis of site B in “wet” water conditions (~ 13%). .....	121
<b>Figure 5. 12a, b and c:</b> Histogram/bar graphs of Site A showing FOS < 1 for the slope on Site B in a) dry water conditions, b) optimum water conditions and c) wet conditions. ....	122
<b>Figure 6. 1:</b> Showing the soil reaction to pressure under compaction, with emphasis on the driven-out water at the base of the proctor mould. ....	126
<b>Figure 6. 2:</b> General properties of gabion wire mesh (Uray Ve and Tan, 2015; Toprak <i>et al</i> , 2016).....	130
<b>Figure 6. 3a and b:</b> Showing construction of Gabion walls as rehabilitation of the failed slope and mitigation of further slope failure on Site B. ....	131

## LIST OF TABLES

<b>Table 2. 1:</b> Modes of slope failure (Das, 2009).....	8
<b>Table 3. 1:</b> Summary of sites used in this research project.....	32
<b>Table 3. 2:</b> Parameters recorded from site A, for use in stability analysis.....	34
<b>Table 3. 3:</b> Parameters recorded from site B, for use in stability analysis.....	36
<b>Table 3. 4: TP1 Soil Profile</b> .....	37
<b>Table 3. 5: TP2 Soil Profile</b> .....	38
<b>Table 3. 6:</b> List of tests and testing standards .....	40
<b>Table 4. 1:</b> Sample designations during laboratory testing.....	72
<b>Table 4. 2:</b> Natural Moisture Contents of all samples tested .....	73
<b>Table 4. 3:</b> Results and interpretations from Particle Size Distribution curves .....	75
<b>Table 4. 4:</b> Specific Gravity (Gs) of all samples tested .....	76
<b>Table 4. 5:</b> Calculated void ratio ( $e$ ) and porosity ( $n$ ) of all four samples .....	77
<b>Table 4. 6:</b> Results from Atterberg Limit tests conducted on all samples .....	79
<b>Table 4. 7:</b> Derived parameters from Compaction Testing.....	82
<b>Table 4. 8: Sample 1</b> results from Consolidation testing .....	89
<b>Table 4. 9: Sample 2</b> results from Consolidation testing .....	92
<b>Table 4. 10: Sample 1</b> results from DSB testing .....	96
<b>Table 4. 11: Sample 3</b> results from DSB testing .....	99
<b>Table 4. 12: Sample 4</b> results from DSB testing .....	102
<b>Table 4. 13:</b> Results from Triaxial Testing conducted at optimum conditions.....	103
<b>Table 4. 14:</b> Summary of results from set of Triaxial tests on Sample 1.....	104
<b>Table 4. 15:</b> Summary of results from set of Triaxial tests on Sample 3.....	105
<b>Table 4. 16:</b> Summary of results from set of Triaxial tests on Sample 4.....	106
<b>Table 5. 1:</b> Summary of materials and material properties.....	109
<b>Table 5. 2:</b> Soil properties and shear strength parameters used during slope stability analysis, under varying moisture conditions.....	110
<b>Table 5. 3:</b> Results of Factor of safety (deterministic) and “overall” probabilistic slope stability analyses considering spatial variability, for Site A and B .....	123
<b>Table 6. 1:</b> Summary of various water conditions assessed for both sites.....	124

## LIST OF ABBREVIATIONS

AEV -	air entry value
AIC -	Akaike Information Criterion optimiser
CD -	Consolidated Drained test
COV -	Coefficient of variability
COVID-19 -	Novel Coronavirus outbreak in November 2019
CU -	Consolidated Undrained test
DSB -	Direct Shear Box test
FDM -	Finite Different Method
FEA -	Finite Element Analysis
FEM -	Finite Element Method
FOS -	Factor of Safety
FOSM -	First Order Second Moment
FSI -	Free Swell Index
GWT -	groundwater table
kPa -	Kilopascals
KZN -	KwaZulu-Natal
LEM -	Limit Equilibrium Method
LL -	Liquid Limit
Ma -	Million years ago
mbegl -	metres below existing ground level
MC -	moisture content
MCS -	Monte Carlo Simulation
MDD -	Maximum Dry Density
M-P -	Morgenstern-Price method
N -	Newtons
NMC -	natural moisture content
OMC -	Optimum Moisture Content
PDF -	Probability density function
PEM -	Point Estimate Method
PI -	Plasticity Index
PL -	Plastic Limit

POF -	Probability of Failure
PSD -	particle size distribution
RFEM -	Random Finite Element Method
SL -	Shrinkage Limit
SOF/ $\lambda$ -	Scale of Fluctuation
SRT -	Strength reduction technique
SSR -	Sum of Squared Residuals
SWCC -	soil-water characteristic curve
TP -	Test pit
UKZN -	University of KwaZulu-Natal
USCS -	Unified Soil Classification System
UU -	Unconsolidated Undrained test

### List of Symbols

~ -	approximately
$\beta$ -	Reliability index
Pf -	percentage finer
PA -	adjusted percentage finer
D -	particle diameter
Rh -	hydrometer bulb reading
Ws -	mass of soil (g)
F200 -	percentage of soil retained on the #200 (0.075mm) sieve.
$k$ -	permeability
L -	corrected length
T -	time interval reading in minutes.
Gs -	Specific Gravity
e -	void ratio
n -	porosity
Sr -	saturation degree
$\rho$ -	density
m -	mass of the compacted sample
v -	volume of compacted sample
$\mu_F$ -	mean value
$\sigma_F$ -	standard deviation
$^{\circ}\text{C}$ -	degrees Celsius
Cu -	Coefficient of uniformity
Cc -	Coefficient of curvature
$k$ -	Coefficient of Permeability
$a_v$ -	Coefficient of compressibility

$m_v$ -	Coefficient of volume change
$C_c$ -	Compression Index
$C_v$ -	Coefficient of consolidation
$H_s$ -	height of soil solids
$H_o$ -	initial height of the specimen
$\gamma_w$ -	unit weight of water
$A$ -	area of the specimen
$c'$ -	effective cohesion
$\sigma_n$ -	normal stress
$\mu$ -	pore water pressure
$\phi'$ -	effective friction angle
$\mu_a$ -	pore air pressure
$\phi^b$ -	friction angle related to changes in pore water pressure ( $\mu$ )
$\tau_f$ -	shear strength of the material
$\tau_n$ -	shear stress
$\sigma_n$ -	normal effective stress
$G$ -	shear stiffness
$\gamma$ -	Unit weight
$C_T$ -	Total Cohesion
$C'$ -	Effective Cohesion
$\sigma_T$ -	Total Angle of Internal Friction
$\phi_f'/\sigma'$ -	Effective Angle of Internal Friction
$\mu_p$ -	excess pore water pressure
$(\mu_a - \mu)$ -	matric suction
$P_k$ -	Total and Matric Soil Suction

# CHAPTER ONE

## INTRODUCTION

---

### 1.1 General Background

Slope stability is defined as the resistance of inclined surfaces to failure by sliding or collapse. Slope failure is a completely natural phenomenon. According to United Nations reports in 2014, natural disasters caused around 2 trillion USD damage globally and affected more than 4 billion people since 1994 (Kellet *et al*, 2014). In the United States each year, slope failure is responsible for a range of 25 to 50 deaths and in excess of one billion dollars in damages (United States Geological Survey, 2014).

Slope failure within a slope or soil mass may occur through the action of gravitational forces, seepage forces, excavation or undercutting of the slope foot or due to gradual disintegration of the soil structure. Slope stability analysis is conducted to assess the design of natural and engineered slopes, such as embankments, road cuts, open-pit mining, excavations and landfills and to check their safety, stability and equilibrium conditions. The process of analysing slope failure involves identifying endangered slopes, investigating the potential failure mechanisms related to the slope, determining the slopes sensitivity to a variety of triggering mechanisms and then designing an optimal slope with regard to safety, stability and cost-efficiency. Possible mitigative and remedial measures are provided as well. The core competence of a geotechnical engineer involves the development of reliable and stable slopes in order to mitigate risk associated with slope failure. (Punmia *et al*, 2005)

There is no standardised process to measure a slopes factor of safety (FOS). Global concepts are randomly used to provide some degree of safety, mainly driven by a professionals' judgement or previous experience in deterministic geotechnical design. Too high FOS, although conservative, are usually not cost-effective. Whereas a too low FOS will result in casualty and economic consequences. More advanced methods of slope stability analysis (such as probabilistic analysis) are considered better because they are able to account for soil variability and uncertainty with accuracy. This would aid geotechnical engineers to make economically informed decisions for safe slope stability design. (Fenton and Griffiths, 2008)

A report according to Paige-Green (1989) illustrates a slope instability susceptibility map based on rainfall, infiltration, topographic terrain, geology, and engineering reports. Garland and Olivier (1993) later updated this map, and a revision was provided by Paige-Green and Croukamp (2004) (Figure 1.1). Based on the initial report by Paige-Green, slope instability in South Africa tends to occur in the mountainous regions of Kwazulu-Natal (KZN) namely the Drakensberg, the Western Cape, and the eastern coastal regions of KZN where dune soils are predominant. High slope instability susceptibility within mountainous nature reserves (KwaZulu-Natal and Western Cape) does not pose a direct threat to people or even property and thus there are not many recorded incidences of slope failure or landslides in these areas (Paige-Green, 1989).

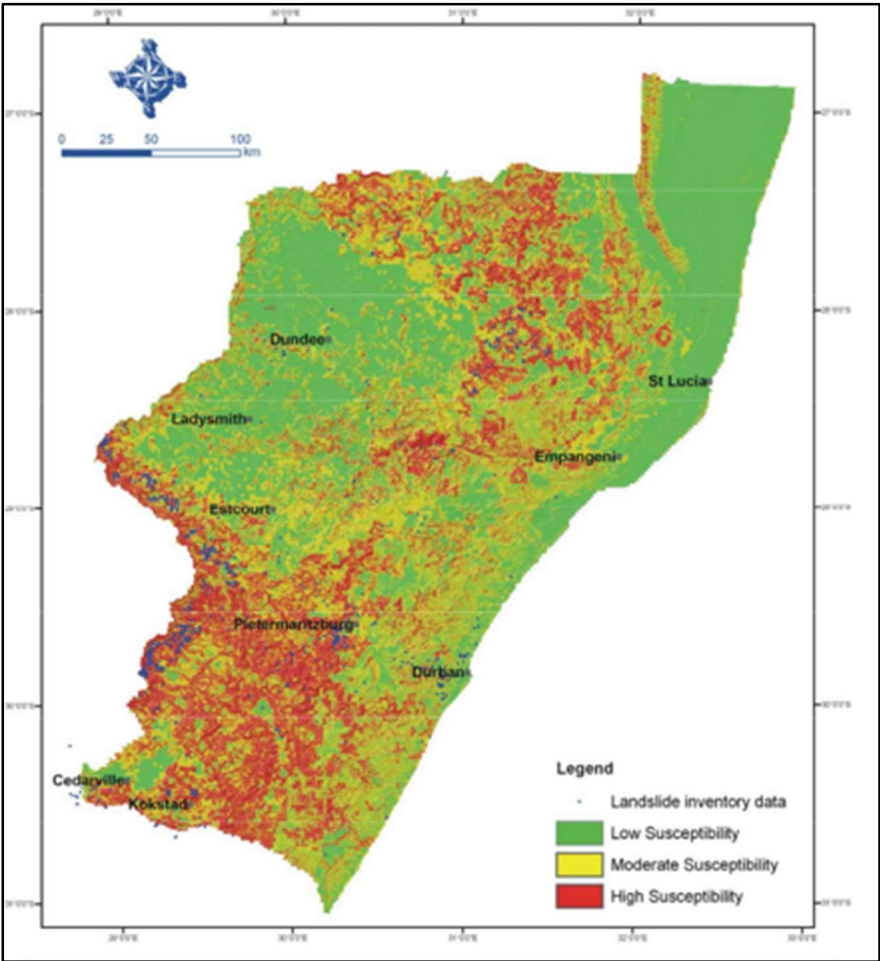


**Figure 1.1:** Landslide susceptibility map of South Africa (Chiliza and Richardson, 2008)

The landslide susceptibility map demonstrates the landslide incidence and susceptibility of slope failure at the provincial scale. In this way it serves as an enlightenment for geohazard to the public and government. In hilly areas where rural community development is constrained, national

landslide-mapping programs are now available as a safety guide. As unexpected heavy-rainfall events and flash floods are increasing in frequency, there is a need to rapidly map this geohazard to mitigate deaths and damages (Wieczorek, 1984; Chiliza and Richardson, 2008). As development continues to surge in South Africa, real estate developers tend to develop properties very close to highly susceptible areas. Under these circumstances, the need for continuous studies and monitoring of slopes becomes imperative.

## 1.2 Problem Statement

Slope instability is a significant problem in Durban, due to the topography and the weather condition of the area. Topographically, the city of Durban consists of multiple ridges and valleys, parallel to the coast. Examples are that of the Berea suburb, situated on a ridge of hills encircling the harbour and beach, and the Bluff area which is a series of hills formed from ancient tidal activity, separating the natural Durban Harbour from the sea (Cawthra *et al*, 2012). As such, this triggers vulnerability of slopes to failure due to topographical formation. Climatic conditions around Durban are generally humid and the climatic stratification depends on the annual gross rainfall and moisture flux in slopes. As Durban is a coastal city, it comprises dune sands of the Berea Formation, Karoo Supergroup. The Berea Formation soils vary greatly in soil type ranging from fine grained sands to silts and clays. This great variability makes them very unreliable in engineering structures. Both the aforementioned ridges, that of the Berea suburb and the Bluff, are underlain at depth by these problematic soils. On steeper embankments they are mostly associated with shallow non-circular flows, generally triggered by rainfall (Singh *et al*, 2009; 2011). The Berea Red soil is classified as a “Collapsible material”. They can withstand relatively large vertical loads at low moisture contents, however, upon wetting, the soil exhibits a volume decrease and collapse of the soil structure. This phenomenon displays as settlement of the soil mass. Both sands and clays of the Berea Formation are known to undergo significant settlement and are highly compressible, especially those of looser or softer consistency (Clayton, 1989). The Engineering Council of South Africa (ECSA) issued a practice notice, attributing many of the concrete retaining block (CRB) wall failures, to the moisture sensitive nature of Berea Red sands, which were poorly compacted when used as backfill. It was observed that the failures occurred due to water ingress into the soil, leading to the formation of slip planes behind the walls (ECSA, 2017). Garland (1978) investigated a landslide failure of an embankment made up of Berea Red sands. He found that this failure also occurred due to the effects of soil moisture on the slope material, with a 5 %

increase in moisture content resulting in a shear strength decrease of up to 8.2 kN/m<sup>2</sup>. Uniformly graded, rounded fine sands such as much of the Berea dune soils, are found to be very susceptible to liquefaction. Upon interaction with water they may act like a fluid, leading to mass failures such as landslides (Poulos *et al.*1985). Based on the above, the slope stability analysis of both sites in the study area, especially those underlain by problem soils, has to be strictly analysed in order to mitigate slope failure occurrences. Awareness around the potential of failure associated with these soil slopes, can help to avoid loss of life and property, in the future.

### **1.3 Research Objectives**

This research aims at investigating and quantifying the effects of soil variability due to associated geological threats, on the stability of two natural slopes in Durban, KwaZulu-Natal. Another aim is to provide more insight into common soil types and geotechnical problems that arise within the study area. The specific objectives of the study are to:

- Conduct geotechnical site investigations of each site, involving visual inspection of the site to make important observations, and to physically measure parameters on site for use in slope stability analyses;
- Collect samples from the sites for laboratory testing to obtain soil properties and parameters for use in slope stability analyses;
- Conduct laboratory testing under varying moisture contents where possible, to obtain the necessary parameters for soil/slope modelling;
- Model and conduct slope stability (kinematic) analyses of the two slopes under varying water conditions, using RocScience© Slide Software suite to obtain Factors of Safety and Probabilities of Failure;

### **1.4 Hypothesis**

Slope failures occur largely due to soil variability in a slope and associated geological threats. The analysis of slope stability should analyse the interactions between slope geometry, shear strength resistance, effects of pore-water pressure, and water infiltration, using design software to provide Factors of Safety.

## 1.5 Research Significance

As mentioned in the problem statement above, much of the study area (Durban, KwaZulu-Natal) is underlain by problem soils. Due to the inherent variability of these soils and the fact that they are encountered more frequently during construction and city expansion, slope stability analysis in Durban is necessary to augment information available on common soil behaviour and the measures necessary to avoid failure. Successful outcomes of this research project, in the form of definitive results and conclusions, can aid geotechnical engineers in better understanding soil variability and its effects on a slopes reaction to varying soil conditions. It will also highlight the necessity to properly investigate all soils on site, with full consideration of the geological profile, properties and origin, in order to analyse the stability of soil slopes more accurately. This research was presented at the UKZN Postgraduate Research and Innovation Symposium (PRIS), 2020.

## 1.6 Research Limitations

The following limitations were anticipated during the course of this research project and in arriving at the recommendations and conclusion:

- **Inherent soil variability** makes every soil character and behaviour vastly different from the next, even those soils that are of the same type, texture or origin. This temperamentality brings a great deal of uncertainty at every step of the investigation and was kept in mind throughout the course of the project.
- **Human error** is a major factor to consider during laboratory testing and throughout the undertaking and interpretation of laboratory tests.
- Although the benefits of the more advanced **FEM analysis outweigh the LEM analysis** for slope stability, the software to conduct FEM analysis was not feasible for this study nor was it obtainable due to time constraints.
- The **COVID-19** pandemic led to much uncertainty and anxiety throughout the entirety of 2020 and impacted every aspect of this research project, since conception. Fieldwork and laboratory testing, which made up almost 80% of this study, was postponed indefinitely upon the first lockdown in March 2020. Essentially, the work that was to be completed in

one year, was pushed into a 6 month span. The turmoil and disruption caused by this global pandemic was a major limitation to fulfilling the objectives of this study.

## **1.7 Research Organisation**

The research study is laid out as follows:

Chapter 1 - Serves as the introductory chapter, covering general background to the research, problem statement, hypothesis, research objectives, justification and organisation.

Chapter 2 – Detailed literature review.

Chapter 3 - A detailed description of the methodology adopted in order to achieve the objectives of this research. Specific background into each individual site is discussed, consisting of site descriptions and site geology. Information is provided on standard civil engineering / soil testing procedures and apparatus. The process to undertake the slope stability analysis is discussed, as well as a breakdown of necessary parameters and how they were obtained.

Chapter 4 - Covers the experimental aspect of the research project. This chapter provides detailed results from laboratory testing, scientific interpretations of the test results, and discusses the application of all results and parameters into the slope stability analyses.

Chapter 5 – Provides detailed slope stability analyses of each slope / site, discussions and comparisons of each slope analysis under varying conditions.

Chapter 6 - Discussion of all findings and results thus far.

Chapter 7 - Recommendations and conclusion of the research project.

## CHAPTER TWO

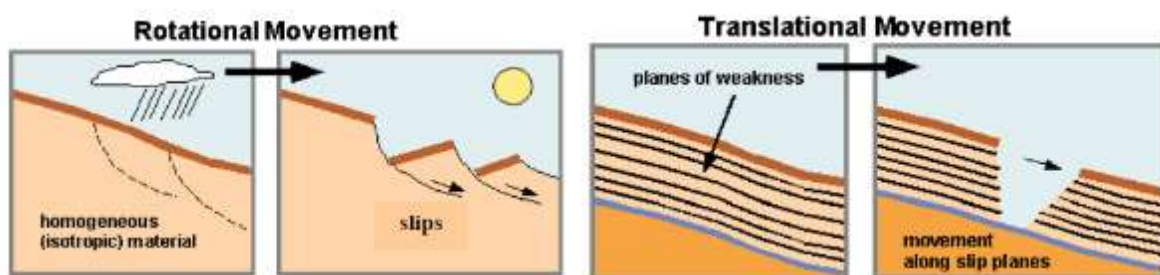
### LITERATURE REVIEW

---

#### 2.1 Background into Slope Stability

Slope instability is regarded as one of the three major geological disasters, along with earthquakes and volcanoes. Slope failures may occur due to gravitational and seepages forces within the soil, and other triggering factors such as the slope geometry, height, excess pore water pressure, and loss of shear strength caused by weathering, and liquefaction. Furthermore, geological events such as earthquakes and volcanic eruptions can also trigger slope failure (Chen *et al*, 2014; Yang *et al*, 2016). The failure of a soil mass within a slope is called a slide. It entails the downward and outward movement of the entire mass of soil that experiences failure. Slides can occur in almost every possible way, slowly or suddenly and without any obvious inducement (Salunkhe *et al*, 2017).

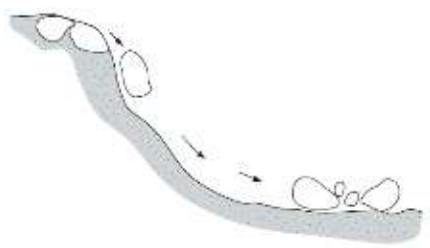
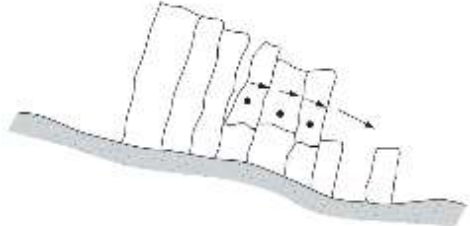
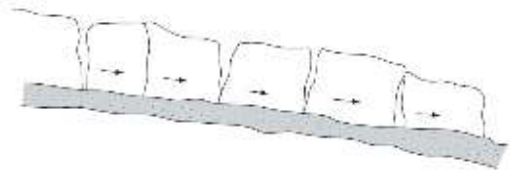
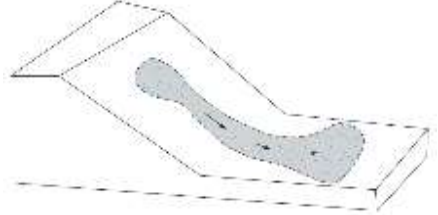
Slides in soil will either exhibit rotational or translational movement, as illustrated in Figure 2.1 below. The slide that occurs depends on the type of material present in the slope: in a slope that is considered homogenous with similar properties in all directions, rotational movement is the most common occurrence, whereas in inhomogeneous slopes with varying planes of weakness, translational movement is anticipated (Niroumand *et al*, 2012).



**Figure 2. 1:** The two general types of sliding slope failures that occur, dependent on soil properties (Niroumand *et al*, 2012)

The mass movement of slopes can be categorised into two types namely, a slope failure and a landslide (Okamura and Yure, 2001). A slope failure occurs very fast on a slope of at least  $20^{\circ}$ , often with no warning signs. This failure is commonly triggered by rainfall which affects a small, localised area. A landslide, however, occurs over a larger area with a slope angle less than  $20^{\circ}$ ,

and is a slow or gradual movement. According to Das (2009), a mass of soil will be in equilibrium provided that the strength of the mass, which is resisting failure, is equal to or greater than, the force of gravity which is driving failure. Slope failure is often generated by processes that increase the shear stresses that the soil mass experiences, and in doing so, decrease the shear strength (Abramson *et al*, 2002). Table 2.1 below is a summary providing illustrations of the main types or modes of failure that occur (Das, 2009).

<b>Table 2. 1:</b> Modes of slope failure (Das, 2009)	
<p><b>Fall</b> – The detachment of soil and/or rock fragments that “fall” down the slope. In the case of soil, it is termed a landslide and in the case of rock it is termed a rockfall.</p>	 <p><b>Figure 2. 2:</b> “Fall” type of landslide failure</p>
<p><b>Topple</b> - This is a rotational slide failure whereby the soil and/or rock mass tilts forward around an axis beneath the centre of gravity of the mass undergoing displacement.</p>	 <p><b>Figure 2. 3:</b> “Toppling” slope failure</p>
<p><b>Spread</b> - This is a translational slide failure involving the sudden lateral movement of water-bearing seams of soil (sand or silt) that were overlain by clays or a heavy overburden.</p>	 <p><b>Figure 2. 4:</b> “Spreading” slope failure</p>
<p><b>Flow</b> - This is a downward movement of a soil mass that has mixed with water to form a viscous fluid.</p>	 <p><b>Figure 2. 5:</b> “Flowing” slope failure</p>

Wedge failure is another important type of slope failure. This is a structurally controlled failure mechanism found mostly in competent rock slopes. Wedge failure occurs in slopes made out of slabs of intact rock joined together by weak discontinuities, like joints, beddings, faults, or shear zones. The intersection of discontinuities, their orientation and whether they “daylight” out of the slope, determines if wedge failure will occur by sliding along discontinuities (illustrated in Figure 2.6 below). (Kumsar *et al*, 2000)

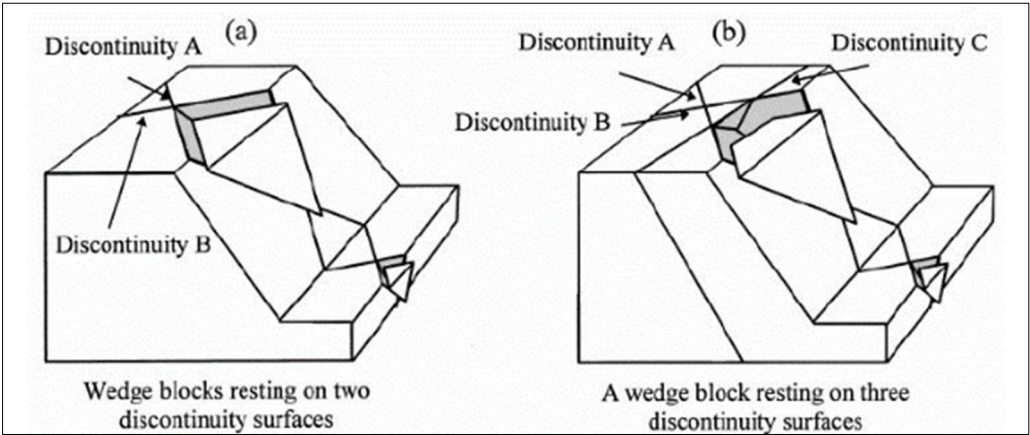


**Figure 2. 6:** Types of wedge failures (Kumsar *et al*, 2000)

Figure 2.7 below illustrates two types of failure mechanisms (FM) that exist, a shallow slide or local failure and deep slide or global failure. A shallow failure is one that affects small and surficial layers of a slope, usually as a result of erosion or runoff during rainfall. Deep failure mechanisms extend well into a slope and outcrops within the foundation layer (Li *et al*, 2019a).

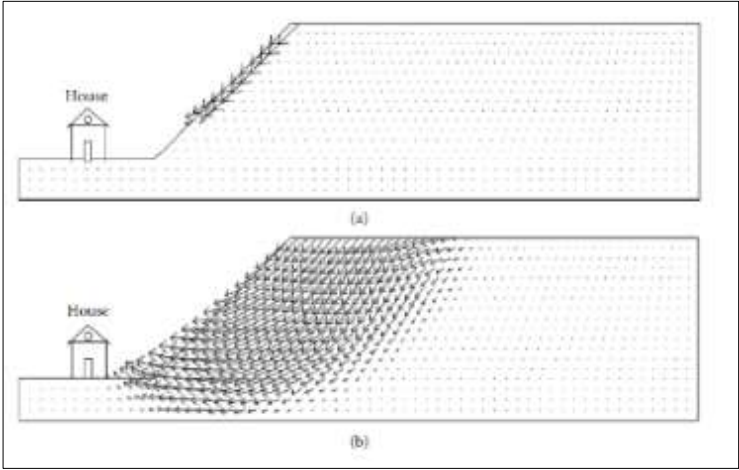


**Figure 2. 7:** The two main failure mechanisms in soil slopes a) shallow slide b) deep slide (Li *et al*, 2019a).

The figure above clearly demonstrates the difference in associated failure consequence. Although failure consequence is generally site-specific regarding loss of life and property, deep slides usually lead to more severe consequences than shallow slides (Li and Chu, 2015; Huang *et al.*, 2013).

Slope stability is influenced by a range of factors such as slope geometry, soil properties and behaviour, shear strength, unit weight, rainfall intensity, hydraulic conductivity, degree of saturation and even the presence of tension cracks or vegetative cover. Although much research has been carried out in this field throughout the years, there are still many unexplained slope failures and the causal factors of slope instability are still not fully understood (Duncan and Wright, 2005). Understandably, slope stability analysis is an important area of geotechnical engineering practice. (RocScience Inc, 2001-2004). In the past, slope stability analysis was performed through tedious and complicated manual calculations. Over time, it has adapted to more advanced methods that can be conducted easily with computer software. This great improvement has made the prospect of slope stability analysis in the geotechnical profession all the more accessible and convenient for practitioners, leading to an increased ability and understanding of the field (Chok, 2009).

## **2.2 Rainfall Induced Slope Failure**

Mapping and classification of mass-movement deposits in KwaZulu-Natal indicated that the largest collapses occurred as paleo-landslides, in areas of high relief and steep foot slopes of the Drakensberg mountains and in major river valleys. The majority of these slopes comprised of thick deposits of sandy colluvium formed from Ordovician Natal Group sandstone bedrock (Bell and Maud, 1996; Singh *et al.*, 2008). Various site investigations have been conducted concerning slope stability problems in this region, such as multiple cases of slope instability which were encountered during the construction of the N3 highway in Rickivvy, near Pietermaritzburg (Maurenbrecher, 1973; Maurenbrecher and Booth, 1975; Maud, 1985). Another example is that of the Maya Place landslide which occurred in the same area, underlain by Pietermaritzburg Formation shale beds that were dipping concordantly to the hillslope (Webb, 1983). Of the multiple case studies researching recent landslide events in KZN and surrounds, heavy rainfall has been identified as a primary causal factor attributed to many slope failures, ranging from small-scale localized collapses to large-scale “global” landslides and mudslides (Beckedahl *et al.*, 1988). Figures 2.8

show some of the catastrophic failures that occurred in Durban as a result of heavy rainfall in April 2019. The consequence of this rainfall event led to 32 loss of lives and 42 injuries due to flooding and slope failure.



**Figure 2. 8a and b:** Showing a few of the failures that occurred during April 2019 rainfall. (Floodlist, 2019)

Another example of rainfall-induced slope failure presented in Kwazulu-Natal with the collapse of a steep embankment of saturated soil, leading to the closure of a rail track when the failed material was deposited 50m below. Accordingly, most landslides identified are small scale/localized occurrences associated with high rainfall intensity mobilized through soil variability. Many researchers have shown that the majority of landslides occur in the rainy season, destroying infrastructure and occasionally resulting in human casualties (Johnson and Sitar, 1990; Fredlund and Rahardjo, 1993; Brand *et al.*, 1984; Lim *et al.*, 1996; Ng and Shi, 1998). As such, the effects of rainfall on slope stability must be considered in landslide hazard assessments (Chowdhury *et al.*, 2010). Much more research needs to be conducted into slope failures that occur as a result of rainfall processes, in order to further understand its effects in slope stability analysis. As soil slopes are usually unsaturated, with degrees of saturation ranging between 75 to 90%, it is widely acknowledged that most landslide incidences that occur in unsaturated residual soils, are caused by infiltrating rainwater (Johnson and Sitar, 1990; Fredlund and Rahardjo, 1993; Brand *et al.*, 1984; Lim *et al.*, 1996; Ng and Shi, 1998). Unsaturated soil is made up of three phases: solid, water, and air. It is important to note that the pore-water pressure of soil is always negative relative to the pore-air pressure. These *in-situ* soil conditions affect the entire concept of slope stability (Fredlund and Rahardjo, 1993). As such, it is not reliable to apply the classical saturated theory to determine the stability of rainfall-induced slope failures in unsaturated soil conditions.

Studies show that the shear behaviour of residual soils is greatly affected during rainfall and wetting episodes. Upon wetting, unsaturated soils undergo a collapse of the soil structure as well as an increase in pore water pressure, both factors which induce slope failure (Zhu *et al.*, 1998; Dai *et al.*, 1999).

In general, soils are divided into two soil-moisture states - saturated and unsaturated. The difference between the two states is determined by the relationship between the soil water content and the soil properties, characterised by parameters such as the degree of saturation and the pore-water pressure. Studies into soil-water interactions have led to enhanced understanding and knowledge of soil mechanics theory. During the dry season, the uppermost soil layers are initially unsaturated with negative pore-water pressure. This negative pore water pressure is defined as the matric suction, which is considered a major contributing factor to the shear strength of soils and ultimately, the stability of the slope. Various studies have been conducted regarding the use of a rainfall simulator to model the effects of rainfall and associated processes, on the stability of natural slopes. The hypothesis was that infiltrating rainwater into an unsaturated soil slope, has a negative effect on the stability of the slope by decreasing the matric suction within the soil and ultimately decreasing the shear strength of the slope. The conclusion reached was that smaller total rainfall could trigger infiltration, whereas larger total rainfall contributes more to runoff than infiltration. The researchers found that all processes related to rainfall, such as infiltration, run-off, and changes in pore-water pressure, all play significant roles in a full assessment of rainfall-induced slope failure. (Zhang *et al.*, 2000; Tsaparas *et al.*, 2003; Rahardjo *et al.*, 2003), As such, the application of unsaturated soil mechanics can help to assess rainfall-induced slope failures.

### **2.3 Soil Variability Induced Slope Failure**

Soils are naturally variable materials due to the processes that form them as well as the processes of the environment that alter them. After deposition, soils are modified continuously by external factors and processes like physical weathering, erosion, chemical reactions, decomposition, the introduction of new substances and even human intervention such as soil improvement techniques, excavation (also known as cutting) and filling. Based on the above, soil profiles are inherently heterogenous and soil properties can be highly variable both horizontally and vertically (multi-layered) (Hight and Leroueil, 2003; Lacasse and Nadim, 1996; Uzielli *et al.*, 2006).

Geotechnical engineers conduct both field and laboratory tests to determine the material properties of soils. Field tests include static penetration tests (SPT), cone penetration tests (CPT) and investigation pits. Laboratory tests are conducted based on the properties or parameters necessary for engineering construction with or on soils. Laboratory tests range from basic tests for soil classification such as Particle size analysis, Atterberg Limits, Free Swell tests, to more complicated tests such as direct shearbox tests or triaxial tests. Results are interpreted based on a limited number of field tests and soil samples. As such, the most conventional tool for dealing with ground heterogeneity is by quantifying safety factors, relying on the engineers experience and judgment (Elkateb *et al.*, 2002). Figure 2.9 shows the different scales of variability, ranging from the microscale level to the geological scale (Phoon and Kulhawy 1999; Huber, 2013)

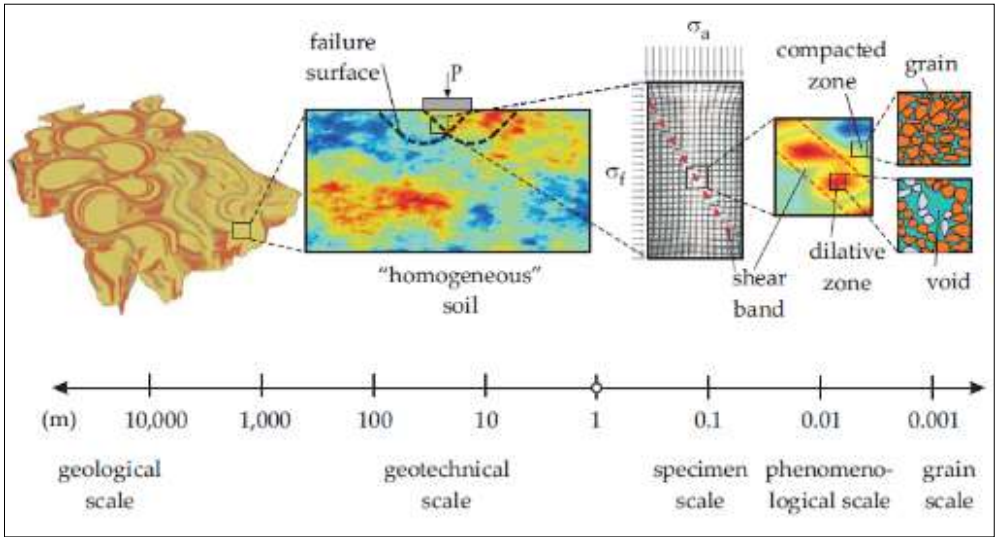


**Figure 2. 9:** Illustration of the multi-scale nature of soil (Huber, 2013)

As illustrated above, there are multiple spatial scales that contribute to soil variability. The geotechnical scale falls between the specimen scale and the geological scale, therefore it can be expected that this large range of variabilities will all play a role in the evaluation of spatial variability of soil properties as well in the evaluation of the effects of soil variability (Huber, 2013). Fenton (1999) is one of many authors to assert that for both natural and man-made soils, the spatial variation of soil properties is more related to the formational processes of the soil, rather than the physical and chemical composition of the soil. The inherent variability in soil properties is known to influence the geotechnical response of soil in unexpected ways, bringing unavoidable uncertainty in design (Lacasse and Nadim, 1996). A relatively simple and popular approach to modelling inherent spatial variability is by using a stationary random field. The spatially variable

soil property (e.g., undrained shear strength) is characterized by a mean value  $\mu$ , standard deviation  $\sigma$ , scale of fluctuation  $\lambda$ , and autocorrelation function (Li *et al.*, 2019b). Vanmarcke (1983) used a scale of fluctuation (SOF) to describe the extent of how soil properties are spatially correlated. “The SOF is one of the important parameters describing a stationary random field. It indicates a measure of distance within which soil properties at different locations are highly correlated.” (Li *et al.*, 2019b). Generally, the mean and variance can be determined efficiently, whereas significantly more effort is required to estimate the SOF of the random field (Nie *et al.*, 2015).

The complex nature of soils as a result of soil variability leads to a suspicious and wary approach. However, soil variability can be viewed in a positive light when we consider its contribution to geotechnical design. A suitable modelling platform that requires limited computations or conceptual effort from the engineer, may lead to a more rational and economic design. (Uzielli *et al.*, 2006). In reality, soil data variability should be site-specific. However, site-specific data is either limited or not accessible. Consequently, the variability of soil properties and associated uncertainty should be considered of the utmost importance when analysing slope stability.

## **2.4 Methods of Slope Stability Analysis**

There are three well-known methods for analysing the stability of a slope i.e., limit equilibrium method, finite element method, and probabilistic method. Geotechnical engineers most commonly use the conventional limit equilibrium method (LEM) (Cheng and Lau, 2008; Abramson *et al.*, 2002). The finite element method (FEM) is more advanced, enabling engineering practitioners to perform accurate 2D or 3D slope evaluation, while also accounting for soil variability (Cheng and Lau, 2008). The probabilistic method is known to quantify some uncertain factors and is most commonly used to design the reliability index of slopes (Peterson, 1999).

### **2.4.1 Limit Equilibrium Methods (LEM)**

The conventional limit equilibrium method assumes the FOS of a slope as a single parameter that remains constant along the entire failure surface. The FOS is a value used to quantify the stability of a slope and can be determined through either force or moment equilibrium, as shown in Figure 2.10 (Abramson *et al.*, 2002). Moment equilibrium is generally used to analyse rotational

landslides, whereas force equilibrium is used for translational or rotational failures (Cheng and Lau, 2008).

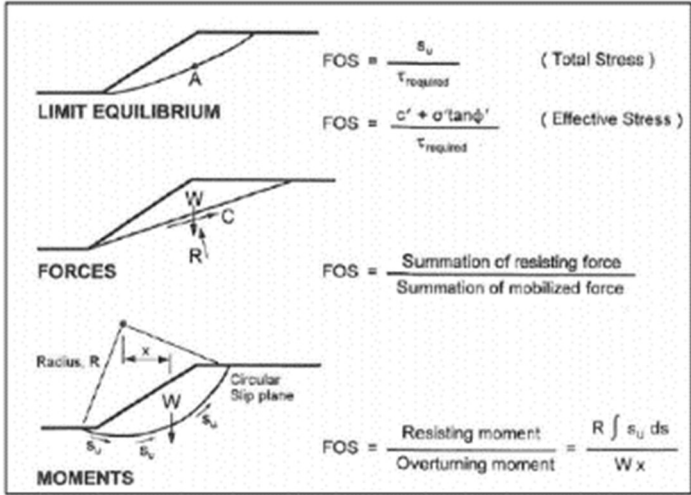


**Figure 2. 10:** Illustration of LEM and theory of FOS (Abramson et al., 2002)

A FOS of 1 (= 1) indicates that a structure or soil mass is just barely stable and cannot support any additional loading factors (Duncan, 1996). If the FOS is less than 1 (< 1), the slope condition is considered as unstable. It is important to note that many natural slopes still prove to be stable, even with a FOS less than 1.0. This inconsistency can be attributed to the inability of software to account for certain common processes that occur in soils (Cheng and Lau, 2008). These are soil parameters such as vegetation or soil suction that provide additional stabilisation and increase the factor of safety. Conventional methods all ignore vegetation as a factor in slope stability analysis because the physical effects of vegetation are too complicated to quantify. This is generally considered the more conservative approach seeing as the anchoring action of vegetation usually serves to improve the stability of a slope (Chok, 2009).

Conventional slope stability analyses such as LEM and method of slices, are **deterministic** analyses that use single best estimates of all soil parameters. In most cases, these parameters are estimated by the engineer based on knowledge and experience with very limited test data. As such, the calculated FOS depends on two factors: 1) the accuracy of the slope stability method selected for analysis, including the assumed failure mechanism and 2) the reliability of the engineers judgements and assumptions regarding the associated uncertainty of the input parameters. Currently, the best way to account for the uncertainty in soil parameters is by adopting a higher and more conservative FOS. (Chok, 2009)

The limit equilibrium method (LEM) uses force and/or moment equilibrium to solve the equilibrium problem. Firstly, the soil mass is divided into slices and the directions of the forces acting on each slice in the slope are assumed. LEM's require that a continuous surface passes through the soil mass. This is the surface upon which the FOS of the slope is calculated (RocScience Inc, 2001-2004). Many LEM's have been developed for slope stability analyses such as the ordinary method of slices (Fellenius 1936), Bishop's modified method (Bishop 1955), force equilibrium methods (Lowe and Karafiath, 1960), Janbu's generalised procedure of slices (Janbu 1968), Morgenstern and Price's method (M-P) (Morgenstern and Price 1965) and Spencer's method (Spencer 1967). When using RocScience software (2001-2004), the Bishop method is generally selected for circular failure surfaces, and the minimum FOS can be filtered out using the "auto refine" search tool. For non-circular failure surfaces, the M-P and Spencer methods are generally selected (Li *et al.*, 2019a). Slope stability charts can be created based on the limit equilibrium methods used, and this can assist with preliminary quick-estimation and analysis (Chok, 2009).

Slope stability analysis with a LEM can be performed using either **total or effective stress**. Total stress analysis applies to embankments and complicated loading problems with emphasis on the short term safety condition. A total stress analysis does not consider pore pressures and therefore only describes the 'undrained' shear strength of the soil. This scenario is also referred to as a ' $\varphi_u=0$  analysis'. An effective stress analysis is more suitable for cases where the long term condition is important. In this case the shear strength of the soil is described by the *Mohr-Coulomb failure criterion*, which is provided in Equation 1 below for fully saturated soils (Duncan, 1996).

$$s = c' + (\sigma_n - \mu) \tan \varphi' \quad (1)$$

Where,  $c'$  is the effective cohesion of the soil;  $\sigma_n$  is the normal stress;  $u$  is the pore water pressure and  $\varphi'$  is the effective friction angle of the soil. (Chok, 2009)

Equation 2 provides the extended form of the *Mohr-Coulomb failure criterion*, which applies to partially saturated or unsaturated soils (Fredlund *et al.*, 1978):

$$s = c' + (\sigma_n - \mu_a) \tan \varphi' + (\mu_a - \mu) \tan \varphi^b \quad (2)$$

Where,  $\mu_a$  is the pore-air pressure;  $\varphi^b$  is the friction angle of the soil as affected by matric suction ( $\mu_a - \mu$ ), when  $(\sigma_n - \mu_a)$  remains constant. The term  $(\mu_a - \mu)$  is known as the *matric suction* and is considered to provide an increase in the apparent soil cohesion. (Fredlund and Rahardjo, 1993)

Prior to starting a LEM analysis, the slip surface is required to be assumed. This can be planar, circular or non-circular in shape. When failure occurs, the obtained FOS is assumed to be constant along the entire slip surface. The analysis is run thousands of times, until the slip surface with the lowest FOS is found and this is then assumed to be the critical slip surface. (Chok, 2009)

#### **2.4.2 Limitations of conventional slope stability methods**

The slope failure incidence has puzzled geotechnical engineers and researchers, due to the challenges of quantifying theoretical failures. This is a limitation that needs to be resolved through the development of the correct mechanics of failure. A study was conducted evaluating the stability of 118 slopes along the Karak Highway in Malaysia. The results showed that 90% of the slopes had factors of Safety less than one, even though the slopes were stable and are still standing (Othman, 1989). This is an obvious indication of something lacking with current conventional slope stability methods. Similarly, in the case of already failed slopes, engineers cannot achieve FOS' less than one directly, but only via back-analysis in an attempt to recreate the failure surface. Brand *et al* (1984) investigated multiple slopes in Hong Kong in a highland area where the groundwater table (GWT) was too far down to have any influence on the failures at the top. This implies that rainfall-induced shallow failures are not associated with a rising GWT and instead are more related to infiltrating rainwater. Even so, it has become a common practice among engineers to model rainfall-induced slope failure by elevating the groundwater table (GWT). A rise in the GWT results in a buoyancy effect that reduces the effective stress between soil particles, thereby reducing the shear resistance or the shear strength of the soil. Failure is triggered when the soil weight or any external loading factors overcome the soil shear resistance, which has been reduced by groundwater (Noor *et al*, 2009). In summary, conventional methods are unable to account for the physical effects of certain complicated soil processes, and other inherent soil properties as factors in a slope stability analysis. As such, conventional methods of slope stability analysis may present poor and inaccurate estimates of the safety or stability condition of a slope (Chok, 2009).

### 2.4.3 Numerical Simulation Method

The application of numerical modelling in slope stability analysis is increasing rapidly due to the multiple advantages it has over the limit equilibrium method. Conventional numerical modelling is based on different methods, such as the finite element method (FEM), boundary element method (BEM), and finite difference method (FDM), all of which has become acceptable for slope stability analysis, especially in cases where the failure mechanism is not completely controlled by discrete geological structures. In those cases where the slope failure mechanism is controlled by discrete geological structures, other numerical simulation methods such as the particle flow code, discontinuous deformation analysis, and universal distinct element code are usually applied. Many researchers achieved suitable results and proved the usefulness of numerical simulation in slope stability analysis (Choi and Chung, 2004; Zheng *et al.*, 2005; Singh *et al.*, 2008; Kainthola1 *et al.*, 2013; Sarkar *et al.*, 2012; Wang *et al.*, 2003; Pradhan *et al.*, 2011). Gasmol *et al.* (2000) conducted a study on an unsaturated residual soil slope, applying the numerical model to investigate the effects of water infiltration on the slope stability. Firstly, the soil-water characteristic curve (SWCC) and the permeability density function (PDF) was used to simulate the flow of water through the slope, followed by a LEM slope stability analysis to determine the FOS. A 3D numerical analysis was conducted by Ng, *et al.* (2001) on a similar cut slope in Hong Kong, with the aim of investigating the slope response to groundwater changes brought about by varying rainfall pattern, frequency, duration and pore water pressures. The study concluded that the pore water pressure in near-surface soil layers is greatly influenced by rainfall pattern. Rahardjo, *et al.* (2001) investigated a residual soil slope in Singapore, to assess the effects of antecedent rainfall. Cho and Lee (2001) conducted a 2D flow-deformation analysis on an unstable unsaturated slope in Korea, that was being triggered by rainwater infiltration. In the case of a layered fill slope that displayed excessive seepage induced instability, Lee, *et al.* (2008) combined numerical analysis software with centrifuge model tests. Gofar *et al.* (2006) investigated a rainfall-induced landslide centred around the hypothesis that tension cracks allow for greater rainwater infiltration into a slope or soil mass. The transient seepage models were simulated in three different conditions: one with no tension cracks, one with some tension cracks near the surface of the slope, and one with tension cracks extending deep into the slope mass. The results indicated that it was the action of suction which triggered the initiation of tension cracks, especially in slopes with expansive soils. It was further suggested that this increase in moisture absorption was the main factor contributing

to slope failure as absorbed moisture causes reduction of shear strength, namely soil cohesion, and matric suction in the soil slope (Gofar *et al.*, 2006; Indraratna *et al.*, 2015).

#### **2.4.4 Probabilistic Slope Stability Analysis: Reliability analysis and Probability of Failure**

In a probabilistic slope stability analysis, the ‘probability of failure’ (POF), also known as the reliability index, is calculated instead of a FOS. In this way, the POF can be defined as the probability of having a FOS less than 1 (Obregon and Mitri, 2019). The POF is presented as a percentage. The lower the percentage, the less likelihood of failure. Vice versa, the higher the percentage the more likely it is for failure to occur. A probabilistic slope stability analysis is generally considered to be a more rational approach when accounting for soil variability and the associated uncertainty of soil properties in geotechnical analyses (Mostyn and Li, 1993). As mentioned previously, conventional methods of slope stability analysis display an inability to fully model spatial uncertainties found within site parameters, such as terrain or topography, geological stratigraphy, geologic origins, variations in soil properties of subsurface materials and varying groundwater levels to name a few. In contrast, the probabilistic method treats the input parameters as random variables and in doing so, ignores the uncertainties posed by the deterministic model altogether (Abramson *et al.*, 2002; Chowdhury and Xu, 1994). In order to treat parameters as random variables, a Probabilistic Density Function (PDF) is created, from which a reliability index ( $\beta$ ) can be estimated and characterized by its mean value ( $\mu F$ ), and standard deviation ( $\sigma F$ ). The reliability index ( $\beta$ ) can then be used to determine the POF (Malkawi *et al.*, 2000). The POF is the most important aspect of design performance. “Failure” becomes a generic term for non-performance and is related to the level of risk involved (US Army Corps of Engineers, 1997; Uzielli *et al.*, 2006).

Although there has been much research contribution regarding this field in recent years, probabilistic analyses still remain a minority discipline, in part due to the perceived computational and material data requirements, and also due to a reluctance by engineering practitioners to move away from conventional methods. In recent years, engineers are more increasingly faced with complicated ground conditions, such as in areas of land contamination. These new challenges raise the possibility of a greater role for stochastic methods in the future (Hicks, 2005). It has been observed that when a probabilistic analysis is conducted without considering the spatial correlation

of soil properties, the POF result is inaccurate and over-estimated. (Vanmarcke, 1977; Li and Lumb, 1987; Mostyn and Soo, 1992; El-Ramly *et al.*, 2002).

Some probabilistic techniques developed are: 1) First Order Second Moment (FOSM) method; 2) Point Estimate Method (PEM) method; 3) Monte Carlo Simulation (MCS); 4) Finite Element Method (FEM) and 5) Random Finite Element Method (RFEM), all of which are briefly expanded on in the sections below (Chok, 2009).

#### **2.4.4.1 First Order Second Moment Method**

The first order second moment (FOSM) is a relatively simple method that accounts for spatial variability of the random variables through the use of a *performance function*, which is the FOS equation of the LEM selected for slope stability analysis, such as the Bishop's simplified method of slices, M-P method or Spencer's method (Chok, 2009). The major difference with the FOSM method is that it does not define a probability density function (PDF) for the random variables and instead the shape and form of the PDF needs to be assumed before the probability of failure can be estimated. (El-Ramly *et al.* 2002).

#### **2.4.4.2 Point Estimate Method**

The Point Estimate Method (PEM) is considered an alternative approach to the FOSM method. It was developed by Rosenbluth in 1975 and is considered a direct method that yields fairly accurate results. In the PEM, PDF's are replaced with sets of discrete point masses, that are multiplied by weighted factors to evaluate the first two moments of the *performance function*. When there are more than two random variables, the computation becomes overly tedious, and the entire PEM analysis loses its advantage (Chok, 2009).

#### **2.4.4.3 Monte Carlo Simulation**

The Monte Carlo simulation (MCS) has recently gained much popularity for its simplicity and availability (Abramson *et al.*, 2002). This method generates sets of random variables based on each assumed PDF, after which, the simulation is run continuously until the *performance function* is

evaluated for each set. The biggest disadvantage of the MCS is the extensive computational efforts required (Chok, 2009). The computer software program SLOPE/W has developed a user friendly interface, using the Monte-Carlo simulation for slope stability analysis (Krahn, 2004). Figure 2.11 provides a breakdown of the Monte Carlo simulation method.

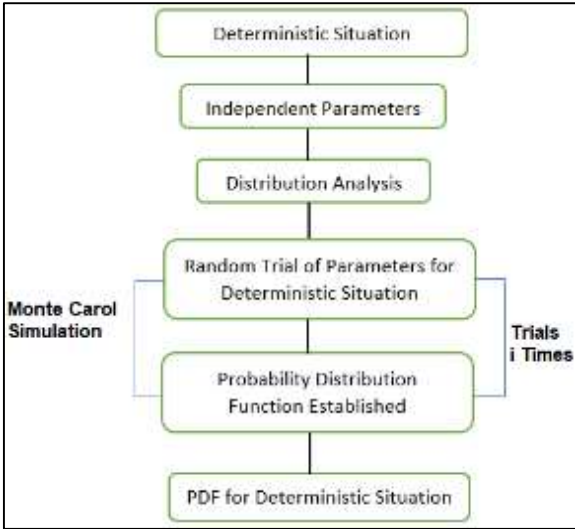


**Figure 2. 11:** General Monte Carol simulation approach (Krahn, 2004)

**2.4.4.4 Finite Element Method**

The introduction of the Finite Element Method (FEM) for use in geotechnical engineering was published by Clough and Woodward (1967). The FEM analysis uses an elastic-perfectly plastic stress-strain law with a Mohr-Coulomb failure criterion. It involves the application of gravity loading, by considering the forces generated by the self-weight of the soil and monitoring the stresses at all Gauss points (which are all initially assumed to be elastic), as shown in Figure 2.12 below. Each stress point is compared with the Mohr-Coulomb failure criterion, and if the stress at any Gauss point lies within the Mohr-Coulomb failure envelope ( $F < 0$ ), then the area around that point is assumed to be elastic. If a point lies out of the Mohr-Coulomb failure criterion ( $F \geq 0$ ), then that area is said to be “yielding”. The process is repeated until each point within the mesh has been compared and classified (Chok, 2009).

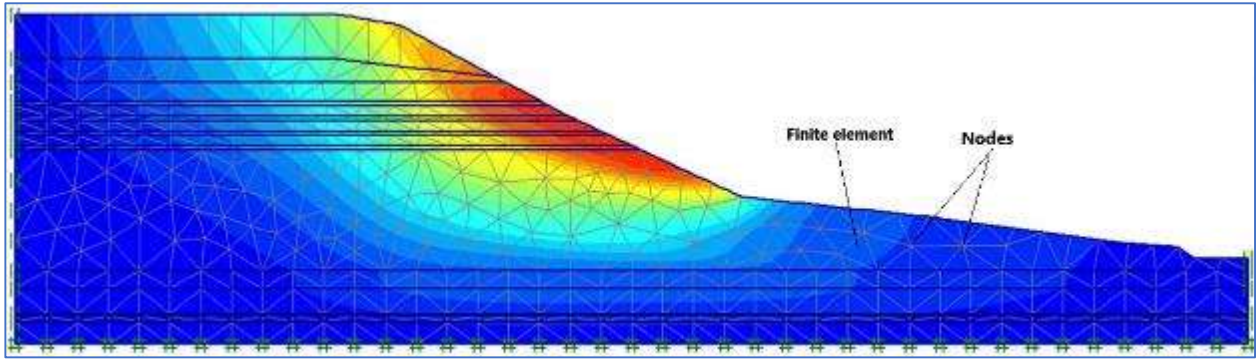


**Figure 2. 12:** Showing the application of FEM of slope stability analysis (adapted from Baba *et al.*, 2012).

Much research has proven that the results of FEM analyses generally agree with the results from conventional LEM analyses (Griffith and Mitchell, 1980). In fact, RocScience Inc. (2001) has suggested that the FEM proves useful in comparing the results of various LEMs. The FEM is considered to be more advantageous than the LEM, because the FEM provides the same accuracy of results without having to assume the shape or location of the critical failure surface, slice side forces, or their direction (Abramson *et al.* 2002). Even complicated slope configurations, multi-layered soil deposits, associated stresses, strains and shear strengths can all be applied using the FEM, in both 2D and 3D (Zaki, 1999; RocScience Inc.,2001). Griffith and Lane (2000) used FEM to monitor overall progressive shear failures, and also to assess the stability of slopes under various drawdown conditions.

There are two generalised approaches to analysing slope stability using FEM. The first approach is to increase the gravity or loading on the surface of the soil mass, and the second approach is to reduce the strength characteristics of the soil mass, also known as the FEM – Strength Reduction Technique (SRT) (RocScience Inc. 2001-2004). The SRT method is the more advanced approach, involving the gradual reduction of the initial strength parameters until the point of failure is reached. As per the Mohr-Coulomb criterion, the FOS is then defined as the factor by which the original strength parameters were reduced, or the strength reduction factor (SRF). The strength parameters at failure, cohesion ( $C_f$ ) and friction ( $\phi_f$ ) can be calculated using equations 3 and 4 below (Matsui and San, 1992).

$$C_f = \frac{C}{SRF} \quad (3)$$

$$\phi_f = \tan^{-1} \left( \frac{\tan \phi}{SRF} \right) \quad (4)$$

The strength reduction technique can determine both the failure zone and the safety factor; however the POF result from the FEM analysis cannot easily be linked to the traditional FOS of the slope (Yang *et al.*, 2016).

A common use of the FEM is to determine the stress field of a slope (Wei *et al.*, 2009). The figures below provide a breakdown of the vertical stress distribution of a 3D soil slope using FEM. As can be seen, the potential slip surface located behind the stress field of the slope, is identified as the critical slip surface of the slope (Yang *et al.*, 2016).

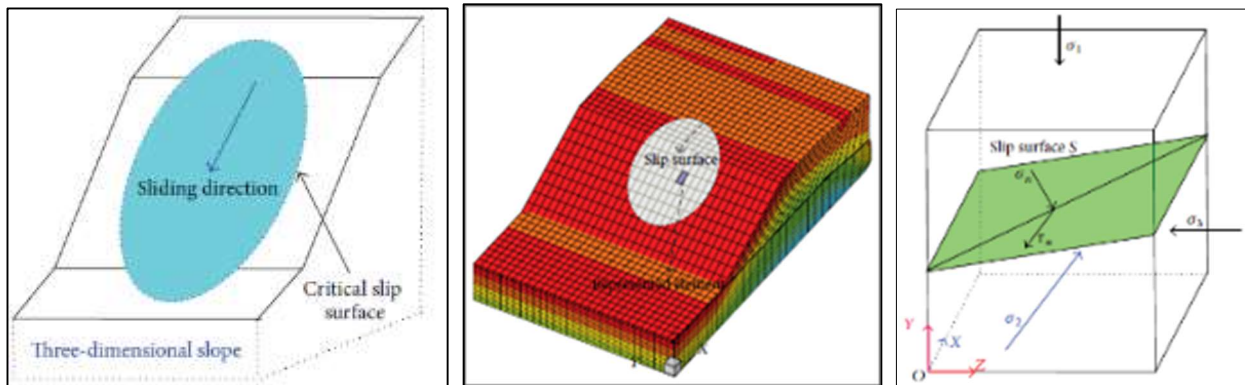


**Figure 2. 13a, b and c:** Stress distribution of 3D soil slope in a FEM stability analysis (Yang *et al.*, 2016)

Yang *et al.* (2016) displayed the above in practice. He used the FEM to calculate the stress fields of a 3D rotational slope failure. The elastic-perfectly plastic soil model, together with the Mohr-Coulomb Criteria and a LEM were all used to determine the safety factors of certain slip surfaces. The critical slip surface was identified thereafter. The two most important results from the FEM analysis were 1) the identification and location of the critical slip surface and 2) the corresponding FOS of this critical slip surface.

#### **2.4.4.4.1 Limitations of FEM**

Although the finite element method is considered a useful and reliable technique for slope stability analysis, deformation analyses and other geotechnical problems, it is still not used as much as conventional limit equilibrium methods. (Duncan 1996; Griffiths and Lane, 1999). Conventional LEM's are simpler to apply, theoretically with quick and relatively accurate FOS estimations, and in practicality as the software is more easily accessible than FEM software. FEM analyses involve more complicated calculations and theory, and also require more input parameters which take time to collect and process (Chok, 2009).

A study by Wong (1984) proved that the biggest disadvantage of FEM for slope stability analyses, is due to the uncertainties of failure criteria. In a finite element analysis, the failure condition occurs progressively because discrete elements of the FEM model do not all fail at the same time. In this way, there is a wide range of failures spanning from the first occurrence of the yield point to the final failure of all elements (Wong, 1984). Popular failure criteria include “bulging of the slope line (Snitbhan and Chen, 1978), shear limit (Duncan and Dunlop, 1969), and non-convergence of the solution (Zienkiewicz, 1971)” (Wong, 1984). Abramson *et al.* (2002) also provided detail on these failure criteria, concluding that proper interpretation of FEM results largely depends on the engineering practitioners experience in modelling the slope and soil response to changes in moisture conditions. In the case of undrained clay slopes, FEM has proved to be unreliable in locating the critical slip surface and also did not adequately model the effects of tension cracks when they arose (Hammouri *et al.*,2008).

#### **2.4.4.5 Random Finite Element Method (RFEM)**

Griffiths and Fenton (2004) proposed the Random Finite Element Method (RFEM) to overcome the limitations posed by conventional LEM's, namely the inability to account for spatial and soil variability. The RFEM is a probabilistic slope stability analysis that combines both the MCS method, with the FEM (Griffiths and Fenton, 2004). The RFEM has proved to be a powerful tool that considers both soil variability as well as the spatial variability and random behaviour of soil properties. During the FEM analysis, the entire slope is divided into multiple discrete elements. Thereafter, the MCS assigns a different random variable to each discrete element and soil property within (Chok, 2009). The greatest advantage of the RFEM over basic probability analysis, is that

RFEM allows slope failure to occur naturally by “seeking out” the most critical mechanism (Griffiths and Fenton, 2004). El-Ramly *et al.* (2002), reviewed literature on RFEM and noted that the geotechnical profession was generally unwilling to adopt more advanced probabilistic approaches, such as RFEM to geotechnical design, especially in the more traditional geotechnical projects such as slope stability and foundation design.

#### **2.4.4.5.1 Limitations of RFEM**

Although RFEM is an excellent advanced method for considering soil and spatial variability in probabilistic slope stability analysis, it is not being fully utilised in geotechnical practice. Practitioners are deterred by the theory which they do not fully understand, as well as by the tedious prospect of performing both a FEM as well as MCS. Another disadvantage of the method is that currently RFEM software is only limited to analysing single layer soil profiles, and not multi-layered ones (Chok, 2009).

### **2.5 Comparison of stability analysis methods**

Geotechnical design has been mostly based on the deterministic approach, where a single analysis using a single representative value of each soil property is conducted to provide a global FOS (Hicks and Spencer, 2010). As mentioned before, although the LEM is the most popular method in slope stability analysis because of the great understanding that comes from decades of use and the relative ease of application, the inherent limitation of the method is that it cannot account for variability in soil properties from one place to another, nor can it consider stress or strain factors in slopes, resulting in inaccurate and unreliable factors of safety (Tschuchnigg *et al.*, 2015). Unlike this, a probabilistic analysis statistically considers soil and spatial variability, leading to the more reliable result of measuring a slopes stability, the POF (Chok, 2009). The LEM methods which are used so predominantly in current slope stability analyses, have not changed since conception, and it is important to realise that they were never designed to be used in geotechnical problems involving highly variable soils and shear strengths (Griffiths and Fenton, 2004).

### 2.5.1 Finite Element Method vs Limit Equilibrium Method

The most obvious downfalls of traditional LEM slope stability analysis is relating to the shape and location of the critical failure surface. Firstly, the shape of the failure surface (either circular or non-circular) is fixed by the selected LEM method and does not “seek out” the critical failure surface (Griffiths and Fenton, 2004). Probabilistic slope stability analyses provides the POF based on the critical slip surface that was obtained from an initial deterministic analysis. The problem arises that the critical slip surface obtained from the deterministic/LEM analysis may not be the same critical slip surface that the probabilistic analysis would have found when accounting for the heterogeneity of a spatially random soil. LEM’s always represents the critical slip surface as circular or wedge, however this is never the case. The critical slip surface can be almost any shape or at any location within the slope mass, as slope failure tends to occur at various points within the soil mass that have low shear strengths (Chok, 2009). This is the major advantage of a FEM or probabilistic approach in slope stability analysis over traditional LEM’s, that no assumption needs to be made in advance about the shape or location of the failure surface, slice side forces and their directions. Using a general soil material model such as the Mohr-Coulomb Criterion, the equilibrium stresses, strains, and associated shear strengths in the soil mass can be computed fairly accurately, for all types of failure mechanisms. (RocScience Inc. 2001-2004) (Griffiths and Lane, 1999).

The main advantages of FEM over conventional LEM in slope stability analyses is summarised as follows (Griffiths and Lane, 1999; Chok, 2009):

1. The shape and location of the critical failure surface is not assumed, instead failure is considered to occur ‘naturally’ through weak zones with low shear strengths.
2. The FEM maintains global equilibrium until actual failure occurs. In this way there are no assumptions made about internal stresses or strains as the LEM makes.
3. The FEM can be used to perform deformation analyses when accurate soil consistency and stiffness parameters are input.
4. The FEM can assess both progressive failures as well as overall shear failure.

Uzielli *et al* (2006) compared a wide variety of studies that used the probabilistic method of analysis and made several important general observations based on the results. Firstly, it was noted that when soils are modelled as spatially variable, the modelled failure mechanisms are very

different and significantly more complex than in the case of deterministic or homogenous soil properties. One example posed is that a footing founded in spatially varying soil will technically fail on one side only, in contrast to the typical symmetrical “punching” failure (Uzielli *et al*, 2006).

A routine slope stability analysis involves a combination of the SRT, with a FEM or FDM together with a LEM such as Bishops Simplified, M-P method or Spencer method. Li *et al* (2019a) undertook a comparative investigation to compare the performance of LEM based SRT with the performance of FEM and FDM based SRT. The conclusion reached was that the Bishop method (LEM) performed as satisfactorily as the numerical based SRT (FEM and FDM), in cases where there were no distinct surfaces such as soft bands or tension cracks to skew the determination of the failure mechanism (Li *et al*, 2019a). As we are working with natural soil slopes which are inherently heterogeneous, the presence of variable surfaces and soils is inevitable. As such, even though the LEM provides satisfactory FOS’s and comparable FM’s, it would be considered better practice to use more advanced numerical methods such as FEM or FDM based SRT for slope stability analysis (Li *et al*, 2019a).

### **2.5.2 Finite Element Method vs Random Finite Element Method**

Li *et al* (2015a) compared the analyses of two hypothetical 3D slope stability problems, both considering the spatial variability of undrained shear strength parameters. The first slope was analysed by Vanmarcke's (1977) simplified FEM and the other was analysed using the advanced RFEM. The following notable observations were made:

- Both methods yielded POF’s and not FOS’s
- The two methods provided significantly different results, based on the scale of fluctuation (SOF) of the undrained shear strength parameters relative to the slope geometry.
- In the simpler (Vanmarcke) model, a pre-defined cylindrical surface was assumed based on simple spatial averages, whereas the RFEM analysis, using the premise of a heterogeneous soil, sought out the weakest or ‘critical’ path.
- The results demonstrated that the RFEM response of the slope was weaker – and therefore more conservative - than the Vanmarcke solution (i.e. the RFEM yielded a lower FOS than that of the simpler model). It was observed that the difference was greatest for small SOF’s (Li *et al*, 2015b). Similarly, Griffiths and Fenton (2004) observed that simplified

probabilistic analyses (such as Vanmarcke's model) which does not account for spatial variability, could lead to unconservative estimates of slope safety. This was observed to occur at lower FOS with high COV.

The study by Griffiths and Fenton (2004) illustrated important relationships between the random field parameters (namely SOF and COV) used in slope stability analysis, within the results of their RFEM. They compared the results yielded from the RFEM and the simpler probabilistic method (both of which accounted for spatial averaging) in terms of the POF, for various COV of normalised undrained strength, as represented in Figures 2.14 and 2.15 below. An obvious crossover point was observed, indicating a change in the relationship between the coefficient of variation, probability of failure and factor of safety (Griffiths and Fenton, 2004; Uzielli *et al*, 2006).

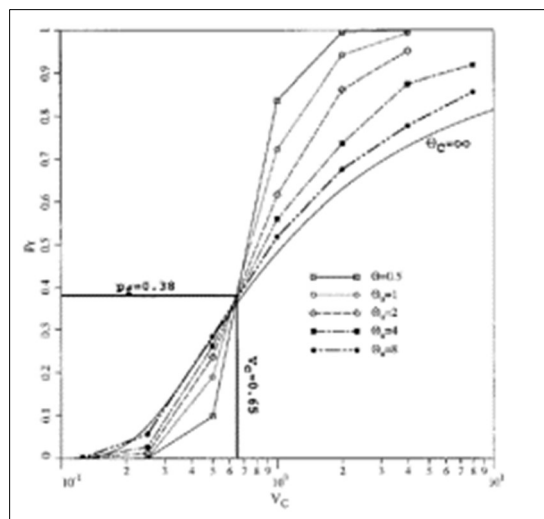


**Figure 2. 14:** Probability of failure versus coefficient of variation for various normalised scales of fluctuation (Griffiths and Fenton, 2004)

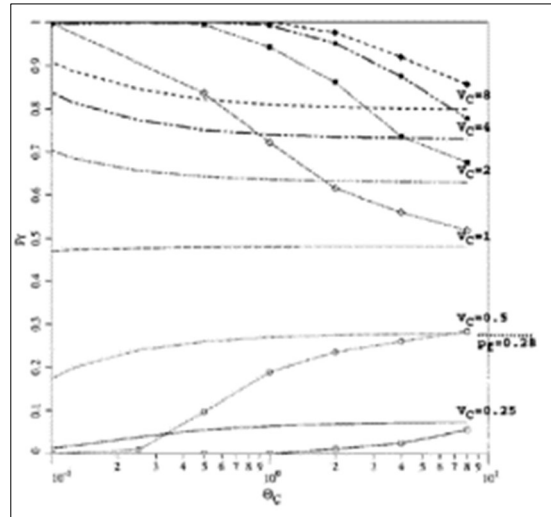


**Figure 2. 15:** Comparison of the probability of failure for various coefficients of variation of normalised undrained strength predicted by RFEM (curves with points) and by probabilistic analyses accounting for spatial averaging (Griffiths and Fenton, 2004)

## 2.6 Summary

The research conducted thus far has shown how influencing the soil properties and associated soil variability contributes to the occurrence of slope instability and failure. In particular, increases in water content (such as rainwater infiltration) are the most common trigger for slope failure and mass-wasting. Initially, under partial saturation of a slope, a strength increase may occur due to positive effects provided by matric suction within soil pores. Thereafter, upon continuous infiltration or slope saturation, the positive effects of matric suction are lost, and the adverse effects of pore water pressure come into play. This is mostly in the form of a decrease in the shear strength parameters, cohesion and internal friction.

The literature review conducted suggests that numerical simulation is the best method to account for the effects of soil variability on slope failure. However, manually providing the statistical values for the coefficient of variability (COV) is not feasible in this study since they are derived from total variability analyses assuming a uniform source of uncertainty. Given the inherent variability of soils, the entropic nature of soil formation and the available level of knowledge and technology needed to analyse it, it is most likely impossible to model the variability of a soil in a completely satisfactory way. As pore-water pressures are known to reduce the shear strength of soils by causing a decrease in their inter-particle stresses resulting in potential failure, it is increasingly imperative to apply numerical simulations with their corresponding factor of safety.

In this regard, the combined effects of numerical simulation and the limit equilibrium method is considered best for effective and accurate slope stability analysis.

Recent design codes such as the Eurocode 7, require that values of soil and rock properties take into account variability of each value. This calls for an increase in understanding of the processes involved in geotechnical problems, and for associated risks to be quantified explicitly. Given the difficult nature of numerical simulations, the better solution would be to investigate problems probabilistically/stochastically, knowing that these methods lead to more realistic definitions of slope and soil response.

## **CHAPTER THREE**

### **METHODOLOGY**

---

#### **3.1 Introduction**

The literature review of this dissertation (Chapter 2) discovered significant gaps in the research available pertaining to soil variability and matric suction, in the context of rainfall induced slope failures. In attempt to address the research gap, as well as to realise the objectives of this study, the following steps were taken to investigate, analyse and model the effects of soil variability on the stability of natural slopes within the study area, under varying water conditions.

##### **3.1.1 Fieldwork**

Two critical slopes were identified in the Durban area of KZN. Site investigations of the two selected sites were conducted, as well as a desktop study of all completed reports and relevant literature pertaining to the sites. All necessary information for the purpose of laboratory testing, slope stability analysis and modelling were obtained such as slope elevations, angles and the strategic collection of samples. The detailed observations and site investigations are presented in Sections 3.2 and 3.3 below.

The fieldwork and subsequent laboratory testing that was required for this study was delayed due to the COVID-19 pandemic and lockdown measures that came into effect in March 2019. By the time the lockdown eased and movement was allowed, an entire semester had passed. The research timeline was heavily constrained and pushed into a 6 month window. Despite the rush under very stressful circumstances, all effort was made to ensure that the geotechnical investigations and each individual laboratory test was performed according to specification/standard. The premise here was to avoid making unnecessary mistakes that would result in a double job at a later stage, which would only further pressurise the timeline.

### 3.1.2 Laboratory Testing

The suite of laboratory tests that were conducted on collected soil samples, as well as detailed descriptions and methods used to conduct each test is provided in Section 3.4 below.

### 3.1.3 Slope Stability Analysis / Numerical Modelling

The two natural slopes were modelled using the **RocScience**© software Slide to assess slope stability and analyse the effects of soil variability and moisture-induced slope failure. These results are presented in Chapter 5 and are used to provide recommendations regarding the slope stability, measures to mitigate future failure and other observations and conclusions in Chapters 6 and 7.

## 3.2 Fieldwork: Observations and Information obtained

The two sites across Durban, were visited multiple times to collect all information necessary for the purpose of this research project. The soils underlying the site were accessed and profiled via hand dug test pits (TP's) till refusal or pit collapse. Table 3.1 below summarises the sites used in this study, providing co-ordinate locations and general soil type of each site. The subsections that follow provide thorough descriptions of each site as well as underlying geology, laboratory test results and all other collected parameters necessary for modelling and slope stability analysis.

Site Designation	Address	Coordinates	General soil type
Site A	117 Plumstead Crescent	29° 48' 39.04" S 30° 57' 33.76" E	Silty sand
Site B	Beachwood Golf Club	29° 46' 56.05" S 31° 02' 59.65" E	Clayey and silty sands

### 3.2.1 Site A Description

Site A is located at 117 Plumstead Crescent in the Reservoir Hills Suburb of Durban, KwaZulu-Natal (as shown in the site map in Figure 3.2). This site is an empty plot of land situated on the bank of a perennial stream which is a branch of the Umgeni river to the North. The site is densely vegetated comprising bushes, branches, trees, and thicket with a very sharp drop at the end of the

plot towards the stream. There is also some refuse and rubble scattered throughout as can be seen in figures 3.1a, b and c below, which provide some perspective of Site A. The site generally slopes in a northerly direction, initially at a gentle angle of 12 degrees ( $^{\circ}$ ), then at a steeper angle of 24 $^{\circ}$  before dropping off steeply towards the stream at an angle greater than 50 $^{\circ}$ . The slope face under analysis is considered from the initial drop till the stream (shown in Figure 3.3). The geometry of certain key points of the slope was recorded and is tabulated below (Table 3.2).



**Figure 3. 1a, b and c:** Northerly views of Site A showing stream in the distance, vegetation on site and first initial drop.



**Figure 3. 2:** Site map showing location of Site A in relation to road and stream (Adapted from Google Earth)

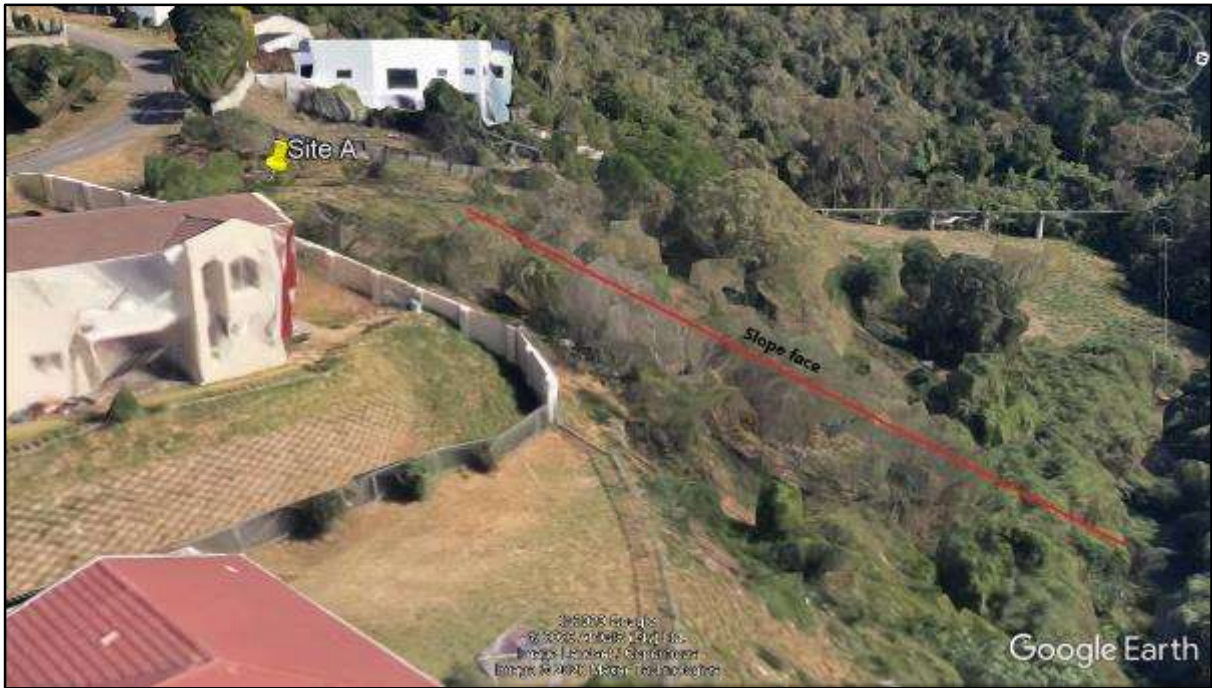


**Figure 3. 3:** Westerly view of Site A showing slope face (adapted from Google Earth)

<b>Table 3. 2:</b> Parameters recorded from site A, for use in stability analysis			
<b>Area of slope</b>	<b>Elevation (m)</b>	<b>Length of slope face (m)</b>	<b>Average angle of slope (degrees<sup>0</sup>)</b>
Crest of slope (at initial drop)	43	~45	~58
Toe of slope (at stream)	19		

### 3.2.2 Site B Description

Site B is located at the Beachwood Durban Country Club in Durban North, KwaZulu-Natal (as shown in the site map in Figure 3.5). The embankment to the east of Fairway Drive is beach-facing on the perimeter of the golf course. The portion of the embankment located at the site coordinates (recorded in Table 3.1), has experienced failure and the overlying house has been undercut as a result. The figures below provide an idea of the site. A vertical water pipe is evident leading from the house on the crest of the slope down into the embankment, which is the apparent cause of slope failure. Slight cracking is also observed on the walls and underside of the overburden property. The embankment is densely vegetated with evidence of waterlogging throughout, extending into the golf course itself. The failed slope (figure 3.4b) is currently lying at a very steep angle of 60 degrees, followed by a 40° embankment leading off onto the gentle golf course at 18°. The slope face is

shown in Figure 3.4a and Figure 3.6 below. The geometry of certain key points of the slope was recorded and is tabulated below (Table 3.3).



**Figure 3. 4a and b:** showing Site B and close up of failure on top of slope



**Figure 3. 5:** Site map showing location of Site B in relation to roads (adapted from Google Earth)



**Figure 3. 6:** Close-up view of Site B, showing slope face. (Adapted from Google Earth)

**Table 3. 3:** Parameters recorded from site B, for use in stability analysis

Area of slope	Elevation (m)	Length of slope face(m)	Average angle of slope (degrees <sup>0</sup> )
Crest of slope	19	~15	~54
Toe of slope	11		

### 3.3 Geological Background

The regional geology of KwaZulu-Natal is made up of a basement called the Kaapvaal craton, which was formed in the Archaean period between 3650-2650 *Ma*. It consists of igneous intrusions, predominantly granitoids with subordinate gneisses. These Archaean rocks have intruded the ancient basaltic and ultramafic lavas (~3500 *Ma*) of the Greenstone Belts. Unconformably overlying the Archaean and Proterozoic basement is the Natal Group, which is made up of arkosic and quartz-arenitic sandstones, conglomerates and subordinate argillaceous rocks. Disconformably overlying the Natal Group is the sedimentary sequence of the Karoo Supergroup which is the geology that is mainly encountered during civil construction in Durban (Johnson *et al.*, 2006).

### 3.3.1 Site A Local Geology

The underlying geology of Site A, as encountered during the site investigation, is a thin layer of residual soil, underlain by the parent rock comprising highly weathered to completely weathered diamictite of the Dwyka Group, Karoo Supergroup (indicated in Figure 3.8 below). Test Pit #1 (TP1) was dug on site (as shown in figure 3.7a and b below) and the soil profile, measured as metres below existing ground level (mbegl), is provided in table 3.4 below. Those layers selected for soil testing are also indicated with the designated sample number.

<u>Depth</u> <u>(mbegl)</u>	<u>Soil Description</u>	<u>Sample No.</u>
0.0-0.1	Dry, orangey brown, slightly clayey, gravelly sandy SILT. Residual Diamictite.	1
0.1-0.26	Reddish brown, completely weathered, highly jointed, Diamictite Rock, Dwyka Group. Recovered as: Dry, reddish and orangey brown, silty sandy GRAVEL.	-
0.26-0.6	Reddish brown, generally highly weathered, occasionally completely weathered, highly jointed, Diamictite Rock, Dwyka Group. Recovered as: Dry, reddish, yellowish, and orangey brown silty sandy GRAVEL, with angular cobbles and pebbles.	2



**Figure 3. 7a and b:** showing TP1 dug on Site A and exposed bedrock within 0.1 mbe gl.

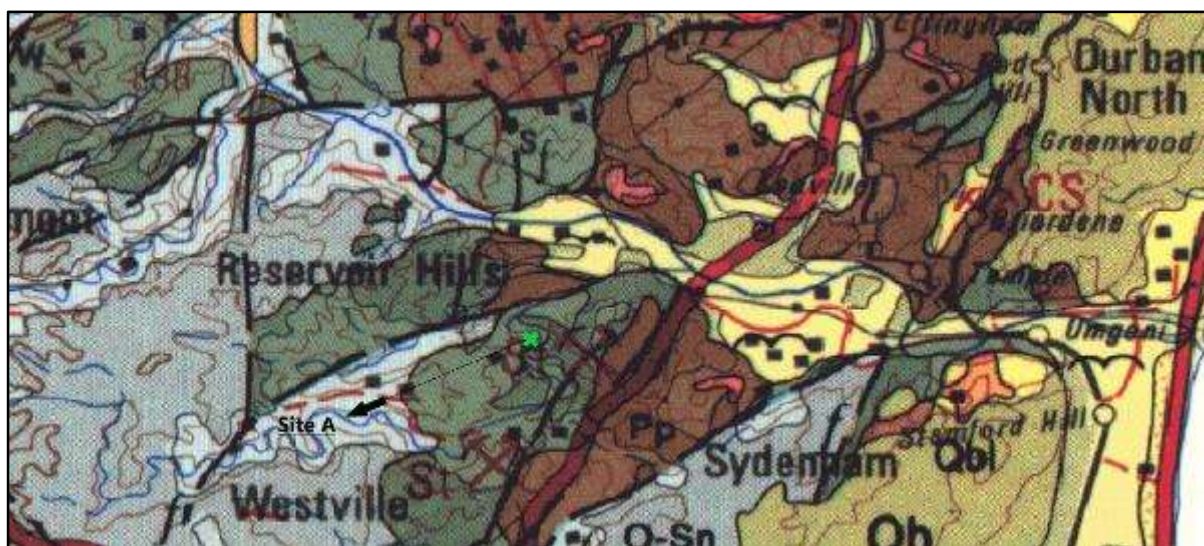


**Figure 3. 8:** Map showing local geology underlying Site A, indicated by the green X (Source: Council for Geoscience, 2008. Adapted from Durban map, area 2930)

### 3.3.2 Site B Local Geology

The underlying geology of Site B, as encountered during the site investigation, is a thick layer of Dune soils, namely Berea Sands of the Durban formation, Karoo supergroup (Figure 3.10 below), further underlain by Beach Sands. The adjacent golf course would be comprised of specialized imported fill. Test Pit #2 (TP2) was dug on site (as shown in figures 3.9a and b below) and the soil profile, measured as metres below existing ground level (mbegl), is provided in table 3.5 below. Those layers selected for soil testing are also indicated with the designated sample number.

<b>Table 3. 5: TP2 Soil Profile</b>		
<u>Depth</u> (mbegl)	<u>Soil Description</u>	<u>Sample</u> <u>No.</u>
0.0-0.32	Moist, reddish dark brown becoming blackish brown with depth, soft to slightly stiff, slightly silty, sandy CLAY. Berea Formation, Natal Group. Recovered as blocks of soil.	3
0.32-1.00	Very moist to wet, light brown to medium brown, stained red, orange and black, speckled black and white, very loose, slightly silty SAND. Beach Sands.  1. At 0.5m – layer of orange oxidation between lighter moist sand and darker wet sand.	4

	<p>2. Soil becomes wet and dark brown, stained black, medium dense with depth.</p> <p>3. Standing water noted at 0.90 m bgl.</p>	
--	----------------------------------------------------------------------------------------------------------------------------------	--



**Figure 3. 9a and b:** Showing TP2 dug on Site B, with evidence of water table at base of pit.



**Figure 3. 10:** Map showing local geology underlying Site B, indicated by the green dot (Source: Council for Geoscience, 2008. Adapted from Durban map, area 2930)

### 3.4 Laboratory test methods and standards

The list of tests conducted on the samples shown below (Figures 3.11a and b), their purpose in this study and the associated international standards are summarised in Table 3.6 below and are discussed in detail in the sections that follow.



**Figure 3. 11a and b:** Images of samples collected from the two sites.

<b>Table 3. 6:</b> List of tests and testing standards		
<b>Test type</b>	<b>Aim of test</b>	<b>International Standards</b>
Moisture Content	<ul style="list-style-type: none"> <li>• To determine natural moisture content of soils as soon as taken from site (<i>in situ</i>)</li> <li>• To determine percentage of water present in soils</li> </ul>	<ul style="list-style-type: none"> <li>- ASTM D2216</li> <li>- BS 1377: Part 2 (1990)</li> </ul>
Particle Size Analysis	<ul style="list-style-type: none"> <li>• To determine soil type in terms of predominant soil sizes.</li> <li>• To create a Particle Distribution Curve that will determine soil grading and sorting.</li> <li>• To calculate Cu and Cc.</li> </ul>	<ul style="list-style-type: none"> <li>- ASTM D6913 / D6913M-17</li> <li>- ASTM D5519</li> <li>- ASTM D7928</li> <li>- ASTM D2487</li> <li>- ASTM D422-63</li> </ul>
Specific Gravity	<ul style="list-style-type: none"> <li>• To calculate G<sub>s</sub> in order to correct for <i>k</i> in hydrometer testing.</li> </ul>	<ul style="list-style-type: none"> <li>- ASTM D854-14</li> <li>- ASTM D792, ISO 1183</li> </ul>

		<ul style="list-style-type: none"> <li>To calculate void ratio and porosity using correlations.</li> </ul>	
Atterberg Limits	Liquid Limit (LL)	<ul style="list-style-type: none"> <li>To determine consistency of soils and their behaviour under different water conditions.</li> <li>To determine Plasticity Index (PI) parameter for use in calculations.</li> </ul>	<ul style="list-style-type: none"> <li>ASTM D4318-00 (LL and PL)</li> <li>BS 1377: Part 2 : 1990 (SL)</li> </ul>
	Plastic Limit (PL)		
	Shrinkage Limit (SL)		
Free Swell test		<ul style="list-style-type: none"> <li>To determine free swell index, swell potential, and inferred degree of expansivity.</li> </ul>	IS: 2720 (1977)
Compaction testing		<ul style="list-style-type: none"> <li>To determine soil compaction characteristics – MDD and OMC</li> </ul>	ASTM D698
Soil-Suction test		<ul style="list-style-type: none"> <li>To determine the degree of pore water suction.</li> <li>To indicate the state of desiccation of clays.</li> </ul>	<ul style="list-style-type: none"> <li>BRE Information Paper IP 4/93</li> <li>ASTM 5298-03</li> </ul>
Consolidation testing / Oedometer test		<ul style="list-style-type: none"> <li>To determine collapse potential of soils in terms of heave or settlement.</li> </ul>	ASTM D4546
Direct Shearbox test		<ul style="list-style-type: none"> <li>To determine soil shear strength characteristics – Total cohesion and the total angle of internal friction.</li> </ul>	ASTM D3080
Consolidated Undrained Triaxial test		<ul style="list-style-type: none"> <li>To determine effective cohesion of soils and the effective internal angle of friction for use in shear strength calculations.</li> </ul>	BS 1377: Part 8: 1990

### 3.4.1 Moisture content

The percentage *moisture content* of the soil is determined using the oven-drying method as per ASTM D2216 (Head, 2006). A sample of soil was weighed in its original condition, and then weighed again after 24 hours of oven drying at 110 degrees Celsius ( $^{\circ}\text{c}$ ), as shown in Figure 3.12 below. Water content was calculated using equation 1 below.



**Figure 3.12:** Showing samples after oven-drying.

$$W = \frac{W_w - W_s}{W_s} \times 100\% \quad (1)$$

Where  $W$  is the water content,  $W_w$  is the weight of the water in the soil sample and  $W_s$  is the weight of the soil sample without any water (after oven drying) (Head, 2006).

### 3.4.2 Particle Size Analysis

Particle size analysis is carried out to determine particle size distribution (PSD) via separation of a soil sample into different fractions based on their particle sizes. This is needed for soil classification and profiling in order to comply with the Unified Soil Classification System (USCS) as per ASTM D2487 (ASTM, 2011). The percentage of soil sizes determines the soil type, for example a soil with majority sand, a small percentage of silt and an even smaller percentage of clay would be classified as a slightly clayey silty SAND. The results from the analysis are plotted to create a PSD curve which provides information on soil gradation and sorting (illustrated in Figure 3.4 below). The PSD curve is used to calculate the coefficient of uniformity ( $C_u$ ) and the coefficient of curvature ( $C_c$ ) parameters, which are required in construction during dynamic compaction, grouting and selection of fill materials. Soil classification and gradation is important in engineering in order to determine

properties such as permeability, shear strength, and compressibility for construction purposes. (ASTM Int., 2017)

This analysis is carried out via mechanical sieving for the coarse grained soil fraction and hydrometer tests for the fine fraction. During composite sieving (the use of multiple sieves) the percentage by mass passing each sieve size is recorded to the nearest 1 %. (Arasan *et al*, 2011)

Test method D5519 is used for gradation of a sample with particles larger than the 75 mm sieve. Test method D7928 is used for gradation of samples with particles smaller than 75  $\mu\text{m}$  ( No. 200 sieve) (ASTM Int., 2017).

The apparatus needed to perform the Particle Size Analysis and sedimentation analysis is provided below.

<b><u>List of Apparatus</u></b>
➤ Oven
➤ Scale (accuracy of 0.01g)
➤ Mechanical Sieve Shaker
➤ Sieve sizes: No.4 (4.75mm) to No.200 (75 $\mu\text{m}$ )
➤ Bouyoucos cylinder, graduated at 1130 and 1205 ml
➤ Hydrometer bulb for sedimentation analysis
➤ Distilled water
➤ Dispersing agents sodium oxalate and sodium silicate
➤ Water bath and thermostat
➤ Stopwatch

## **Method**

The samples were oven dried overnight, and then put into the mechanical sieve shaker, as shown in figure 3.13 below, until the entire sample had been separated into individual size fractions.



**Figure 3. 13:** Showing mechanical sieve shaker as sample is being separated.

The “percentage finer” than each particle size range was then calculated on the basis of total mass initially taken. From the results of the sedimentation analysis and the mechanical sieving process, the Particle Size Distribution graph (gradation curve) was plotted as percentage finer (%) versus particle size (diameter in mm). Thereafter, the Coefficient of Uniformity ( $C_u$ ) and Coefficient of Curvature ( $C_c$ ) was calculated from values  $D_{10}$ ,  $D_{30}$  and  $D_{60}$  as derived from the PSD curves, using the following equations:

$$C_u = \frac{D_{60}}{D_{10}} \quad (2)$$

$$C_c = \frac{(D_{30})^2}{D_{10} \times D_{60}} \quad (3)$$

Adapted from: Head (2006)

### 3.4.2.1 Hydrometer Test

The hydrometer test was undertaken according to ASTM D422-63 (Head, 2006). 100g of soil fines passing the 0.075mm sieve (sieve no. 200), were weighed out and transferred into a canning jar. 5 ml of each dispersing agent as well as 400 ml of distilled water was added to the jar and stirred thoroughly with a glass rod. This mixture, as shown in the figure below, was left to sit overnight as shown in Figure 3.14 below.



**Figure 3. 14:** Samples 1 and 2 after being weighed out and mixed with the dispersing agents.

The mixture was dispersed again by mixing with an automatic egg whisk for 5 minutes (Figure 3.15).



**Figure 3. 15:** Sample 3 being stirred with an automatic whisk for 5 minutes.

The mixture/suspension was then poured into the Bouyoucos cylinder and topped up with distilled water till the 1130 ml mark. The cylinder was stoppered and inverted a few times before being placed into a thermostat bath for approximately 1 hour or until the sample reached a constant 20° in temperature. The cylinder was then shaken again end over end before the hydrometer test begun (shown in figures 3.16a and b below).



a.

b.

**Figure 3. 16a and b:** Showing Samples 1 through 4 during hydrometer analysis; a) Sample 1 and 2, b) Sample 3 and 4.

The intervals at which the hydrometer readings were taken were: 18 seconds, 15 minutes (mins), 30 minutes, 60 minutes, and 120 minutes. The hydrometer bulb was inserted approximately 10 seconds before each recording interval. Percentage finer (Pf), adjusted percentage finer (PA) and particle diameter (D) were calculated using the equations below, and these results are plotted on the PSD curve.

$$\text{Pf (\%)} = \frac{a \cdot R_h}{W_s} \times 100 \quad (4)$$

Where,  $a$  is taken as a constant of 1,  $R_h$  is the hydrometer bulb reading and  $W_s$  is the mass of soil used in test.

$$P_A = P_f \times \frac{F_{200}}{100} \quad (5)$$

Where, F200 is the Percentage of soil retained on the #200 (0.075mm) sieve.

$$D \text{ (mm)} = k \sqrt{\frac{L}{T}} \quad (6)$$

Where, k is the corrected value obtained from the graph of Temperature vs Gs, L is the Corrected length and T is time interval of reading in minutes.

(Adapted from: Standard Test Methods, 1986)

### 3.4.3 Specific Gravity of Soil Solids

The Specific Gravity (Gs) of a soil is defined as the ratio between the weight of a volume of soil to the weight of an equal volume of distilled water. Specific gravity is a soil parameter that is particularly important for calculation of the weight-volume relationship and is also to correct for *k* values during the hydrometer test (sedimentation analysis). Other correlations have been found to determine void ratio (*e*) and subsequently porosity (*n*), using equations 7 and 8 below. (ASTM, 2014; Barounis and Philpot, 2017).

<b><u>List of Apparatus</u></b>
➤ Vacuum pump
➤ Scale (accuracy of 0.01g)
➤ 100ml volumetric flask with stopper
➤ Funnel
➤ Distilled water
➤ Glass rod

### Method

50g of soil fines passing the smallest sieve (0.075mm, in this study) were weighed out ( $W_s$ ). The weight of the empty and dry volumetric flask was also recorded to the nearest 0.01 gram. The flask

was filled with distilled water up till the mark and the weight of flask plus water was recorded as  $W_{bw}$ . Some of the distilled water was emptied out to avoid spillage, and the measured soil was added into the flask using a funnel. The flask was then filled again with distilled water up to the mark. The solution was stoppered and then gently agitated. At this point, a vacuum pump was inserted into the top of the flask (as shown in figure 3.17 below) and a gentle vacuum was maintained for approximately 30 mins in order to remove all air bubbles.



**Figure 3. 17:** Sample under vacuum to remove air bubbles, during specific gravity test.

Without agitating the mixture further, the weight of the flask and water and soil was recorded as  $W_{bws}$ . Specific Gravity ( $G_s$ ) of the sample was calculated using Equation 6, with other correlations provided below.

$$G_s = \frac{m_s}{m_s + [(m_{bw}) - (m_{bws})]} \quad (7)$$

Where,  $m_1$  is the mass of soil used in the test,  $m_{bw}$  is the mass of flask + water and  $m_{bws}$  is the mass of flask + water + soil.

$$e = \frac{w.G_s}{S_r} \quad (8)$$

Where,  $w$  is the water content (%) and  $S_r$  is the Saturation degree, taken as a constant of 1.

$$\text{Porosity } (n) = \frac{e}{1+e} \quad (9)$$

(Barounis and Philpot, 2017).

### 3.4.4 Atterberg Limits

Fine grained soils (clays and silts) display significant behavioural changes based on water content. Albert Atterberg developed the series of tests called the Atterberg Limits which quantifies a soils consistency relative to its water content. The four states of soil consistency are 1) solid, 2) semi-solid, 3) plastic, and 4) liquid. (Brown, 2015)

The Atterberg Limits is used to determine the following (Kaliakin, 2017):

- The Liquid Limit (LL), also known as the ‘upper plastic limit’ which is the moisture content at which a fine-grained soil no longer flows like a liquid. This is the minimum moisture content at which a soil begins to flow, with the application of very small shear force.
- The Plastic Limit (PL), also known as the ‘lower plastic limit’ which is the moisture content at which a fine-grained soil can no longer be remolded without cracking. Once cracking occurs, the soil is considered to change from a plastic state to a semi-solid state. The Plasticity Index (PI) is calculated from the result of the liquid and plastic limits.
- The Shrinkage Limit (SL) is the moisture content at which a fine-grained soil no longer changes volume upon drying. Loss of moisture is replaced by the entry of air into the soil pores.

By performing the Atterberg Limit tests, the soil type can be more easily classified through the use of a Casagrande plasticity chart. The chart is split into regions of low to extremely high plasticity, and the soil behaviour is inferred by plotting on this graph. A soil with a similar LL and PI will display similar behaviour with regard to strength versus water content (Head, 2006; Kaliakin, 2017). A soil exposed to water contents greater than its LL, will fail under static shear stress. When exposed to water contents less than the LL, the soil behaves as a plastic. The PI is the range over which a soil behaves plastically. At water contents less than the PL, soils behave as semi-solids with a brittle nature. At water contents less than the SL, a soil no longer experiences any further volume decrease (Holtz, 2001).

The Atterberg Limits are tested according to international standard ASTM D4318-00 (ASTM, 2003). Each limit has its own testing procedure as discussed in the sections below.

### 3.4.4.1 Liquid Limit

The name of the procedure used to determine the liquid limit is the Casagrande Method, which follows the ASTM D4318 standard (Head, 2006). Below is the list of apparatus needed to perform the test.

<u>List of Apparatus</u>
➤ Oven
➤ Scale (accuracy of 0.01g)
➤ Casagrande cup
➤ standard grooving tool

### Method

Before beginning the Atterberg Limit tests, the percentage water content of the soil was determined using the method laid out in section 3.4.1. After calibrating the Casagrande cup (shown in figure 3.18a), oven dried soil sample was mixed with water (in small increments) and placed as a paste into the cup (figure 3.18b). A standard grooving tool was then used to cut a groove into the centre of the soil pat (Figure 3.18c). Using the apparatus handle, the Casagrande cup was lifted to a height of 10 mm and dropped repeatedly (blows).



a.



b.



c.



d.



e.

**Figure 3. 18a, b, c, d and e:** a) Casagrande cup once calibrated; b) sample once arranged into a pat, c) groove created before start of test; d) Sample after completion of one liquid limit test; with groove closure evident; e) removal of sample at the source of closure for moisture content testing.

The Liquid Limit (LL) was then determined which is defined as the percentage moisture content required to close a distance of approximately 10mm along the bottom of a groove after 25 blows in the cup (shown in figure 3.18d and e). The test was repeated three times for the same soil sample at different moisture contents in order to obtain an average. This is because it is difficult and time consuming to perfectly adjust the moisture content in the soil to meet the required groove closure at 25 blows (N25). The percentage moisture content versus number of blows required for groove closure was plotted on a semi-logarithmic graph, and a best fit line drawn. The moisture content corresponding to N25, was derived from the curve, to provide the liquid limit of the soil.

(Adapted from: Head, 2006)

#### 3.4.4.2 Plastic Limit

The Plastic limit (PL) test follows standard ASTM D4318 (Head, 2006) and is performed by hand without the use of any specialised apparatus. The plastic limit is defined as the water content at which a thread of soil starts to crumbles when it is rolled out to a diameter of 3 mm.

## Method

An ellipsoidal sample of soil was mixed with tiny increments of water and rolled out by hand on a non-porous surface, in this case a glass plate. A soil thread that crumbles at a diameter less than 3 mm, is considered too wet. Whereas, if the thread crumbles at a diameter greater than 3 mm, the soil is drier than the plastic limit. The sample was remolded many times in order to achieve crumbling at a maximum diameter of 3mm (figure 3.19).



**Figure 3. 19:** Sample crumbling at 3mm diameter

At this point, the percentage moisture content of the thread is determined as described previously (through oven-drying). The Plasticity Index (PI) of the sample was calculated using the following equation:

$$PI = LL - PL \quad (10)$$

(Adapted from: Head, 2006)

### 3.4.4.3 Shrinkage Limit

The Shrinkage limit test follows standard BS 1377: Part 2 : 1990 (Head, 2006), and is performed using the following apparatus.

<u>List of Apparatus</u>
➤ Oven
➤ Scale (accuracy of 0.01g)
➤ Mercury
➤ Porcelain evaporating dish
➤ Glass cup
➤ Glass plate with 3 prongs

### Method

The mass of the clean empty dish to be used in the test, was recorded first followed by the volume of the shrinkage dish ( $V_1$ ).  $V_1$  is also the volume of the wet soil pat before shrinkage. Approximately 50 g of soil passing the standard 425  $\mu\text{m}$  sieve was mixed with distilled water until the soil resembled saturation and was pasty enough to be readily worked into the shrinkage dish. The inside of the shrinkage dish was coated with a thin layer of Vaseline. The saturated soil was placed into the dish centre starting with about one-third of the dish's volume, and then tapped gently on a surface until the soil flowed to the edges of the dish. This is done in order to avoid the inclusion of air bubbles. The remaining soil was added in instalments with the same tapping process in between. Once the dish was full, the excess soil was scraped off, and the outside of the dish cleaned (figure 3.20). The dish with soil was then weighed.



a.



b.

**Figure 3. 20a and b:** Sample before (a.) and after (b.) oven drying.

The mass of the wet soil pat ( $M_1$ ) was calculated by subtracting the mass of the dish filled with soil by the mass of the dish itself. The dish was then placed in the oven, where the soil experienced volumetric shrinkage upon drying (illustrated in Figure 3.20). The new volume that the soil occupied in the trough was measured after shrinkage ( $V_2$ ). The mass of the dry soil pat ( $M_2$ ) was then measured. Shrinkage limit (SL) was calculated using the following equation:

$$SL = \frac{(M_1 - M_2) - (V_1 - V_2) \rho_w}{M_2} \times 100 \quad (11)$$

Where  $M_1$  is the initial wet mass of soil,  $M_2$  is the final dry mass of soil,  $V_1$  is the initial volume of soil,  $V_2$  is the final volume of dry soil and  $\rho_w$  is the Density of water.

(Adapted from: Head, 2006)

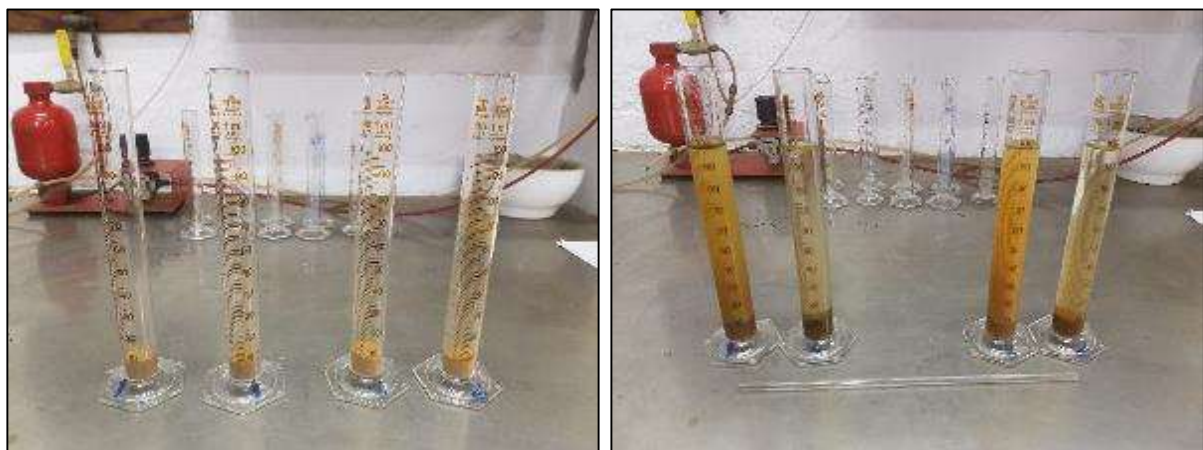
### 3.4.5 Free Swell test

Free swell (or Differential free swell) is defined as the increase in volume of soil when submerged in water without any external constraint. The differential free swell of a soil is represented as the free swell index (FSI) and is conducted according to IS: 2720: 1977 (Head, 2006).

<u>List of Apparatus</u>
➤ Oven
➤ Scale (accuracy of 0.01g)
➤ 100ml glass cylinders
➤ Distilled water
➤ Kerosene oil
➤ Glass rod

#### Method

Two 10g specimens of pulverised soil that had passed through the 425 $\mu$ m sieve were oven dried. Each specimen was then placed into 100ml glass cylinders. Distilled water was added into one specimen and kerosene oil into the other, up to the 100ml mark (shown in Figure 3.21 below). Entrapped air was removed by gently stirring with a glass rod.



a.

b.

**Figure 3. 21a and b:** Sample before (a.) and after (b.) addition of water and kerosene (water is the murkier solution).

The specimen was allowed to rest for at least 24 hours so as to reach a state of equilibrium, after which the final volume of soil in each cylinder was recorded as shown in figure 3.22 below.

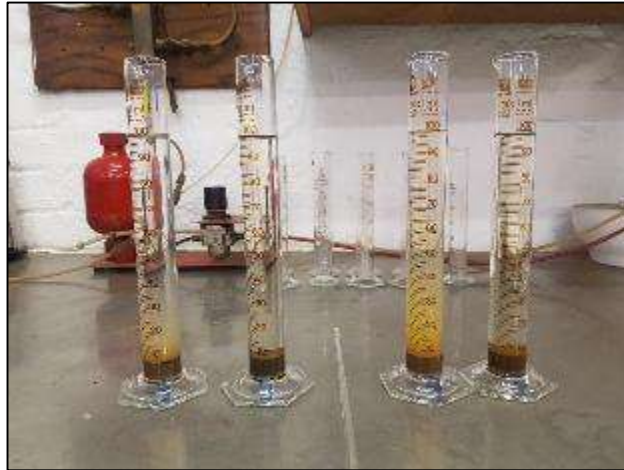


**Figure 3. 22:** Showing free swell of samples after 24 hours. In this case, it is evident that the sample had not increased in volume, i.e., there was no swelling.

The Free Swell Index (FSI) of the soil was calculated using the following equation:

$$FSI = \frac{V_d - V_k}{V_k} \times 100\% \quad (12)$$

where,  $V_d$  is the volume of soil specimen from the cylinder with distilled water, and  $V_k$  is the volume of soil specimen from the cylinder with kerosene.

### 3.4.6 Compaction testing

Compaction is the process by which solid soil particles are packed together using physical or mechanical force, thereby causing a reduction of air in soil voids and no major reduction in water content. Compaction is used to improve the engineering properties of soils by increasing the soils density. At maximum density (MDD), soil is considered to be at its highest strength. The amount of moisture or water content that is necessary to bring a soil to MDD, is known as the soils Optimum Moisture Content (OMC). A sample of soil is compacted under increasing amounts of water in order to draw a compaction curve, from which to derive the compaction characteristics, namely MDD and OMC (Head, 2006).

<b><u>List of Apparatus</u></b>
➤ Oven
➤ Scale (accuracy of 0.01g)
➤ Proctor manual compactor/2.5kg hammer
➤ Distilled water
➤ Mixing trough
➤ Proctor mould and base plate
➤ Extruding jack

## **Method**

Following the steps for light compaction as per ASTM D698 (Head, 2006), the samples were compacted using a 2.5kg proctor hammer and mould with base plate, as shown in figure 3.23 below.



**Figure 3. 23:** Showing apparatus used for compaction testing.

Approximately 3kg of sample was oven dried and passed through the 2mm sieve (size 10). The volume and weight of the mould and base plate was recorded. Each sample was put through five different compaction tests at increasing water contents. Distilled water was measured out for each test and mixed thoroughly with the soil in a mixing trough. The mixed soil was then placed into the compaction mould in 3 layers, with each layer receiving 25 blows, until the soil was flush with the top of the mould (see Figure 3.24 below). Between each test, the sample was removed from the mould using an extruding jack (Figure 3.25).



**Figure 3. 24:** Sample 3 after compaction



**Figure 3. 25:** Extrusion of Sample 1

The compacted soil including the mould was weighed. This weight was converted into a density ( $\rho$ ) using equation 13 below.

$$\rho = \frac{m}{v} \quad (13)$$

Where  $m$  is the mass of the compacted sample minus mould, and  $v$  is the volume of compacted sample within the mould.

The density of the soil at each water content was plotted as a compaction curve in order to derive MDD and OMC at the peak of the curve.

### 3.4.7 Soil-Suction testing

The Soil Suction test is based on the BRE Information Paper IP 4/93 written by Crilly and Chandler in 1993. It is used to determine the pore water suction or pressure of a soil sample in relation to the equilibrium water content of the Whatman No. 42 filter paper. This test is also known as the Filter Paper Method and a similar test is described in ASTM D5298-03 (ASTM, 2003). Soil suction is one of the most important parameters used to describe the moisture condition of unsaturated soils and is crucial in defining their hydro-mechanical behaviour. Matric suction is also known as the capillary

pressure of the soil, which is the pressure difference between the air and water components in soil voids. In the Filter Paper Method, the filter paper comes to equilibrium with the soil through vapor flow (which is the total suction measurement) or liquid flow (the matric suction measurement). The gravimetric water contents of the filter papers are converted to suction values using calculations derived from predetermined calibration curves (Bicalho *et al*, 2007; Chandler *et al*, 1992).

<b>List of Apparatus</b> (Figure 3.26b)
➤ Oven
➤ Scale (accuracy of 0.01g)
➤ Proctor manual compactor
➤ Distilled water
➤ 100mm by 120 mm sealable glass jars
➤ Whatman no. 42 filter papers
➤ Sealing tape
➤ Insulated containing box
➤ Tweezers

**Method**

The previously compacted samples (as described in Section 3.4.4 above), were kept in airtight bags and left in a regulated bath until commencement of the soil-suction test (as shown in Figure 3.26a below).



a.

b.

**Figure 3. 26a and b:** a) Compacted samples being preserved prior to soil suction test; b) apparatus used in soil suction testing.

The samples were trimmed to size (approximately the diameter of the filter paper), turned on the side and sliced into 2 equal discs. Using tweezers, 1 filter paper (known as the matrix) was sandwiched between 2 other filter papers and placed between the 2 separate halves of the sample, and another filter paper (known as the isometric) was placed on a plastic spacer on top of the sample (once re-assembled). Importantly, the positions of each filter paper were marked accordingly as shown in Figures 3.27 below.



a.

b.

c.

**Figure 3. 27a, b and c:** a) Sample trimmed and cut in half; b) filter paper placed between the two halves of the sample (within 2 other buffer filter papers); c) plastic spacer used to separate top filter paper from top of sample.

The sample was re-assembled and swiftly placed into a jar that was then sealed thoroughly so as to avoid any air infiltration. The sealed samples were placed into a contained environment and left for approximately 5 to 10 days (see figures 3.28 below).



a.



b.

**Figure 3. 28a and b:** a) Sealed sample in airtight container; b) kept in contained environment for 5 to 10 days with temperature regulation.

The sample was removed from the jars using a tweezer and separated into its 2 discs. Each (now moist) individual filter paper was placed in a jar and weighed. Extreme care was taken not to interfere with the moisture content of the filter papers, not by hand or by exposing them to open air for extended periods of time. The filter papers were oven-dried for 24 hours and the dried weight of each filter paper was recorded, in order to calculate the moisture content on each filter paper (using Equation 1 above). The average moisture content of all 3 filter papers was calculated so as to determine the Total and Matric Soil Suction ( $P_k$ ) on each filter paper, using the equations below.

Matric Suction:

If the calculated water content is greater than 47%:

$$\text{Log}_{10}P_k = 6.05 - 2.48\text{Log}_{10}x W_p \text{ (Kpa)} \quad (14)$$

If the calculated water content is less than or equal to 47%:

$$\text{Log}_{10}P_k = 4.84 - 0.0622 x W_p \text{ (Kpa)} \quad (15)$$

Total Suction:

If the calculated water content is greater than 45.3%:

$$\text{Log}_{10}P_k = 2.412 - 0.0135 \times W_p \text{ (Kpa)}$$

If the calculated water content is less than or equal to 45.3%:

$$\text{Log}_{10}P_k = 5.327 - 0.0779 \times W_p \text{ (Kpa)}$$

(Bicalho *et al*, 2007; Chandler *et al*, 1992; Head, 2006)

### 3.4.8 Consolidation testing / Oedometer test

Consolidation is the process by which soil particles are packed closely together over a period of time, under the application of a constant external pressure. Both air and water are driven out of the soil voids during consolidation. Primary consolidation is the total compression that the sample undergoes during active loading, whereas secondary consolidation is the compression that occurs after primary consolidation and over the long term. The Consolidation test is also referred to as the standard Oedometer test or One-dimensional compression test and is used to determine the rate and magnitude of either **settlement or heave** in soils. This rate is determined by the swell or collapse potential of the soil (Head, 1994).

<u>List of Apparatus</u> (Figure 3.29)
➤ Consolidometer or oedometer <ul style="list-style-type: none"> <li>○ Consolidation ring</li> <li>○ Two porous stones</li> <li>○ Two filter papers</li> <li>○ Loading pad</li> </ul>
➤ Loading plates of various weights
➤ Dial gauge (accuracy of 0.002mm)
➤ Oven
➤ Scale (accuracy of 0.01g)
➤ Knife or spatula
➤ Distilled water
➤ Stopwatch



**Figure 3. 29:** Showing oedometer apparatus.

## Method

Following standard ASTM D4546 (Head, 1994), the *loading-after-wetting test* was used. Oven dried sample passing the 1.18mm sieve was tested for consolidation under 3 water contents, one on the dry side of the compaction curve, one at OMC, and one on the wet side.

The metal ring of the oedometer was cleaned and dried before its weight, inner diameter, and height was measured. The sample was lightly compacted within the oedometer ring after which, excess soil was trimmed off the top and bottom of the ring, and the ring was weighed again with the specimen neatly inside. The porous stones were saturated by submerging in distilled water for 4 to 8 hours. The consolidometer was then assembled with a porous stone at the base, followed by filter paper, the oedometer ring with sample and then filter paper again topped off with the second porous stone. The loading pad was placed on the top porous stone and the consolidometer was locked into place using metal screws. The assembled specimen is then saturated by adding distilled water.

The initial load was 5kPa, with vertical settlement being recorded of the dial gauge at the following intervals: 6 secs, 15 secs, 30 secs, 1 min, 2 min, 4 min, 8 min, 15 min, 30 min and 1 hour. After the 1 hour reading, the load was doubled and then doubled again every 24 hours for 5 days. On the 5<sup>th</sup> day, the load was reduced to a quarter of the heaviest load. Settlement was recorded every 24 hours (Figure 3.30). After completion of the test, the loads were removed, and the apparatus was

dismantled in order for the sample within the ring to be weighed again (Figure 3.31). The specimen was then oven dried to determine its final dry weight.



**Figure 3. 30:** Showing loading of oedometer



**Figure 3. 31:** 3 Saturated specimens (Sample 1) after test in preparation for final moisture content determination.

The consolidation test provides the following results/parameters as given by the respective equations:

- Height of soil solids ( $H_s$ )

$$H_s = \frac{W_s}{G_s \cdot \gamma_w \cdot A \left(1 + \frac{MC}{100}\right)} \quad (16)$$

Where,  $W_s$  is the weight of the sample,  $G_s$  is the Specific Gravity of the soil,  $\gamma_w$  is the Unit weight of water and  $A$  is the area of the specimen.

- Void ratio ( $e$ )

$$e = \frac{H_o - H_s}{H_s} \quad (17)$$

Where,  $e$  is the void ratio,  $H_0$  is the initial height of the specimen and  $H_s$  is the height of soil solids.

- Coefficient of compressibility ( $a_v$ ): Using graph of Final void ratio Vs. Effective stress

$$a_v = -\frac{\Delta e}{\Delta \sigma} \quad (18)$$

Where,  $\Delta e$  is the change in void ratio and  $\Delta \sigma$  is the change in effective stress.

- Coefficient of volume change ( $m_v$ ): Using graph of Final void ratio Vs. Effective stress

$$m_v = \frac{-\Delta e}{1+e} \left( \frac{1}{\Delta \bar{\sigma}} \right) \quad (19)$$

Where,  $\Delta \bar{\sigma}$  is the change in total effective stress.

- Compression Index ( $C_c$ ): Use graph of Final void ratio Vs logarithmic of effective stress

$$C_c = \frac{-\Delta e}{\log \frac{(\sigma_o + \Delta \sigma)}{\bar{\sigma}_o}} \quad (20)$$

Where,  $\bar{\sigma}_o$  is the initial total effective stress.

- Coefficient of consolidation ( $C_v$ ):

Using Dial gauge reading Vs. square root of time:

$$C_v = 0.848 \frac{d^2}{t_{90}} \quad (21)$$

Where,  $d^2$  and  $t_{90}$  are read off the graph.

### 3.4.9 Direct Shearbox test

The Direct Shear Box (DSB) test is the oldest and simplest procedure for determining the shear strength of soils in terms of their total strength properties, namely total cohesion and total angle of internal friction. When the shear stresses exerted upon a soil mass exceed the maximum shear

resistance that the soil inherently has (its shear strength), shear failure can occur. The standard shearbox apparatus does not allow for the control of drainage and therefore there is no way to measure pore water pressure. This is the main advantage of the triaxial test over the direct shearbox test. Shear strength results obtained from these tests are necessary in carrying out slope stability analysis, in order to mitigate the disastrous consequences of shear failure. (Head,1994)

<b>List of Apparatus</b> (Figure 3.32)
➤ Oven
➤ Scale (accuracy of 0.01g)
➤ Direct shearbox apparatus, including bottom grid and top lid with ball bearing
➤ Porous stones
➤ Distilled water
➤ Horizontal dial gauge
➤ Mixing trough
➤ Loading plates of various weights
➤ Stopwatch



**Figure 3. 32:** Direct shearbox apparatus

**Method**

According to ASTM D3080 (Head, 1994), the small shearbox-rapid test was performed. Approximately 800g of oven dried sample, having passed the 1.18mm sieve was set aside for each test. As with the consolidation test detailed in section 3.4.6, each sample was tested under 3 water

contents, one on the dry side of the compaction curve, one at OMC, and one on the wet side. Three different normal stresses were applied to each of these water contents – 20 kPa, 40kPa and 80kPa. This meant that a total of 27 Direct shear box tests were conducted for the purpose of this study. The soil was thoroughly mixed with the required water content, before being carefully and lightly packed into the three shearboxes. The shearbox was assembled into the machine, saturated with distilled water and locked in place using screws. A metal ball bearing was used to hold the lid in place on top of the specimen during testing. The specimens were allowed to consolidate under their respective loads for 1 hour (Figure 3.33), after which the shearing process began. The gears were engaged, and the motor was switched on to begin horizontal shearing of the specimen. Both the horizontal gauge and the loading gauge readings were recorded every minute up until failure occurred (Figure 3.34). This was obvious by an evident drop in the load gauge readings after a peak.



**Figure 3. 33:** DSB tests under active loading



**Figure 3. 34:** Showing failure of a specimen after shearing.

The DSB machine was dismantled, cleaned and dried between each test. Tiny samples were taken from each shearbox after the completion of each test for moisture content determination. The loading values in Newtons (N) were converted using the area of the shearbox to give shear stress values (kPa). The peak shear stress at failure was then obtained from a plot of horizontal displacement vs shear stress. Peak stress at failure was plotted against normal stress used in each test and a best fit line was drawn. This best fit line is called the failure envelope and is expressed by Coulombs Law in the Equation below. Extrapolation of the best fit line to the y-axis gives the soils cohesion (kPa), and the angle of the best fit line to the horizontal is the angle of internal friction.

$$\tau_f = C' + \sigma_n \tan \phi_f' \tag{22}$$

Where,  $\tau_f$  is the shear strength of the material,  $C'$  is the effective cohesion,  $\sigma_n$  is the normal effective stress on the failure plane and  $\phi_f'$  is the effective angle of internal friction.

### 3.4.10 Triaxial test - Consolidated Undrained

The triaxial test is one of the most significant and versatile geotechnical laboratory tests, providing some of the more important parameters necessary for geotechnical design. It is used to determine the shear strength of soil or rock, with the aim of observing the specimen's response under conditions that come as close as possible to those experienced *in-situ*. Unlike the simpler direct shear test, a triaxial test allows for the control of specimen drainage and thus a measurement of pore water pressures along with the shear strength and stiffness of the soil. Primary parameters obtained from a triaxial test may include the angle of shearing resistance / angle of internal friction ( $\phi'$ ), cohesion ( $c'$ ), and undrained shear strength ( $C_u$ ), as well as additional parameters such as the shear stiffness ( $G$ ), compression index ( $C_c$ ), and permeability ( $k$ ) which may also be determined.

The three types of triaxial testing are Unconsolidated Undrained test (UU), Consolidated Undrained test (CU), and Consolidated Drained test (CD). Each test yields different soil responses and subsequent observations are made for different engineering applications. Therefore, the choice of test depends on the results or parameters required by the engineer. The CU test is the most common triaxial procedure because it is based on the effective stresses within a specimen, therefore allowing **effective** shear strength parameters to be determined (i.e.  $\phi'$  and  $c'$ ) whilst also allowing for a faster rate of shearing as compared with the CD test. This is possible because the excess pore pressure changes are recorded during the shearing process.

There are multiple stresses applied to the specimen during testing. The first is the confining pressure ( $\sigma_c$ ) which is applied by pressurising the cell fluid surrounding the specimen and is active in all directions. This stress is also known as the minor principal stress ( $\sigma_3$ ). An axial stress ( $\sigma_a$ ) is then applied to the specimen, which is also known as the major principal stress ( $\sigma_1$ ). A deviator stress ( $q$ ) is generated by the application of the axial stress ( $\sigma_1$ ), and  $q$  acts in addition to the confining pressure ( $\sigma_3$ ).  $q$  plus  $\sigma_3$  is therefore equal to  $\sigma_1$ . When  $\sigma_1 = \sigma_3$ , the stress state of the specimen is said to be isotropic, when  $\sigma_1 \neq \sigma_3$  the stress state is anisotropic.

(Adapted from: Head, 1994)

<b><u>List of Apparatus</u></b> (Adapted from: Head, 1994) (Figure 3.35)
➤ Long sample tubes with sharp cutting edges and rubber end caps
➤ Extruder for U-100 tube samples
➤ Split mould for forming specimen to 2:1 height/diameter ratio
➤ Trimming knife, wire saw or spatula
➤ Vernier Calipers
➤ Scale (accuracy of 0.01g)
➤ Oven
➤ Stopwatch
➤ Distilled water



**Figure 3. 35:** Showing basic triaxial testing apparatus (in UKZN soils laboratory).

### **Method**

According to international standard ASTM 2850 (Head, 1994), there are four basic processes involved in triaxial testing: 1) Preparation, 2) Saturation, 3) Consolidation and 4) Shearing. Three specimens are prepared from each sample using a different confining pressure for each. Selected

confining pressures were 50, 100 and 200 kPa. Disturbed sample was reconstructed to MDD and OMC specifications, and a 2:1 height/diameter ratio before being loaded into the triaxial cell.

The specimen was saturated using distilled water and left until total saturation was achieved. The “B-check” was performed to quantify Skempton’s B-value and the degree of saturation. At a B-value of approximately 1, the specimen is considered saturated and the triaxial test began.

While ensuring a constant back pressure throughout, the specimen was consolidated to bring it to the effective stress state required for shearing. The method for consolidation is similar to that detailed in section 3.4.7 above.

Once consolidation was complete to the necessary degree, the shearing process began. The specimen was loaded axially in compression to the required confining pressure (e.g., 50, 100 or 200kPa). The rate of strain selected was 0.3% per hour in order to allow for more readings and a more detailed result. The triaxial machine was engaged and all gauges were set in place. The test was continued until obvious failure of the specimen occurred (see Figure 3.36 below) or a strain of 20% was reached. The figure below shows one of the samples after failure occurred. After unloading and dismantling the machine, a standard moisture content test was taken from each specimen.



**Figure 3. 36:** Showing the failure of Sample 3 at an effective constant stress of 200kPa.

The values of  $\sigma_{1f}$  and  $\sigma_3$  were used to draw Mohr circles of failure for each specimen. The scale of the Mohr diagram should be 1:1 on both axes. In a Mohr diagram, semicircles are plotted with shear stress ( $\tau_n$ ) on the vertical axis versus normal stresses ( $\sigma_n$ ) on the horizontal. A tangent to all three curves defines the failure condition of the sample. This is called the Mohr–Coulomb failure criterion and is quantified by the same Equation 22 above. Extrapolation of the tangent to the y-axis gives the effective cohesion ( $C'$ ) of the sample. The effective angle of internal friction ( $\varphi_f'$ ) is measured by the angle between the tangent and a line drawn parallel to the x-axis/normal (Head, 1994).

## CHAPTER FOUR

### LABORATORY RESULTS AND INTERPRETATION

---

#### 4.1 Introduction

This chapter provides a comprehensive analysis of the results of all laboratory tests conducted for the purpose of this research project, followed by interpretations of the results according to published literature. The raw data obtained during laboratory testing was collated on Microsoft Excel which was then used to create and customise the required graphs/curves. A total of four different soils were encountered between the two sites. Those soils selected for laboratory testing were assigned sample designations, as provided in the soil profiles in Section 3.3 above. Table 4.1 below provides a summary of all laboratory tests conducted on each sample.

		<u>Tests Conducted</u>								
<u>Sample No.</u>	<u>Soil type</u>	<u>PSD</u>	<u>Att. Lims.</u>	<u>SG</u>	<u>Free Swell</u>	<u>Comp-action</u>	<u>Soil Suction</u>	<u>Consolidation</u>	<u>Direct Shear -box</u>	<u>Triaxial</u>
1	Silty Gravelly SAND	X	X	X	X	X	X	X	X	X
2	Silty Gravelly SAND	X	X	X	X	X	X	X		
3	Clayey Sand	X	X	X	X	X			X	X
4	Silty Sand	X	X	X	X	X			X	X

#### 4.2 Natural Moisture Content of Soils

The natural moisture content (NMC) of the four samples were determined using the method described in Section 3.4.1 and calculated using Equation 1. Table 4.2 provides the calculated moisture contents of the samples.

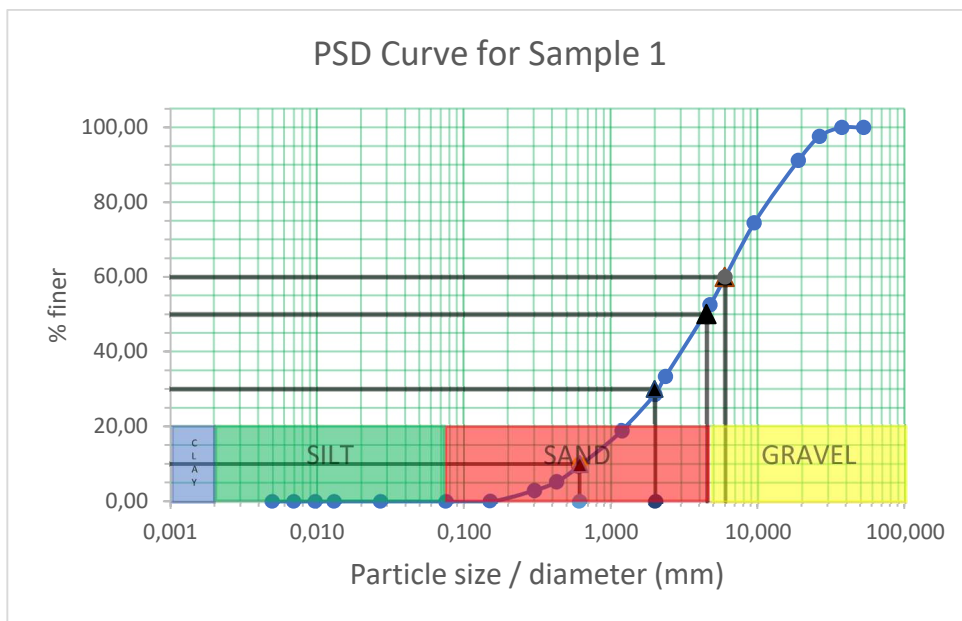
**Table 4. 2:** Natural Moisture Contents of all samples tested

Site	Sample No.	MC (%)	Average NMC%
A	1	8.30	9.5
	2	10.70	
B	3	28.55	27.75
	4	26.94	

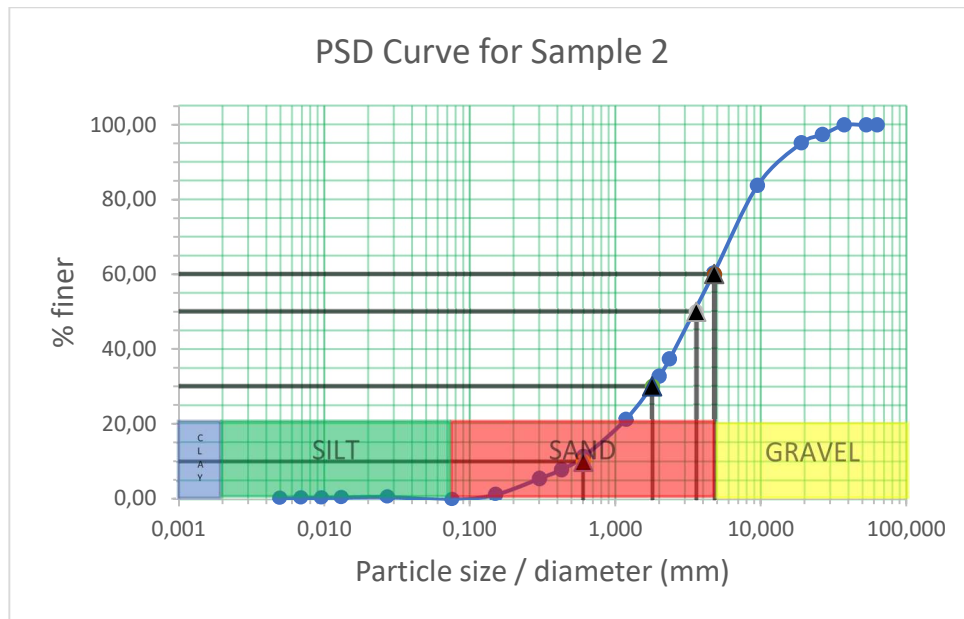
The results indicate that the soils from Site A exhibit relatively low moisture contents and dryer conditions than the soils from Site B. This is due to the fact that Site A comprised rock and residual rock, whereas Site B comprised sands and silts directly overlying the ocean. Sea water was observed in TP2 at 0.90 mbegl, which most likely affected the moisture content of neighbouring soils.

### 4.3 Particle Size Analysis

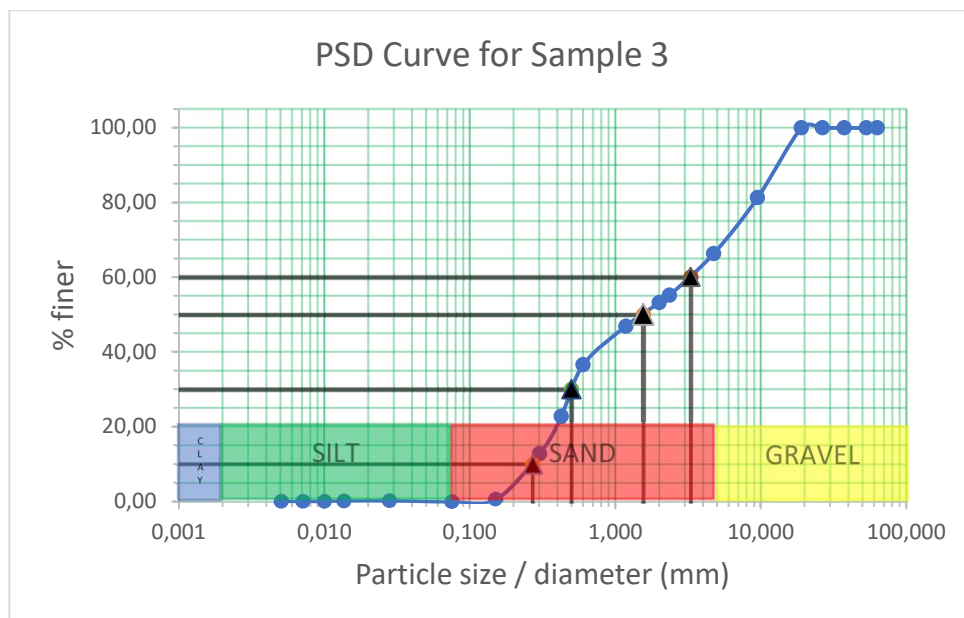
The particle sizes of each sample were determined as described in Section 3.4.2. In order to create the PSD curves, the entire sample was put through mechanical sieving, with the finest portion (passing the 0.075mm sieve) having undergone hydrometer testing. The results from particle size analysis in the form of particle size distribution curves are provided in Figures 4.1 a, b, c and d below.



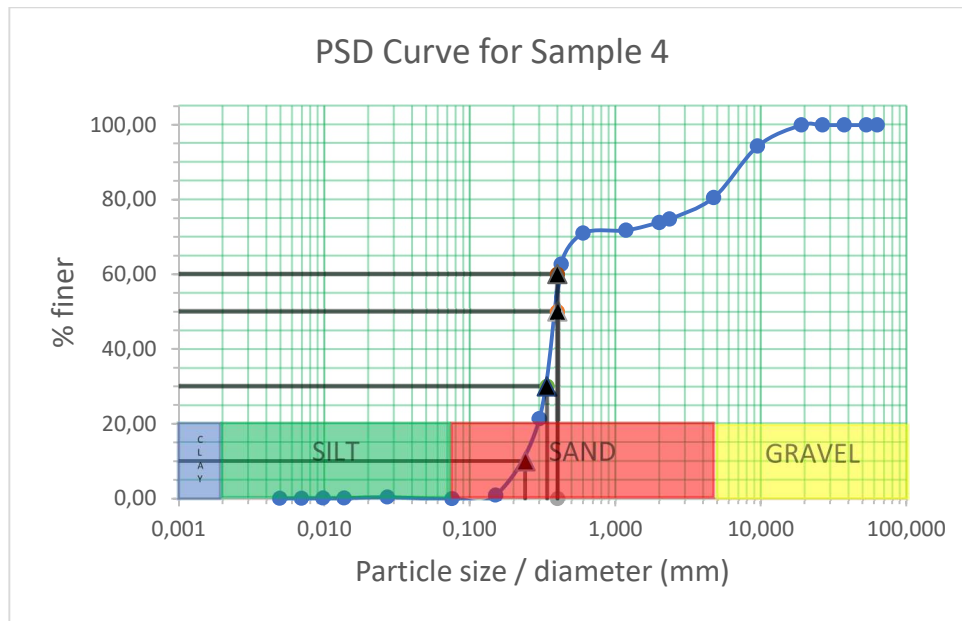
a.



b.



c.



d.

**Figure 4. 1a, b, c and d:** Particle size distribution curves for samples 1, 2, 3 and 4, respectively.

The results from Particle Size analysis and the above plotted distribution curves were used to classify the soils in terms of their soil size and gradation. The Coefficients of Uniformity ( $C_u$ ) and Curvature ( $C_c$ ) were calculated as per Equations 2 and 3 (Section 3.4.2), and the results and interpretations according to Head (2006) are provided in the table below.

<b>Table 4. 3:</b> Results and interpretations from Particle Size Distribution curves					
Sample No.	Soil Classification (as per Head, 2006)	Mean diameter - $D_{50}$ (mm)	$C_u$	$C_c$	Grading
1	Very gravelly SAND	4.5	9,84	1,09	well graded SAND
2	Slightly silty gravelly SAND	3.6	8,00	1,13	well graded SAND
3	Slightly gravelly SAND	1.56	12,22	0,28	Poorly sorted / gap graded
4	Fine grained SAND	0.4	1,67	1,20	Poorly sorted / gap graded

The results from the particle size analysis and derived distribution curves, indicate that both the soils from Site A are well graded SANDS, with particles of all sizes present. The calculated values of  $C_u$  and  $C_c$  confirm this as  $C_u$  is greater than 6 ( $C_u > 6$ ), **and**  $C_c$  lies between 1 and 3 ( $1 < C_c < 3$ ) (ASTM Int., 2017). The soils from Site A can be considered as one soil type, due to the fact that

Sample 1 is derived from the breakdown of Sample 2. In contrast, the soils from Site B are very poorly graded and also gap graded with high contents of only sand size particles and very little to none of other soil sizes.

A study by Robinson and Friedman (2002) investigated the effects of varying soil sizes on the stability of slopes. It was found that in uniform sand slopes with mono-size particles, there were no trends in slope stability or failure regardless of the particle size investigated. However, as particles in a uniform soil mass become smaller the force to mass ratio increases and at a small enough particle size, the electrostatic interaction between particles may contribute to the “flowability” of the soil mass indicating the possibility of landslide failure. Mixed soil slopes were found to be the most stable when the ratio of smaller particles to larger particles was 1:3, resulting in an increase in the slope density as well as the number of contact points between particles, due to packing of small particles within the voids. In general, it was concluded that particle shape and not particle size, is the soil property to have the greatest effect on the stability of a slope. More angular particles tend to interlock which also helps to strengthen and stabilize a slope and spread the stress upon loading (Robinson and Friedman, 2002).

**4.4 Specific Gravity**

Specific gravity tests, as described in Section 3.4.3, were conducted on all four samples. The results were calculated using Equation 6 and are provided in table 4.4 below.

<b>Table 4. 4: Specific Gravity (Gs) of all samples tested</b>	
<u>Sample No.</u>	<u>Gs</u>
1	2.48
2	2.48
3	2.56
4	2.63

The specific gravity of the samples was required in order to correct for other values in the particle size analysis and also, using equations 4 and 5, to calculate the soil void ratio (*e*) and porosity (*n*). These results are provided in the table below.

<u>Sample No.</u>	<u><math>e</math></u>	<u><math>n</math></u>
1	20.58	0.95
2	26.54	0.96
3	73.09	0.98
4	70.85	0.99

In general, the samples from Site A are very similar and both display relatively low void ratios and porosities. This could be due to the fact that samples 1 and 2 from Site A are well graded and contain various soil sizes, causing the smaller particles to fill in the voids in the soil mass (Robinson and Friedman, 2002).

The samples from Site B yielded the same approximate porosities as those from Site A, while exhibiting much higher void ratios (average of 71.97). Technically, this is due to the much higher natural moisture contents of samples 3 and 4 (Site B), with the same approximate specific gravities as samples 1 and 2 (Site A). In reality however, the high frequency in voids is due to the uniformity and well-rounded nature of the beach sands with low to no incidence of particle interlocking or infilling of voids (Robinson and Friedman, 2002).

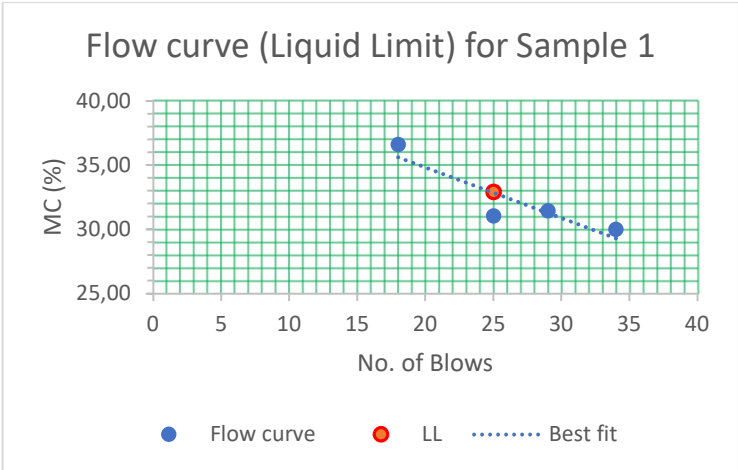
#### 4.5 Free Swell

The free swell of the soils was tested as detailed in Section 3.4.5. **No swell** was observed or recorded in all four samples. 10mm of sample was added to each cylinder (of water and kerosene) and it remained at 10mm after 24 hours. The Free Swell Index (FSI) of all the soils across both sites is 0. The inferred degree of expansivity is therefore LOW to NONE.

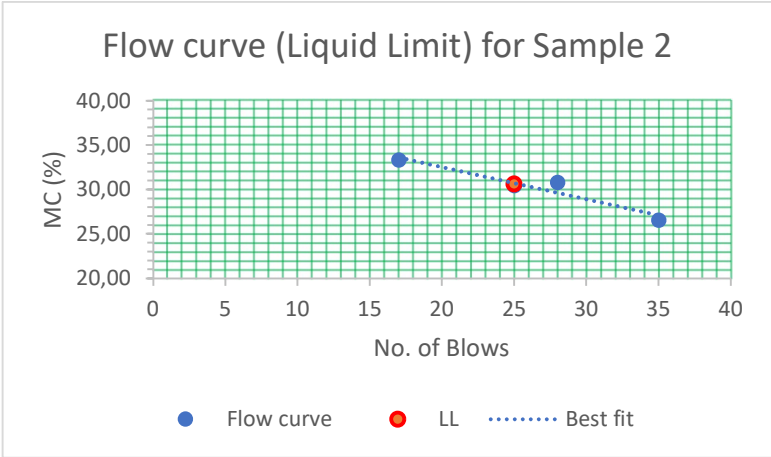
The free swell test is generally performed to indicate the possible expansivity of CLAY soils, or soils containing significant clay content (Head, 2006). As the soils investigated in this study all contain very little fines, this test was mostly conducted as an index test to further classify the soils.

### 4.6 Atterberg Limits

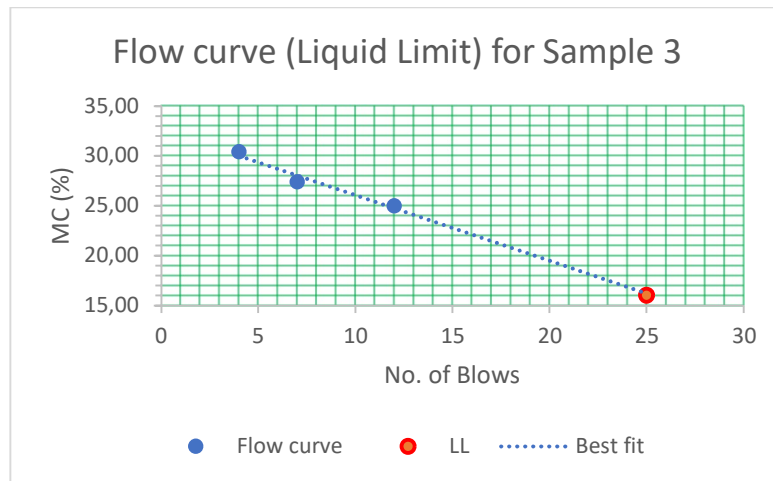
The three Atterberg Limits of the samples were tested in the laboratory following the methods provided in Section 3.4.4. The Plastic Limit (PL) was obtained directly from the test conducted, and the Plasticity Index (PI) was thereafter calculated using Equation 10. The Shrinkage Limit (SL) was calculated using Equation 11. The Liquid Limit (LL) was derived from the plotted flow curves, provided in the following figures (Figure 4.2a, b, c and d). The results from the Atterberg Limits are tabularised below.



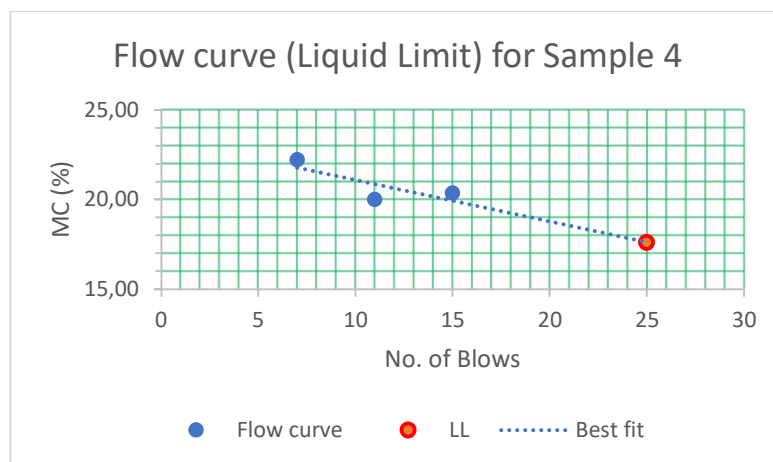
a.



b.



c.



d.

**Figure 4. 2a, b, c and d:** Flow curves to determine LL for samples 1, 2, 3 and 4, respectively.

<u>Sample No.</u>	<u>LL (%)</u>	<u>PL (%)</u>	<u>SL (%)</u>	<u>PI</u>
1	32.90	21.05	36.63	11.85
2	30.60	17.50	31.34	13.10
3	16.00	-	38.83	-
4	18.00	-	21.07	-

The Atterberg Limits for Samples 3 and 4 could not be obtained, as the samples kept failing at all water contents and could not retain any shape. They could not be made into a “pat” for the Casagrande test (to obtain the flow curve and LL), and could not be “rolled” for the Plasticity test. This most likely occurred due to the high sand content of these soils, and their lack of fines (silt and clay). In order to obtain the flow curve, the Casagrande test was modified slightly. Lower ranges

of taps were recorded, at the point where the sample just started to hold the required shape. The SL was able to be obtained, however the PL was not.

Upon inspection of the above results, the two soils from Site A are considered fairly similar in their soil characteristics and behaviour. The ranges between the Atterberg Limits obtained from these samples is so small, that a single average can be given for the soils from Site A. i.e.: LL = 31.75%, PL = 19.28%, SL = 34% and PI = 12.48%.

In general, the soils from Site A exhibit higher LL's than those from Site B. In other words, the soils in Site B require the addition of less water for them to enter a "liquid" state or start to flow. They may therefore be classified as more dangerous than the soils from Site A upon the introduction of water into the soil environment. Furthermore, Site B soils exhibited NMC's (~27.75%) already higher than their calculated LL's (~17%). This indicates that the soils had already been in a potential state of liquefaction when they were first collected from site. This fact was also observed during fieldwork where the stormwater runoff led to small scale failure.

Site A soils exhibited an average shrinkage of 34% upon drying. Site B soils displayed a great variation in the amount of shrinkage that occurred up to a maximum of 38% for the lower beach sands.

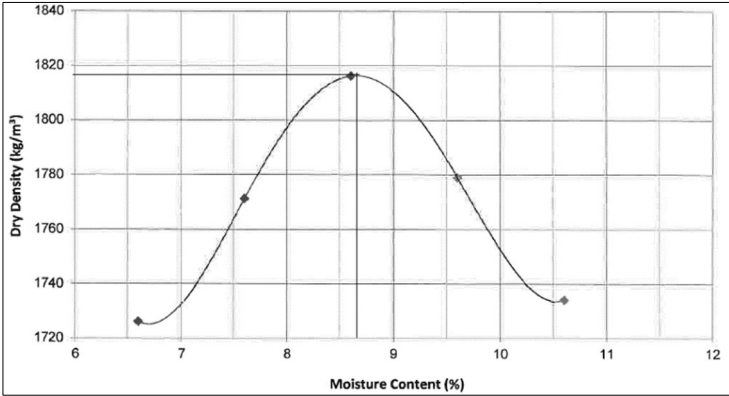
The Atterberg limits are generally conducted on fine grained cohesive soils in order to measure and describe their plasticity range or the activity of the clay content in soils. The soils are plotted on a Plasticity chart to determine their degree of plasticity (low, medium or high) and the soils application in engineering practice can then be determined. For example, clay soils of high plasticity have lower permeability, are more compressible and tend to consolidate over a long period of time. High plasticity clays are therefore more difficult to compact when used in construction, as opposed to low plasticity clays (Head, 2006). As all the investigated soils in this study have low fines content and are classified as SANDS (USCS), the effects of changes to moisture content and associated plasticity in the soils is considered negligible.

#### **4.7 Compaction**

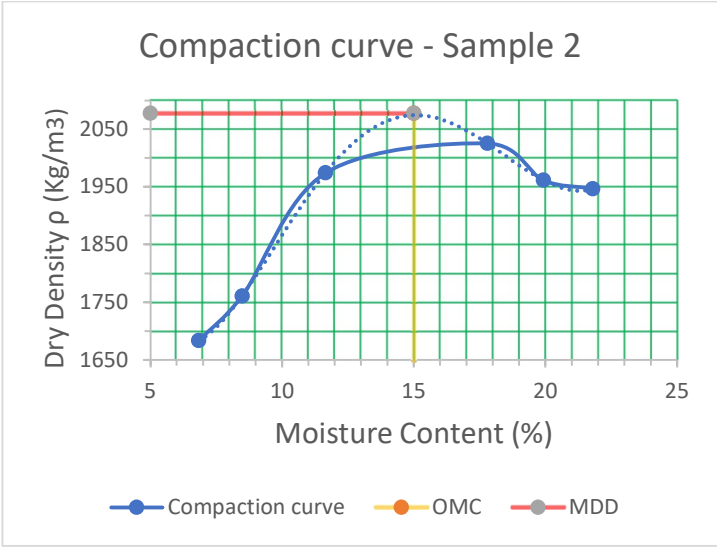
All four samples were put through compaction testing (as discussed in Section 3.4.4). Samples 1 and 2 were compacted in the UKZN soils laboratory and kept in compacted form for use in

subsequent soil-suction tests. Samples 1, 3 and 4 were compacted in an external soils laboratory, Soilco Materials Investigations (Pty) Ltd, in order to obtain the soil parameters necessary for use in triaxial testing, i.e., Optimum Moisture Content (OMC) and Maximum Dry Density (MDD), as derived from compaction curves. The soil compaction character provides a greater understanding of the soil itself and the soil variability. The compaction curves and derived parameters are provided in the figures and table below.

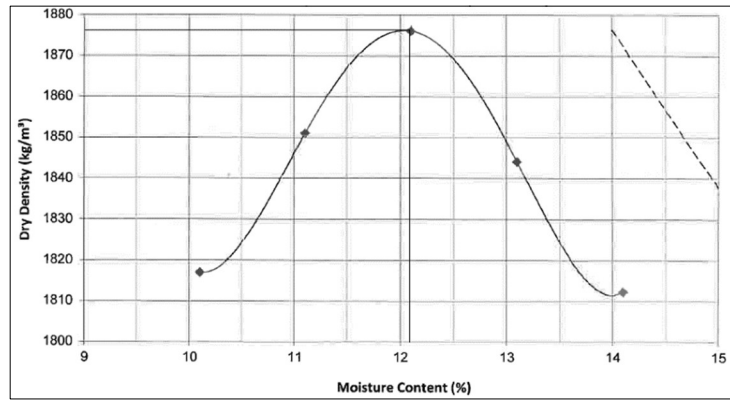
At this point, it is important to mention that the results obtained locally (UKZN laboratory) and the results from the external laboratory are vastly different. This can only be attributed to human error and a lack of technical experience on the researchers part. Due to the fact that the compaction results obtained from Soilco were used in subsequent triaxial testing, these are the results provided below.



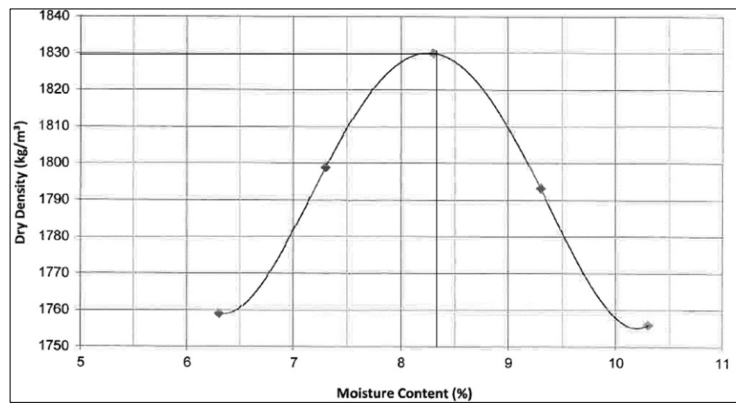
a.



b.



c.



d.

**Figure 4. 3a, b, c and d:** Compaction curves to determine MDD and OMC for samples 1 , 2, 3 and 4, respectively. Samples 1, 3 & 4 as provided by Soilco laboratory.

<b>Table 4. 7: Derived parameters from Compaction Testing</b>			
<u>Sample No.</u>	<u>OMC (%)</u>	<u>MDD (Kg/m<sup>3</sup>)</u>	<u>MDD (kN/m<sup>3</sup>)</u>
1	8.7	1816	17.81
2	15	2078	20.39
3	12	1876	18.40
4	8.3	1830	17.95

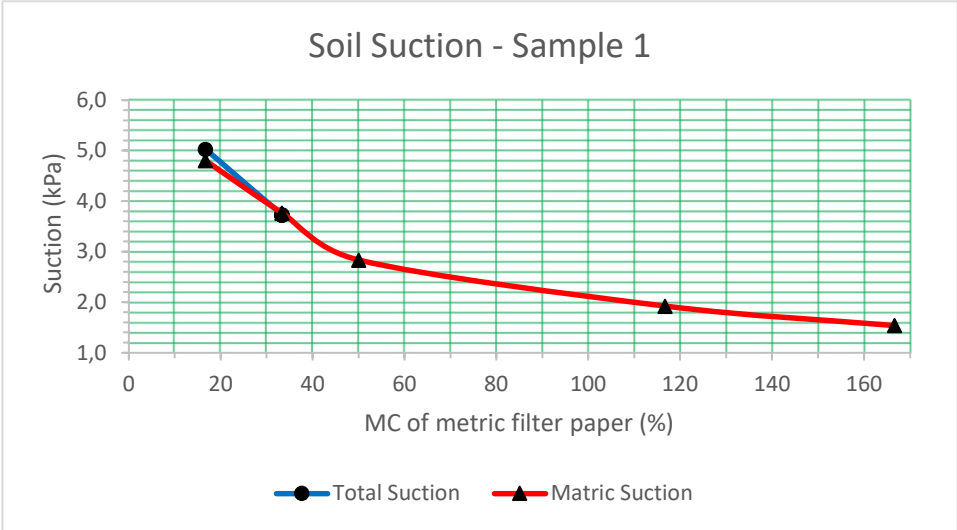
The topsoil from Site A, Sample 1, yielded an OMC of 8.7% in order to achieve a MDD of 1816 Kg/m<sup>3</sup>. Whereas sample 2 from Site A showed very different results. This is likely due to the fact that Sample 2 was mostly bedrock which was occasionally recovered as soil in some places. As such, this result cannot be fully considered as the compaction character of a soil.

The samples from Site B yielded an average OMC of 10%, to achieve an average MDD of 1853 Kg/m<sup>3</sup>.

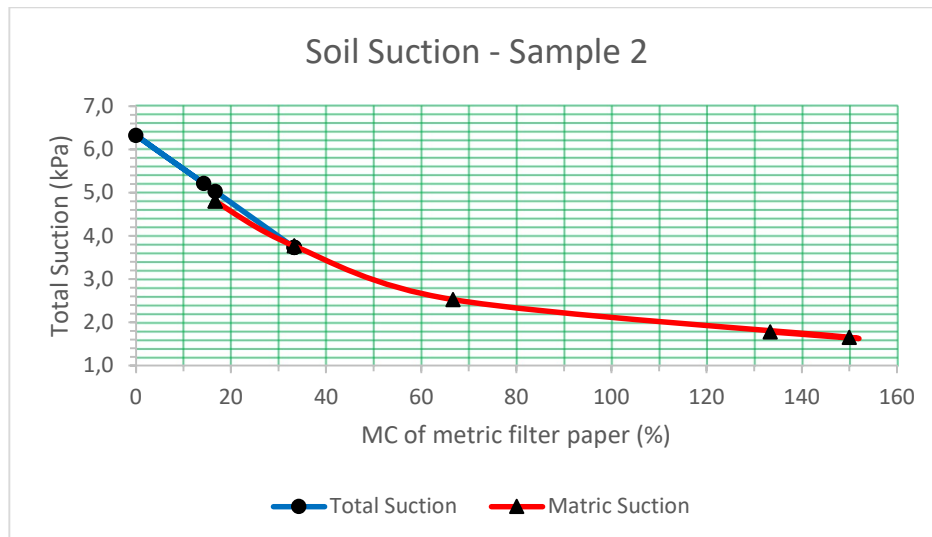
Well graded sandy soils, such as those from Site A show a clearly defined peak in the compaction curve. Whereas uniformly graded, free draining soils such those from Site B generally result in flatter curves where the optimum conditions are more difficult to define. In this case, a better idea of field compaction behaviour can be obtained from an in situ maximum density test. The compactive effort and associated moisture content required to bring a soil to its highest strength, is an important factor to consider when a soil is to be used as fill material in construction. Under-compaction is ineffective as the soil embankment may settle or fail when load is applied, or water is introduced. It is also important to avoid over-compacting soil as they can then absorb water more easily, resulting in swelling, a decrease in shear strength and increased compressibility. When the MDD and OMC of a soil are known, these optimum conditions can be reproduced in the laboratory to test the soil reaction under different *in situ* conditions post construction or remediation, such as to measure the changes in pore pressure due to changing water or stress conditions (Head, 2006).

**4.8 Soil Suction**

Soil suction testing was conducted on samples 1 and 2 from Site A, following the methodology laid out in Section 3.4.4. The total and matric Suction curves for both soils are provided in Figures 4.4 below.



a.



b.

**Figure 4. 4a and b:** Total and Matric soil suction curves for samples 1 and 2, respectively.

As indicated by the above curves, both samples from the Site A displayed similar soil suction behaviour. In general, both **total and matric** pore water suction of the samples decreased as the gravimetric moisture content increased. This concurs with the research that matric suction, although initially aiding slope stability under partial saturation, decreases or may even be lost entirely upon increasing water contents. Increases in water content ultimately reduce the positive effects of matric suction (Indraratna *et al*, 2015).

Research on the topic has found that presence of matric suction increases the soil elasticity as well as the internal angle of friction between soil particles. With increasing confining pressure, maximum shear stress occurs at a larger matric suction. Important correlations between effective cohesion ( $c'$ ), effective internal friction ( $f'$ ) and effective internal friction related to matric suction ( $fb'$ ), were observed by Abd, *et al* (2020). Firstly, effective cohesion ( $c'$ ) increased with increasing clay content and decreased with increasing sand content or increasing particle sizes. Secondly, effective internal friction ( $f'$ ) increased with increasing sand and particle sizes and decreased with increasing fines content. Internal friction related to matric suction ( $fb'$ ) showed no significant correlation to soil properties. The conclusion was that  $fb'$  was independent of soil properties and entirely dependent on matric suction itself. In general, it was found that the shear strength of a soil increases when the matric suction of that soil increased (Abd *et al*, 2020).

The soil-water characteristic curve (SWCC) is used to represent the relationship between volumetric water content and matric suction of the soil. The air entry value (AEV) of a soil, also known as the

bubbling pressure, is the matric suction where air starts to enter the largest pores of a soil. The AEV of a soil tends to increase with an increase in the plasticity of the soil. It is determined from the intersection of the extensions of tangent lines in the saturated zone and the transition zone, as shown in figure 4.5 below. (Fredlund and Xing, 1994; Hong *et al*, 2016).

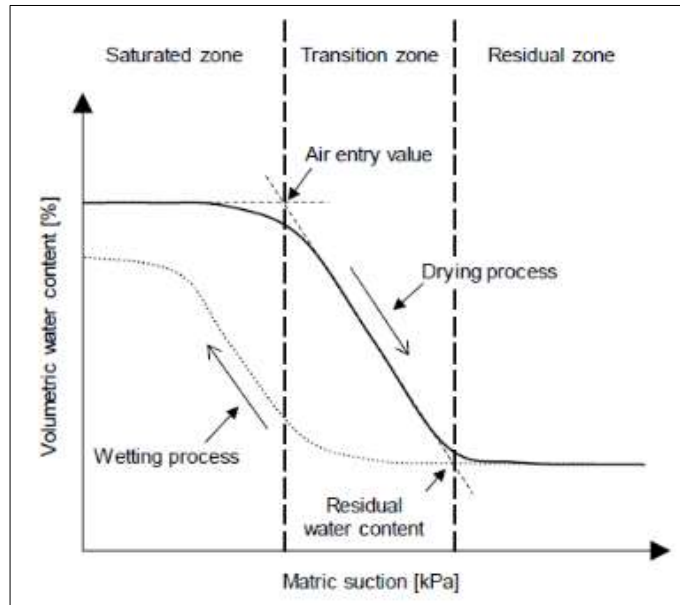


**Figure 4. 5:** Typical Soil-Water Characteristic Curve (SWCC) and zones (Hong *et al*, 2016).

Based on the filter paper dataset, both soils displayed desorptive **unimodal** shapes. As such, the test data best fitted the Fredlund and Xing (1994) SWCC model with a correction factor. These graphs were plotted on an online freeware software called SWRC fit, which is a nonlinear fitting program created by K. Seki (2007). They are provided in Figure 4.6a and b below. An optimiser was used to optimize the parametric models to the measured data, followed by an iterative exercise for the best sum of squared residuals (SSR). The sum of the SSR and Akaike information criterion (AIC) optimiser is an indication of how well the selected model fitted the measured soil suction data (Aneke *et al*, 2019).

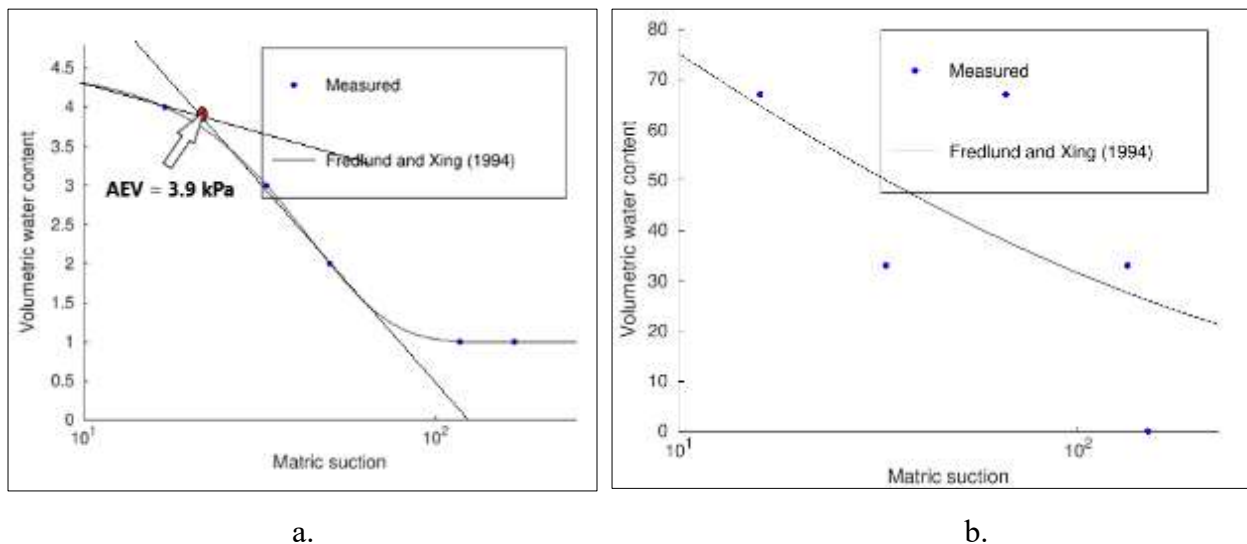
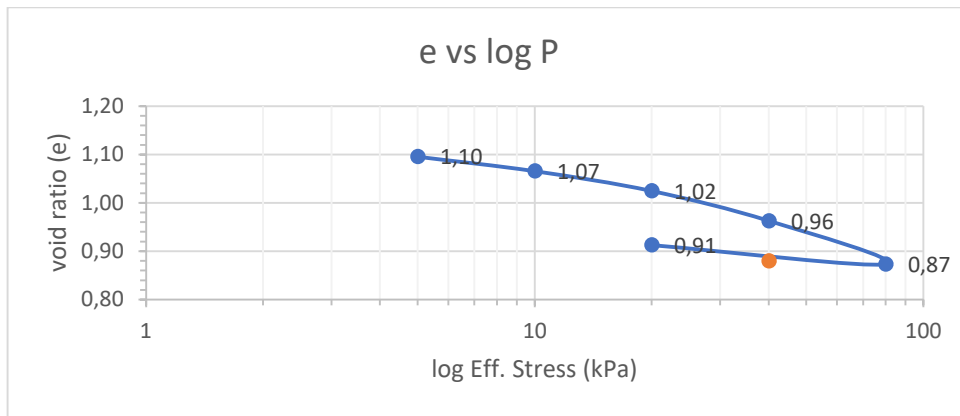


**Figure 4. 6a and b:** Soil-water Retention curves for a. Sample 1 and b. Sample 2 (Created on: SWRC Fit (<http://purl.org/net/swrc/>); Seki, 2007).

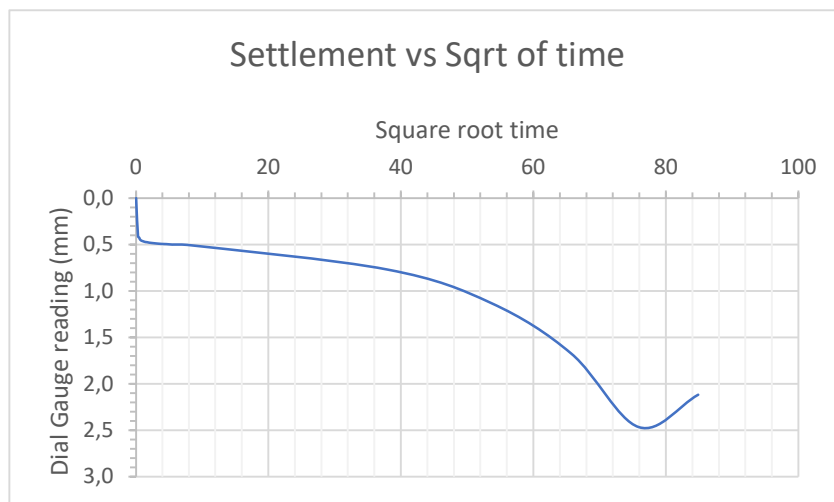
The SWCC for both samples of soil demonstrated increased suction as the volumetric water content decreases. This trend is consistent with other studies such as those conducted by Sivakumar and Wheeler (2000), and Agus and Schanz (2006). The AEV for Sample 1 was determined as approximately 3.9 kPa. This value was used in a Finite Element Analysis (FEA) and groundwater seepage analysis on RocScience Slide, to investigate the effect of matric suction on the pore pressures in the slope and the associated slope stability. This analysis is provided in Section 5.2.1 and discussed thereafter. The soil suction data for Sample 2 appears to be erroneous, as it did not fit the best fit curve or any predetermined trend. As such the AEV for sample 2 was not able to be determined.

#### 4.9 Consolidation

Samples 1 and 2 from Site A were put through consolidation testing under varying moisture contents, as detailed in Section 3.4.5 above. Void ratio versus effective stress was plotted to calculate the compression index ( $C_c$ ), swelling index ( $C_s$ ), coefficient of volume change ( $M_v$ ) and pre-consolidation pressure ( $P_p$ ). Settlement graphs were plotted to calculate the coefficient of consolidation ( $C_v$ ). The most important curves created from consolidation testing are void ratio ( $e$ ) versus effective stress (kPa) and horizontal settlement over time, which are provided in the figures below, followed by all tabulated results from consolidation testing.

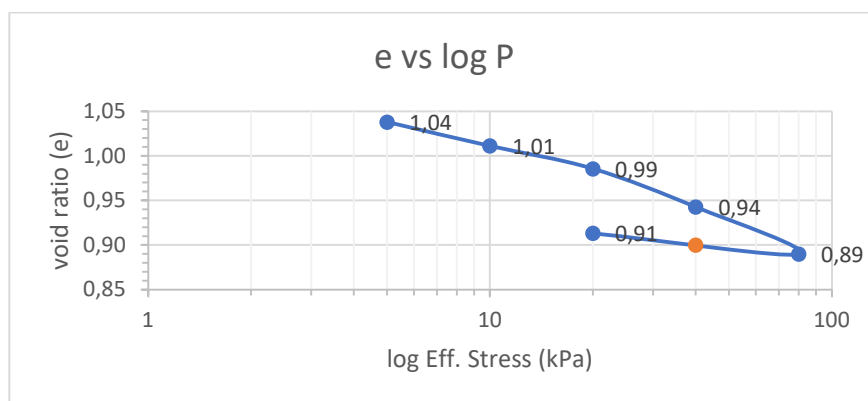


a.

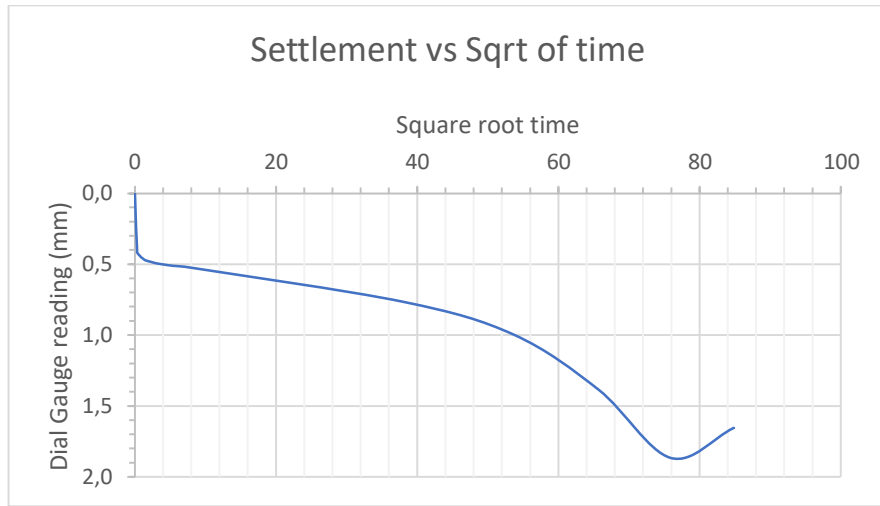


b.

**Figure 4. 7a and b:** Consolidation curves for Sample 1 at 12 % MC

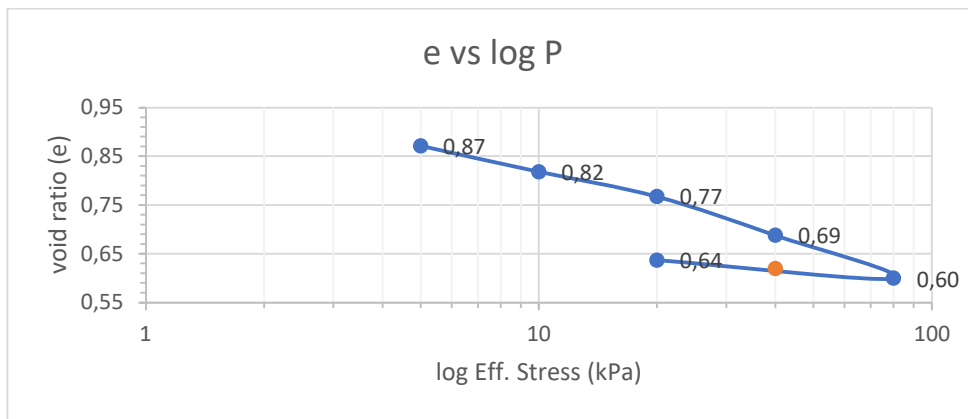


a.

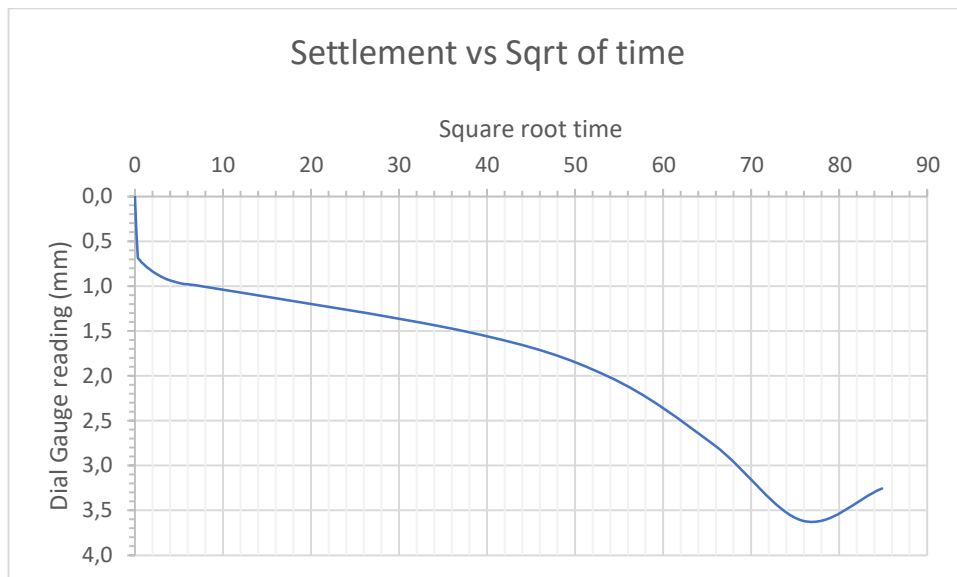


b.

**Figure 4. 8a and b:** Consolidation curves for Sample 1 at 19.56% MC



a.



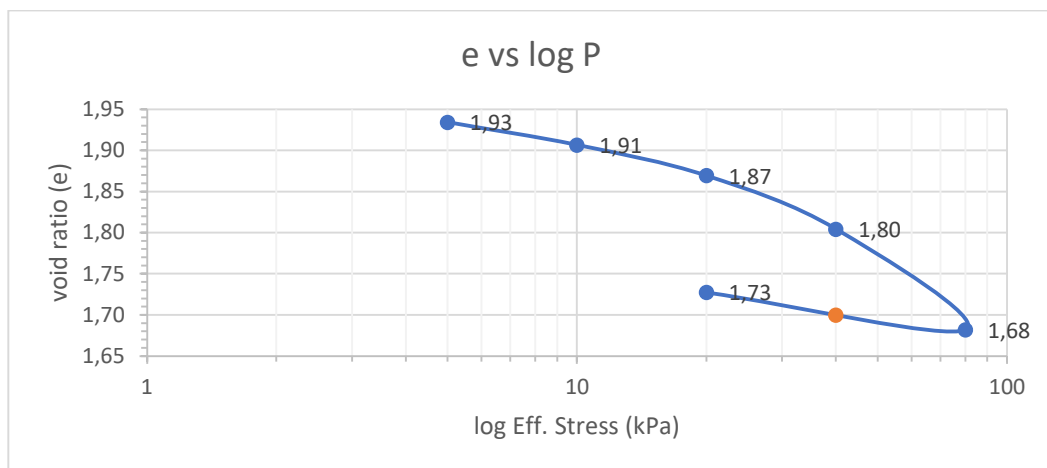
b.

**Figure 4. 9a and b:** Consolidation curves for Sample 1 at 25.76% MC

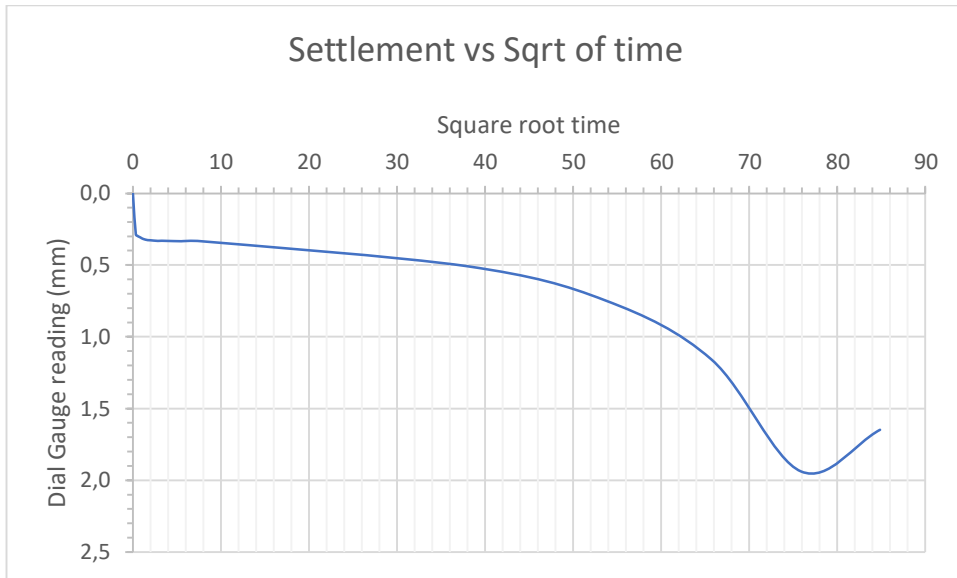
<b>Table 4. 8: <u>Sample 1</u> results from Consolidation testing</b>			
	<b>Dry – 12%</b>	<b>“OMC” - 19.56%</b>	<b>Wet – 25.76%</b>
Cc	0,205	0,143	0,264
Cs	0,110	0,044	0,057
Pp (kPa)	23.0	23,3	20.0
Mv	0,0014	0,0010	0,0020
Cv	6,043	1,595	0,210
<i>k</i> (m/s)	$2,69 \times 10^{-12}$	$5,07 \times 10^{-13}$	$1,31 \times 10^{-13}$

Comparison of results from Sample 1:

Both the Compression Index (Cc) and Swelling Index (Cs) showed significant increases under dry conditions, as compared to optimum and wet conditions. The Coefficient of Consolidation (Cv) as well as the Coefficient of Permeability (*k*) also exhibited large increases under dryer conditions as opposed to wetter conditions. This implies that under dryer conditions, Sample 1 experiences greater permeability where water travels through the soil mass quickly, possibly leading to less build-up of pore water pressure. This also implies less soil-water interaction in the dry condition, which can sometimes be a positive factor due to the effects of matric suction.

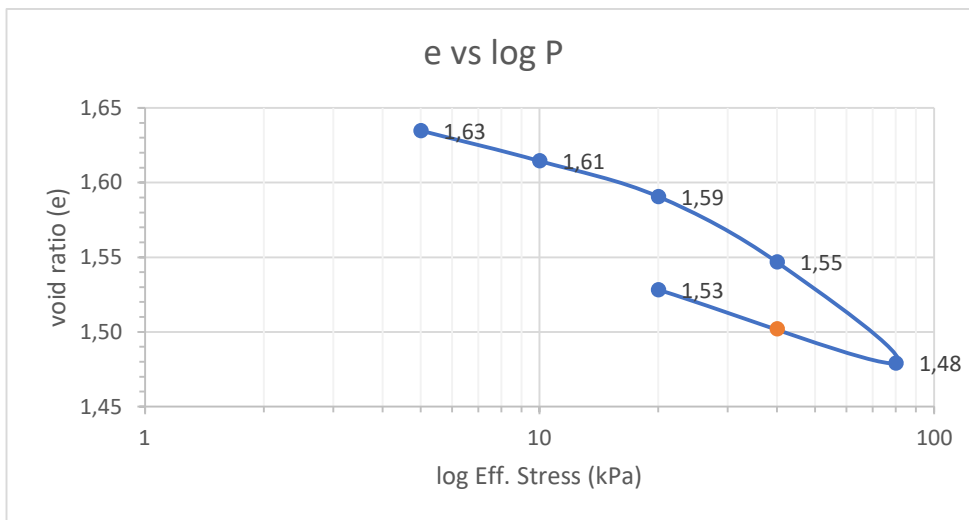


a.

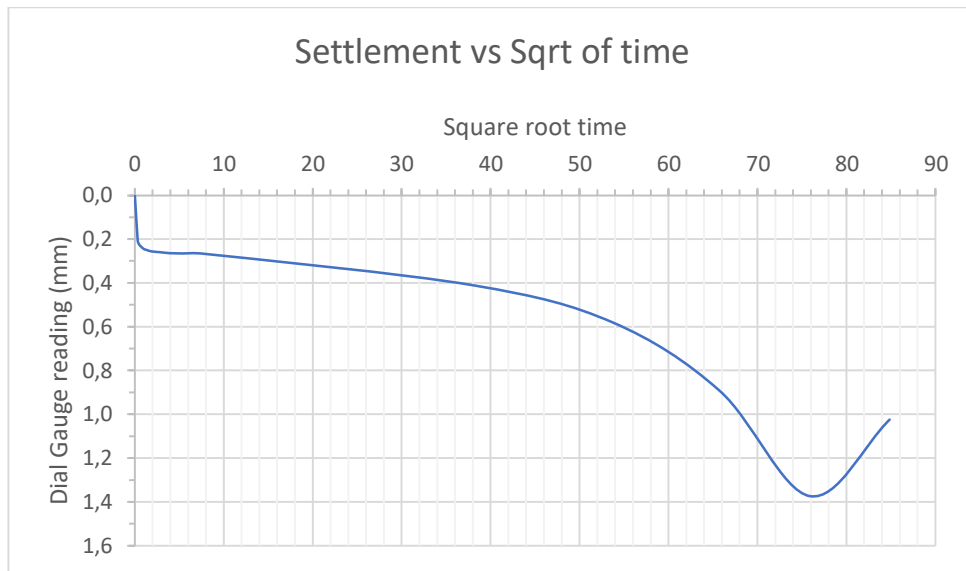


b.

**Figure 4. 10a and b:** Consolidation curves for Sample 2 at 12% MC

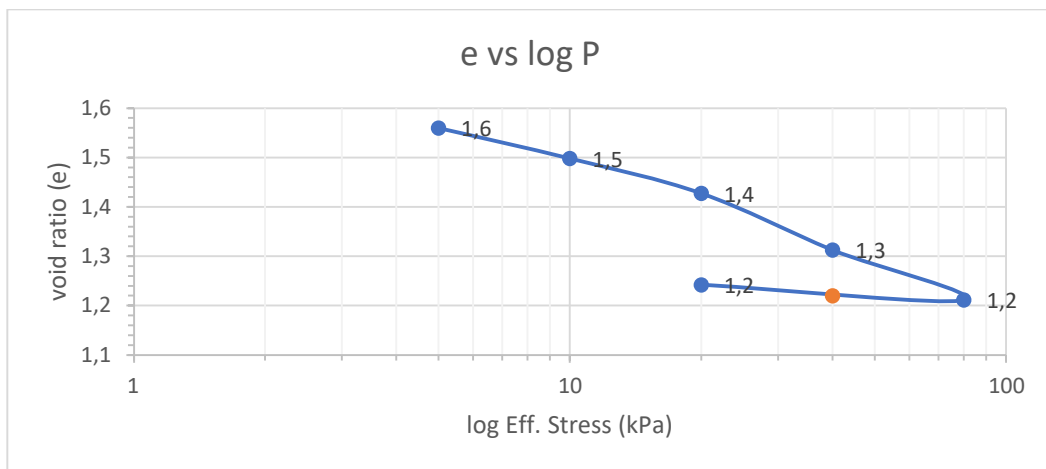


a.

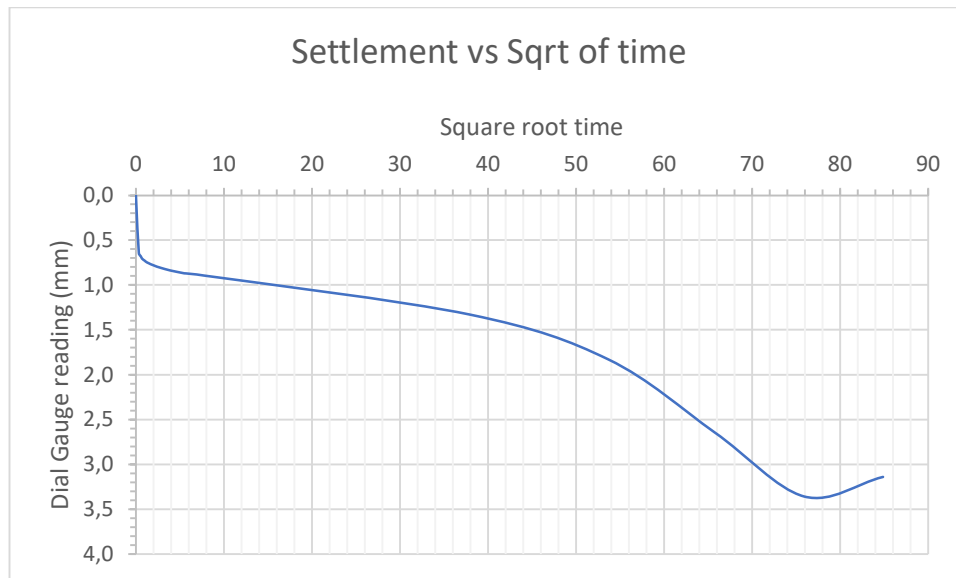


b.

**Figure 4. 11a and b:** Consolidation curves for Sample 2 at 17.79% MC.



a.



b.

**Figure 4. 12a and b:** Consolidation curves for Sample 2 at 21.80% MC

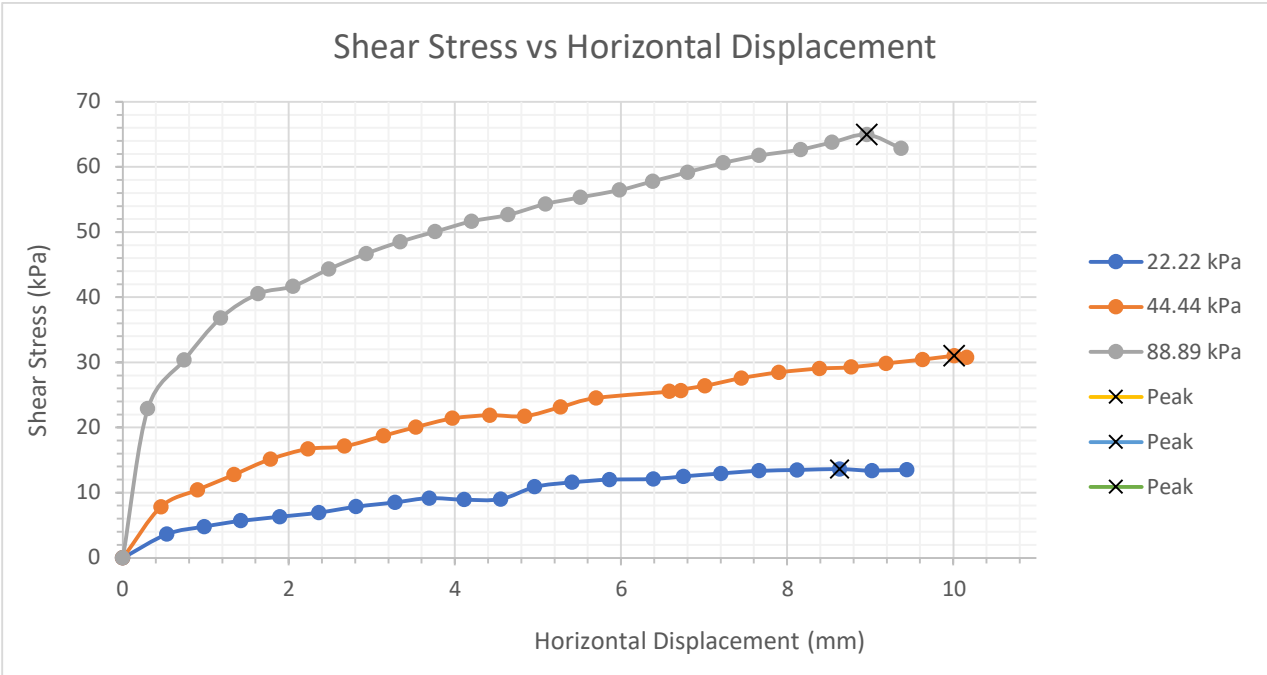
<b>Table 4. 9: <u>Sample 2</u> results from Consolidation testing</b>			
	<b>Dry – 12%</b>	<b>“OMC” – 17.79%</b>	<b>Wet – 21.80%</b>
Cc	0,216	0,146	0,382
Cs	0,092	0,087	0,074
Pp (kPa)	31	30	20
Mv	0,0011	0,0008	0,0021
Cv	1,596	1,713	1,477
$k$ (m/s)	$5,39 \times 10^{-13}$	$4,36 \times 10^{-13}$	$9,80 \times 10^{-13}$

Comparison of results from Sample 2:

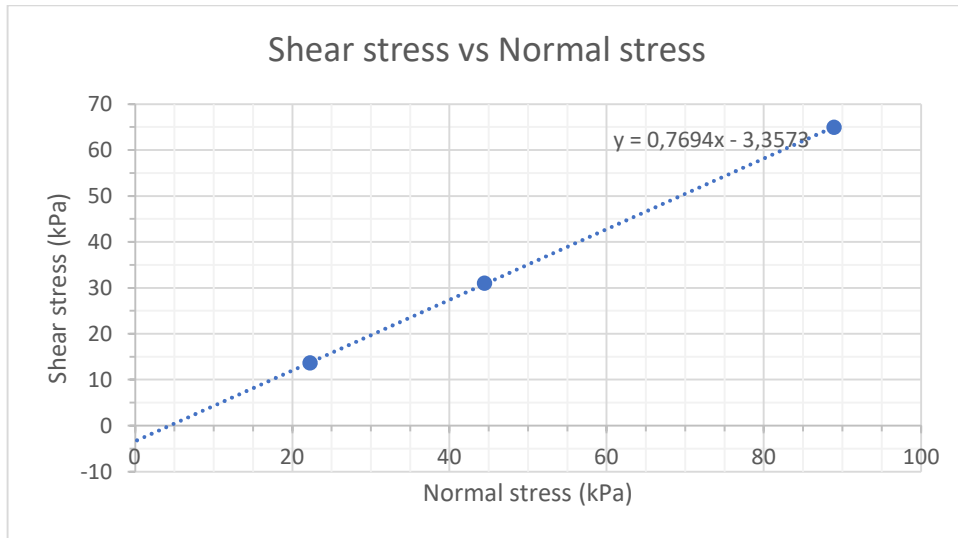
The Compression Index (Cc) increased under “wet” conditions, as compared to optimum and “dry” conditions. The Pre-consolidation Pressure (Pp) dropped significantly from 30 kPa at OMC to 20 kPa in “wet” conditions. The permeability of the sample increased significantly under wetter conditions, as indicated by the large increase in the  $k$  value. The Coefficient of Consolidation (Cv) remained fairly similar under all 3 testing conditions, possibly due to the fact that this sample is derived from weathered rock, crushed down where necessary to form a soil.

**4.10 Direct Shear Box tests**

Due to extensive delays encountered in obtaining the Triaxial test results, a series of Direct Shear Box (DSB) tests were conducted on Samples 1, 3 and 4, to produce the required shear strength parameters (i.e., cohesion and angle of internal friction). A total of 27 DSB tests were performed, as each sample was tested under 3 water conditions - “dry”, “optimum”, and “wet” - and 3 different normal loads – 22, 44 and 88 kPa. Due to COVID-19 lockdown and further delay in obtaining results from the external laboratory, the compaction properties obtained in the UKZN soils laboratory (which are considered less accurate than those provided by the external laboratory) were used here. The moisture contents and conditions used to conduct the DSB tests are provided in the summary tables below. DSB testing was performed according to the method detailed in Section 3.4.7 above. The graphs of shear stress versus horizontal displacement, and the failure envelopes (shear stress vs normal stress) are provided in the figures below. The calculated total cohesion and total internal friction results from DSB testing are provided in the tables below. The results from triaxial testing (provided in Section 4.11 below) will provide effective shear strength parameters, which are more accurate and will therefore be used in the slope stability analyses in Chapter 5.

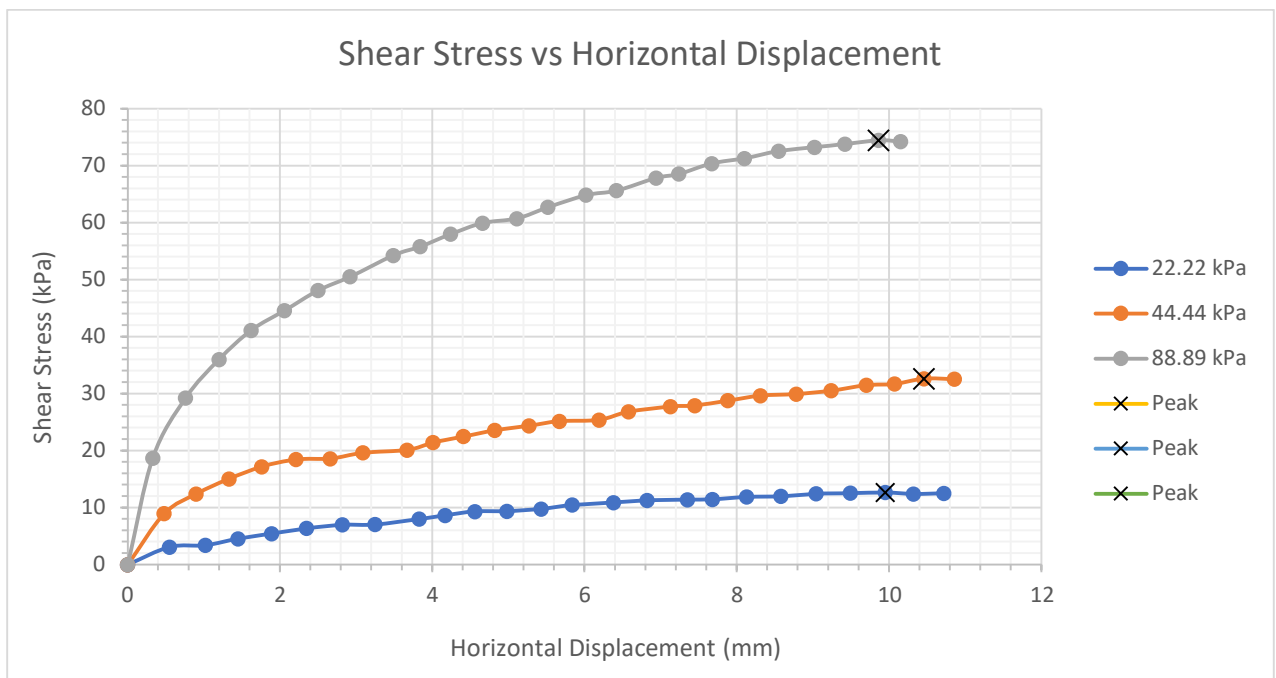


a.

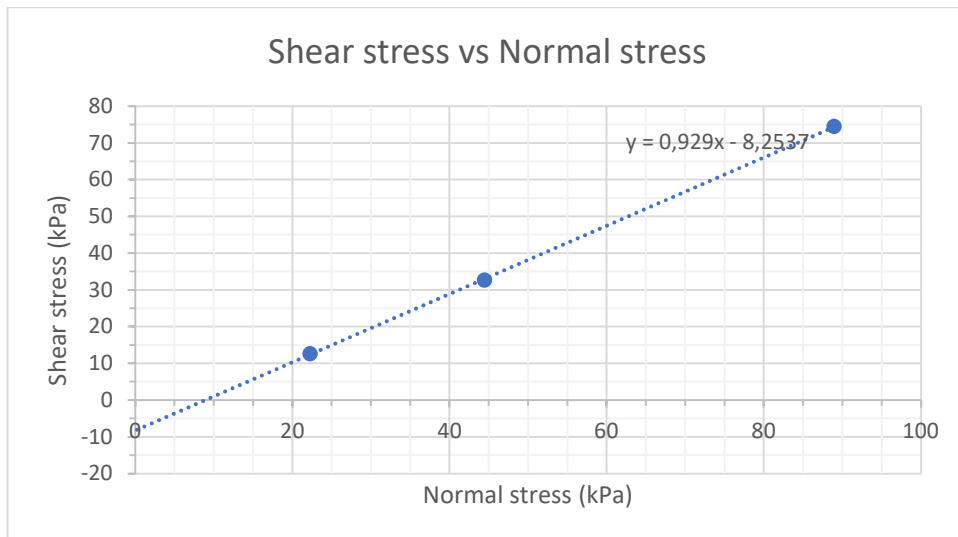


b.

**Figure 4. 13a and b:** Shear stress curves for Sample 1 at 12% MC

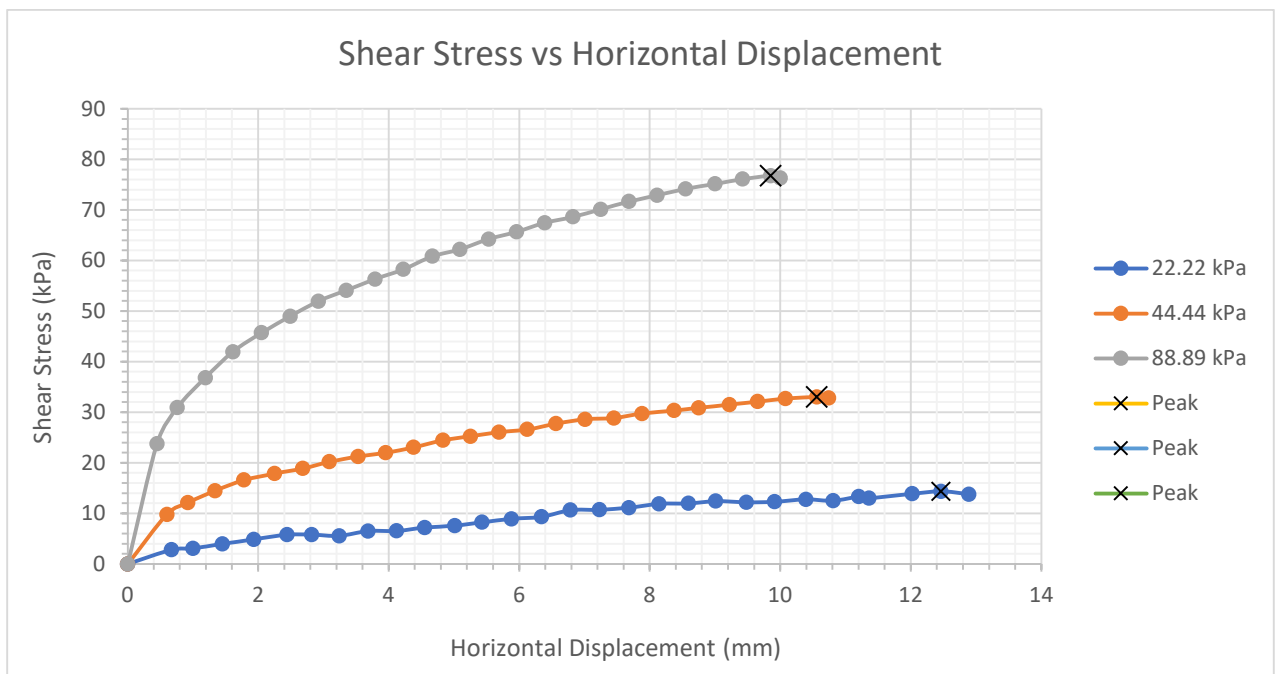


a.

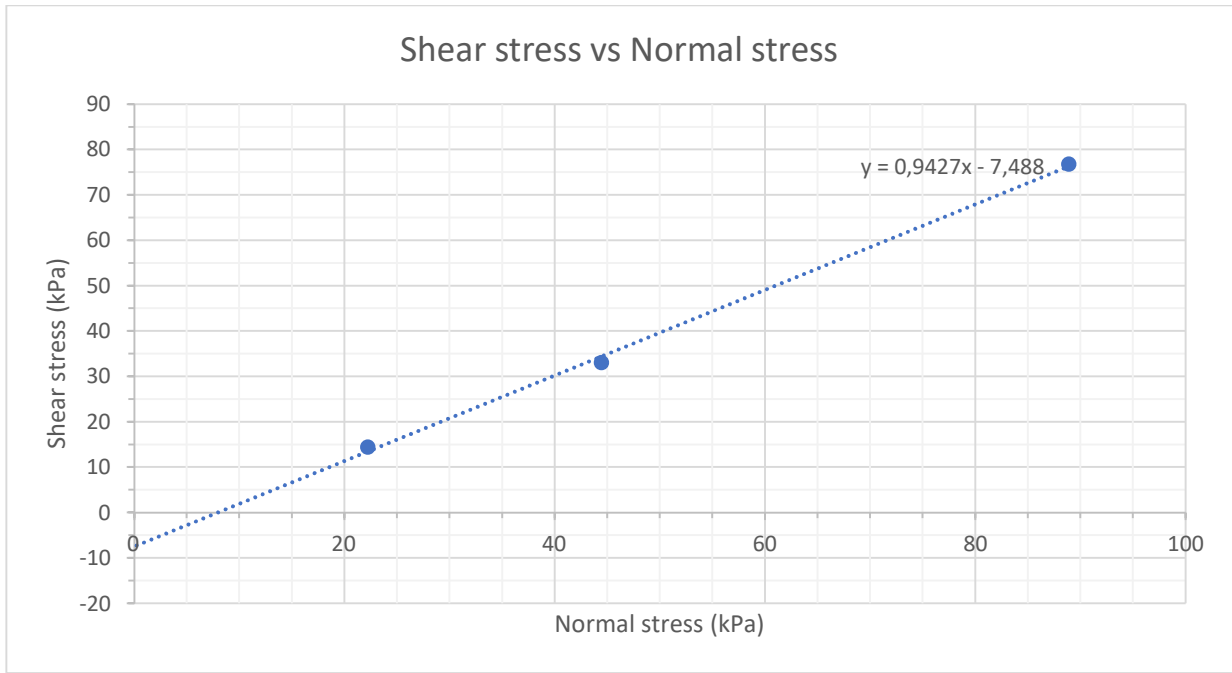


b.

**Figure 4. 14a and b:** Shear stress curves for Sample 1 at 19.56% MC



a.

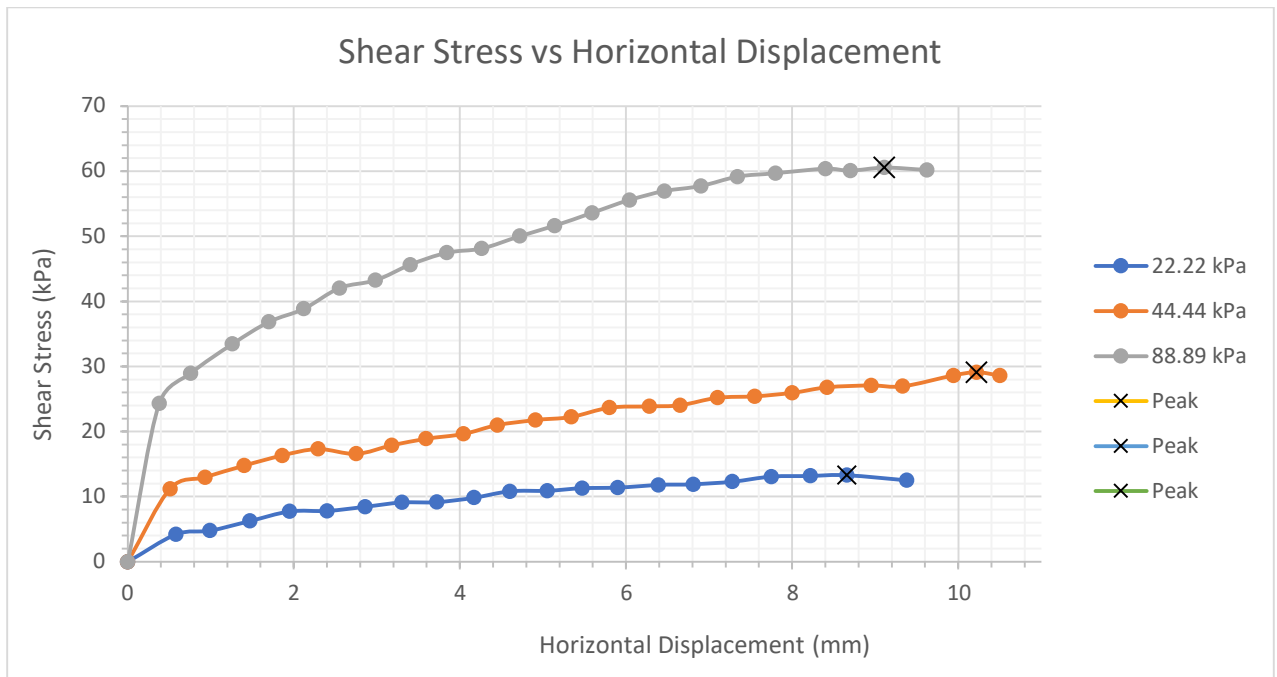


b.

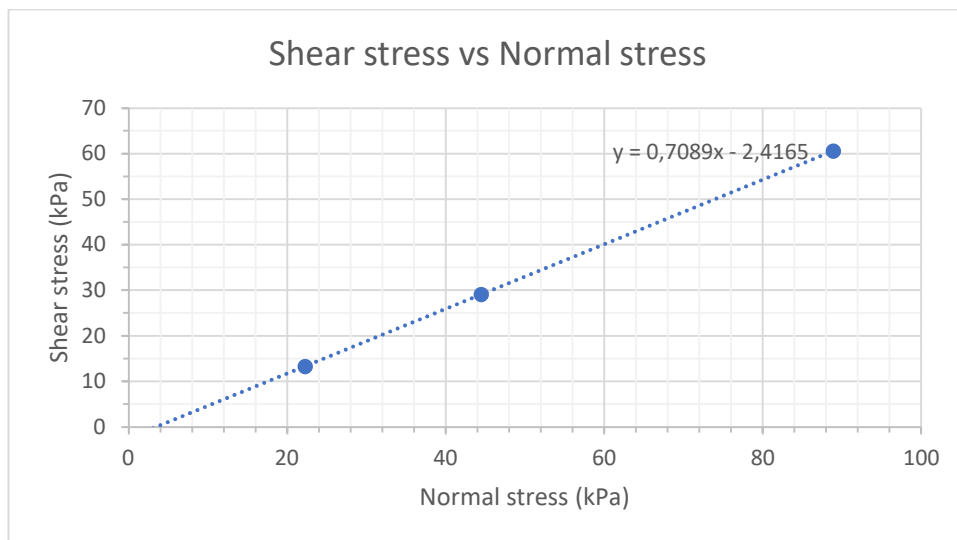
**Figure 4. 15a and b:** Shear stress curves for Sample 1 at 22.34% MC

<b>Table 4. 10: <u>Sample 1</u> results from DSB testing</b>			
	<b>Dry – 12%</b>	<b>“OMC” - 19.56%</b>	<b>Wet – 22.34%</b>
C	0	0	0
$\phi$	37,58	42,89	43,31

The results from Sample 1 indicate that this sand is cohesionless. The angle of internal friction is similar under optimum water conditions and in wetter conditions, however it decreases significantly under dryer conditions or decreasing water content. This implies that the introduction of water into this soil is a positive influence on the soil strength properties up to a certain extent. This soil is more prone to failure without sufficient water content or in dryer conditions.

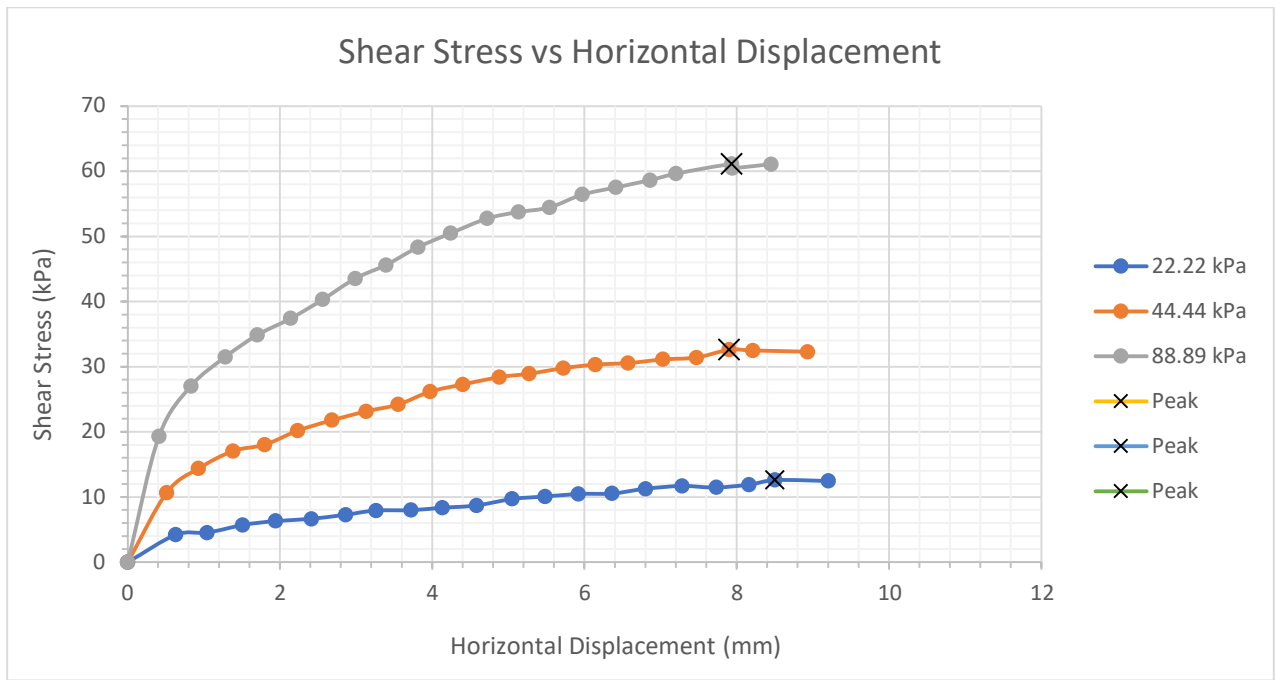


a.

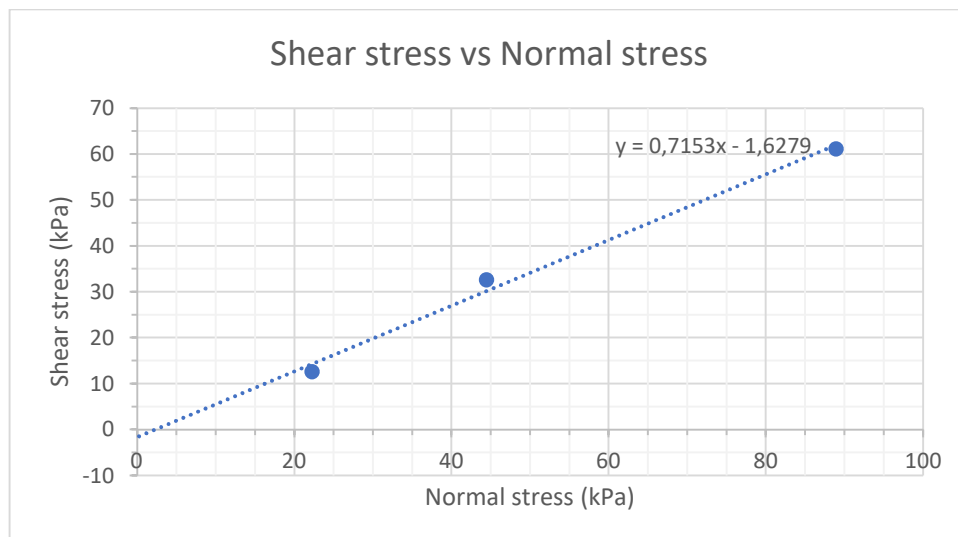


b.

**Figure 4. 16a and b:** Shear stress curves for Sample 3 at 9% MC

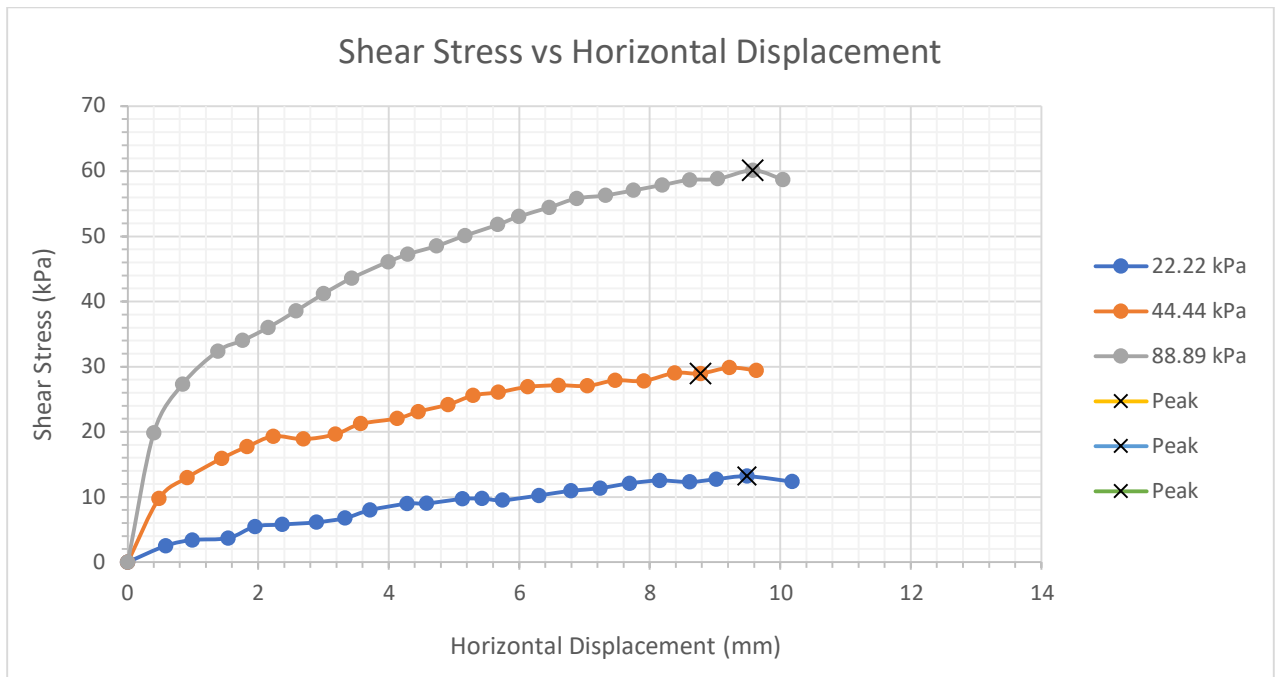


a.

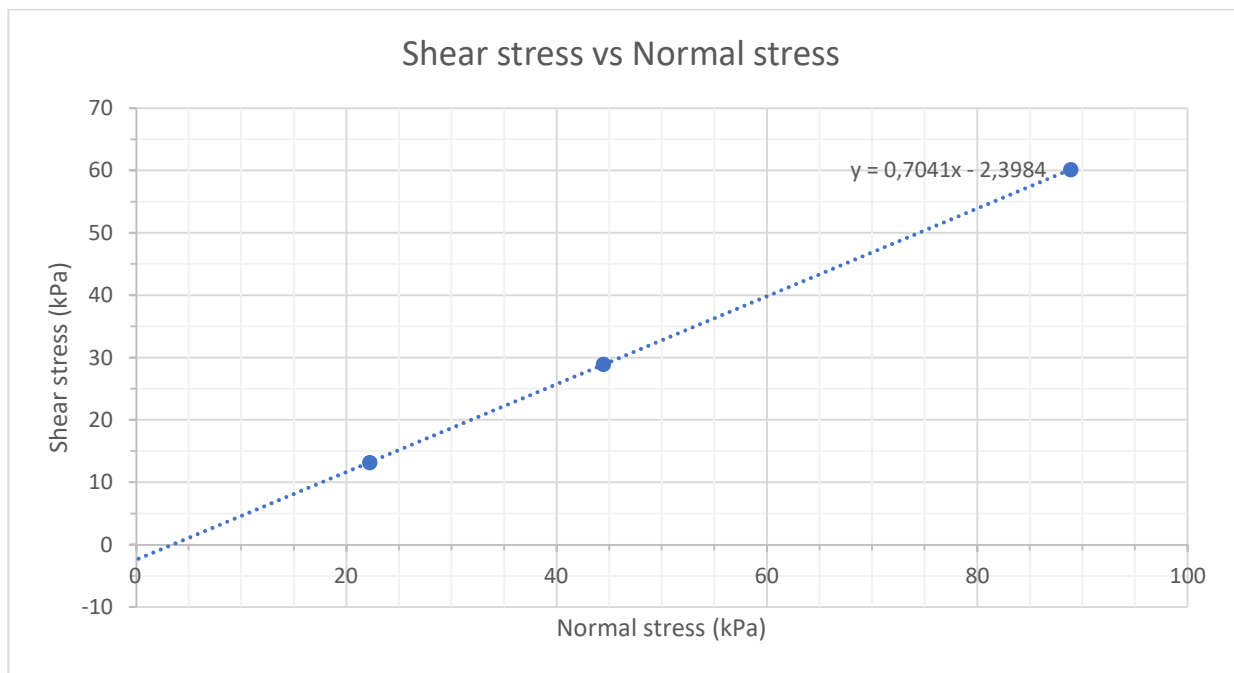


b.

**Figure 4. 17a and b:** Shear stress curves for Sample 3 at 12% MC



a.

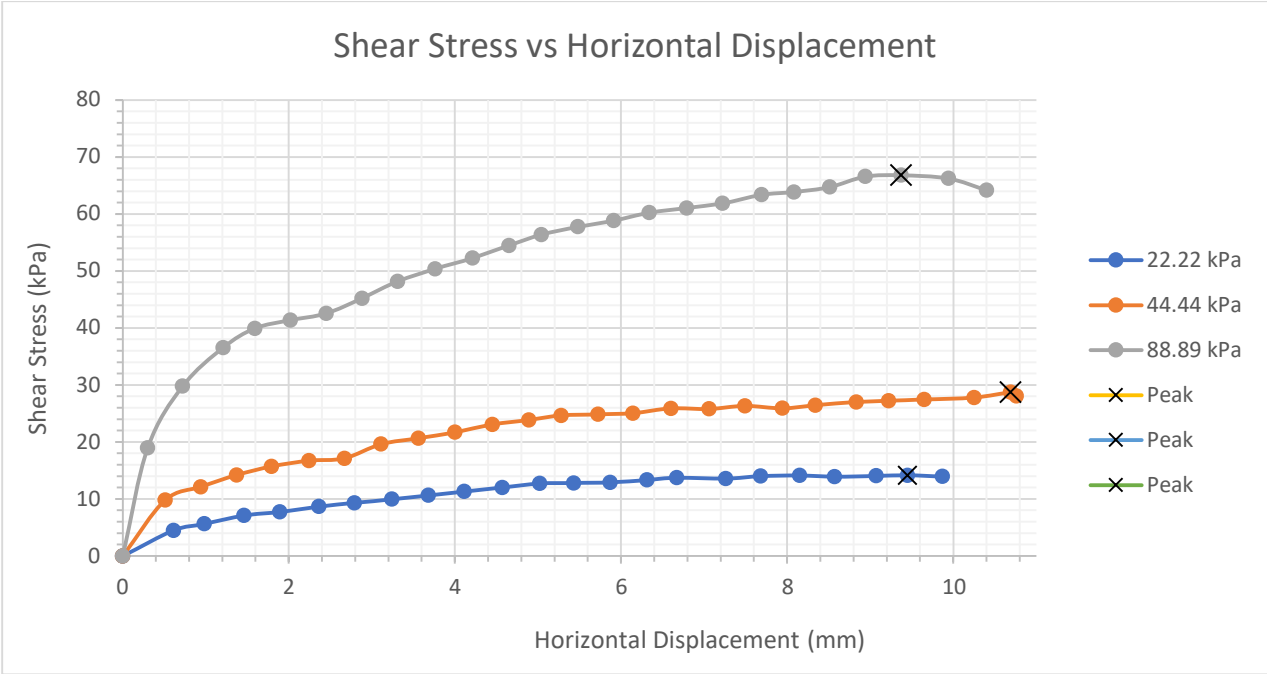


b.

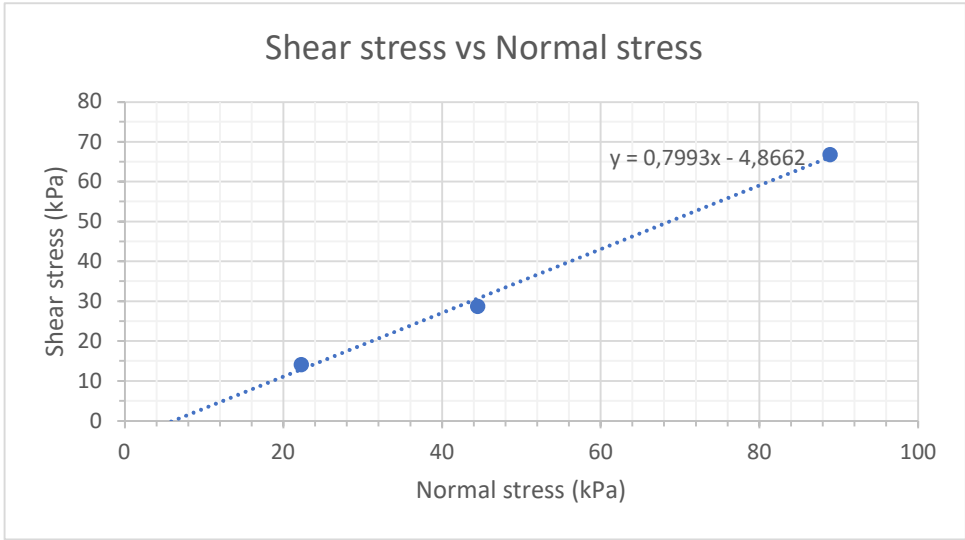
**Figure 4. 18a and b:** Shear stress curves for Sample 3 at 14% MC

<b>Table 4. 11: <u>Sample 3</u> results from DSB testing</b>			
	<b>Dry – 9%</b>	<b>“OMC” – 12%</b>	<b>Wet – 14%</b>
C	0	0	0
$\phi$	35,33	35,58	35,15

The results from Sample 3 indicate that this Berea sand is cohesionless in all water conditions. There is also no significant change in the angle of internal friction, regardless of water content.

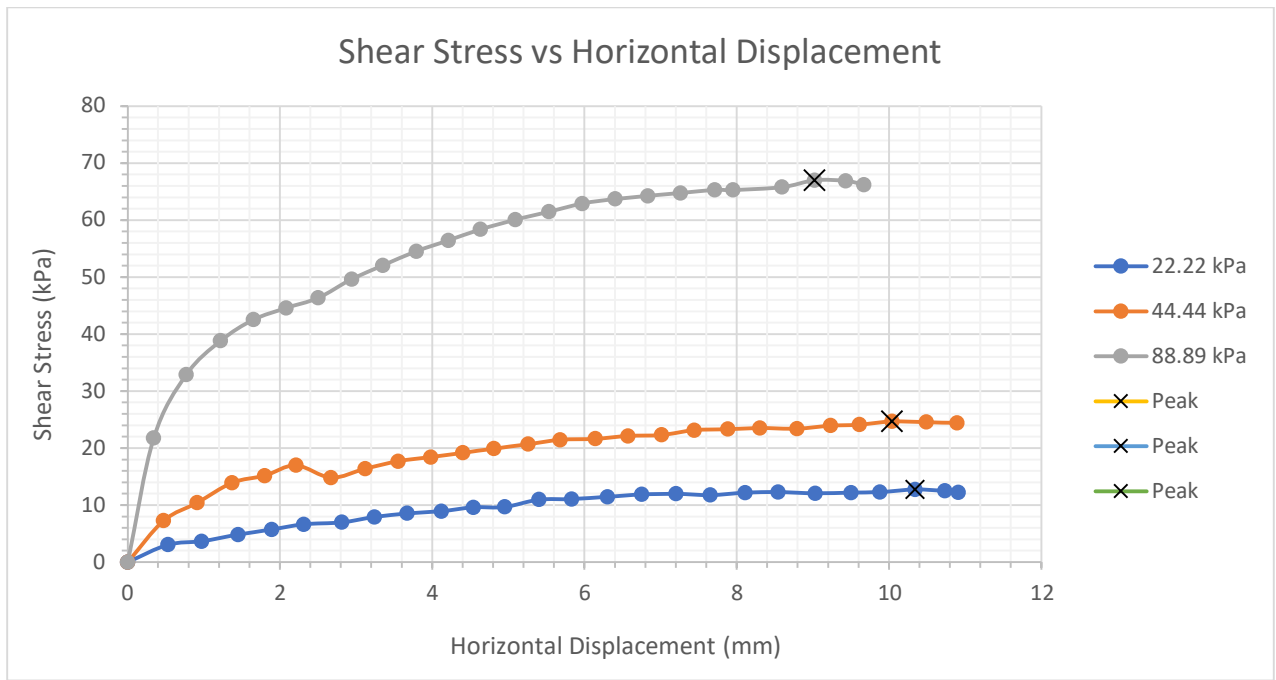


a.

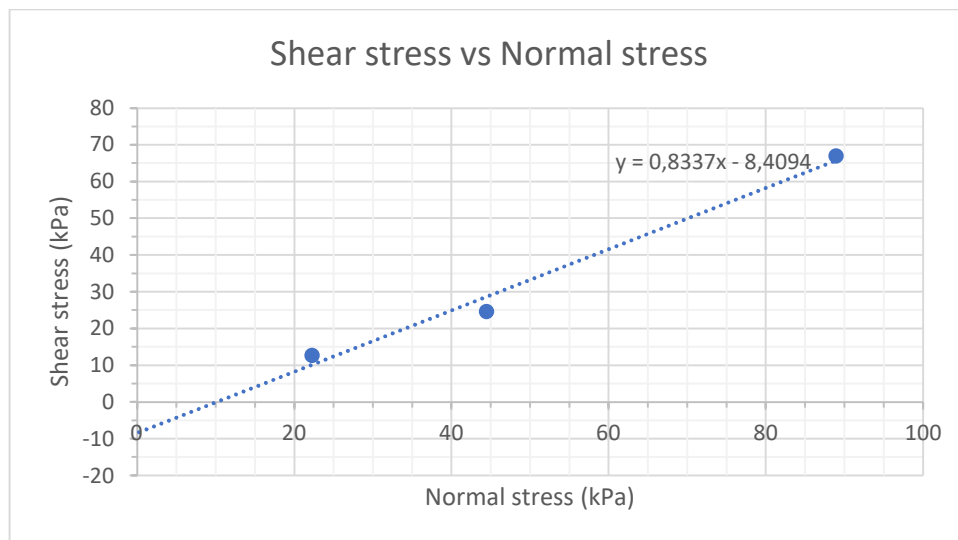


b.

Figure 4. 19a and b: Shear stress curves for Sample 4 at 8% MC

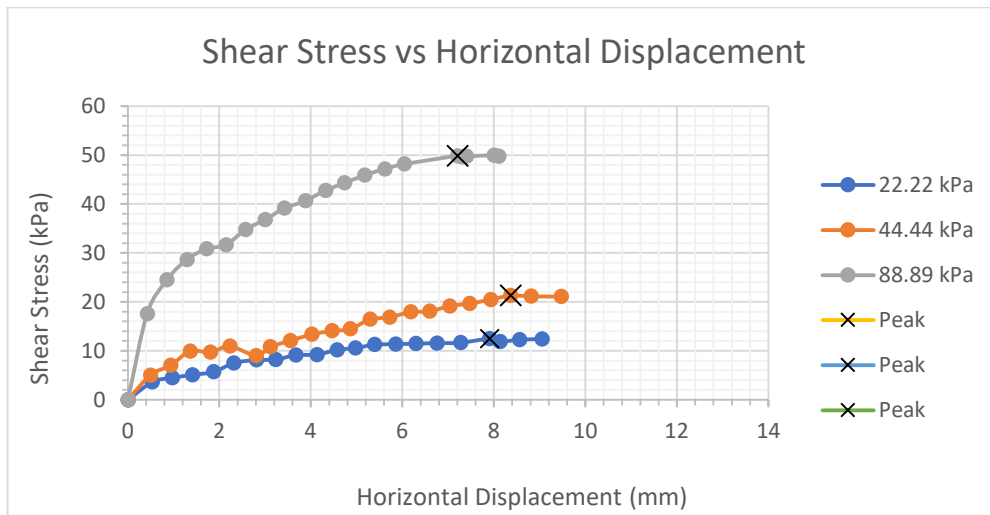


a.

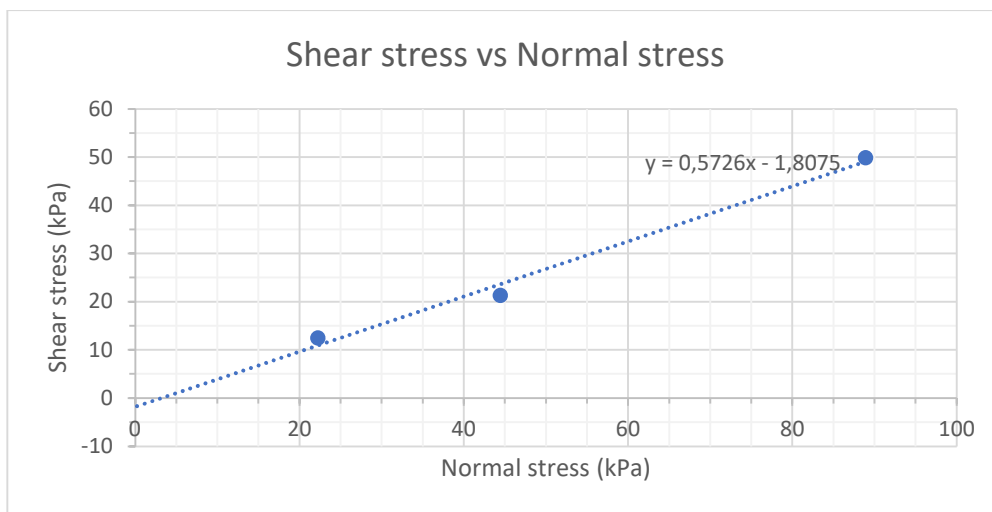


b.

**Figure 4. 20a and b:** Shear stress curves for Sample 4 at 12% MC



a.



b.

**Figure 4. 21a and b:** Shear stress curves for Sample 4 at 13.41% MC

<b>Table 4. 12: <u>Sample 4</u> results from DSB testing</b>			
	<b>Dry – 8%</b>	<b>“OMC” – 12%</b>	<b>Wet – 13.41%</b>
C	0	0	0
φ	38,64	39,82	29,80

The results from Sample 4 indicate that the beach sands are cohesionless in all water conditions. The angle of internal friction is observed to decrease significantly upon increasing water content. This implies that the soil becomes more prone to failure upon the introduction of water, and in wetter conditions.

**4.11 Triaxial tests - Consolidated Undrained**

Consolidated Undrained (CU) Triaxial tests were performed on all soils taken from the 2 sites, namely samples 1, 3 and 4. Sample 2 was excluded for triaxial testing as it was considered rock instead of soil for the purpose of the slope stability analyses. The triaxial tests were subcontracted to Civilab (Pty) Ltd. Unlike the case with DSB testing, which were conducted at 3 varying moisture conditions, the triaxial tests were conducted at optimum conditions, that is OMC and MDD as obtained from the results of the compaction tests conducted at Soilco. (Section 4.7). The Mohr-Coulomb failure envelopes as provided by the external laboratory are provided in the figures 4.22-4.24 below. The results from Triaxial testing such as the deviator stress, axial strain at failure, confining stresses used to plot the Mohr circles ( $\sigma_1'$  and  $\sigma_3'$ ), excess pore water pressure, total and effective cohesion ( $C_T$  and  $C'$ ) and internal angles of friction ( $\sigma_T$  and  $\sigma'$ ), are all summarised in the tables below.

<b>Table 4. 13:</b> Results from Triaxial Testing conducted at optimum conditions						
	OMC (%)	MDD ( $Kg/m^3$ )	$C_T$	$C'$	$\sigma_T$	$\sigma'$
Sample 1	8.7	1816	24.2	<b>6.4</b>	25.3	<b>33.2</b>
Sample 3	12	1876	14	<b>1.7</b>	26.3	<b>41.5</b>
Sample 4	8.3	1830	15.2	<b>7.6</b>	30.3	<b>32.1</b>

The following observations were made regarding the above triaxial results. The total cohesion of the samples was much greater than the actual or effective cohesion. Effective cohesion is the more accurate result as it considers the effects of pore water pressure on the shear strength of the samples (Gibbs and Coffey, 1969). Evidently, without considering the effects of pore water pressure, the cohesion of a sample is grossly over-conservative, and may imply a slope that is safe, when it is far from it. Similarly, the total angle of internal friction is significantly less than the actual/effective values, results which are also misleading of a slopes safety. With regards to the samples excess pore water pressures ( $\mu_p$ ) during triaxial testing, sample 1 from Site A and sample 3 from Site B both exhibit positive pore pressures, indicating soil saturation. This is the expected scenario, as samples are left to achieve saturation prior to starting triaxial testing. In contrast, Sample 4, which is the beach sand above and below the water table (sea level), exhibits negative pore water pressures. This is due to suction in soil voids above the water table when they become partly filled with water as a result of capillary rise from the water table below (Gibbs and Coffey, 1969)

**Table 4. 14:** Summary of results from set of Triaxial tests on Sample 1

Rate of Strain (%/hour)	0.3	Dry Density (kg/m <sup>3</sup> )	MC (%)	Cell Pressure (kPa)	Deviator stress at failure (kPa)	Axial strain at failure (%)	Membrane correction	Excess pore pressure (kPa)	Effective Principal stress ratio	$\sigma_1'$	$\sigma_3'$
Specimen A		1719	13.4	50	140.3	2.53	1.1	0.3	3.811	190.2	49.9
Specimen B		1707	12.9	100	242.2	2.91	0	12.5	3.784	329.3	87
Specimen C		1681	13.6	200	367.4	3.08	1.1	56.7	3.566	510.6	143.2

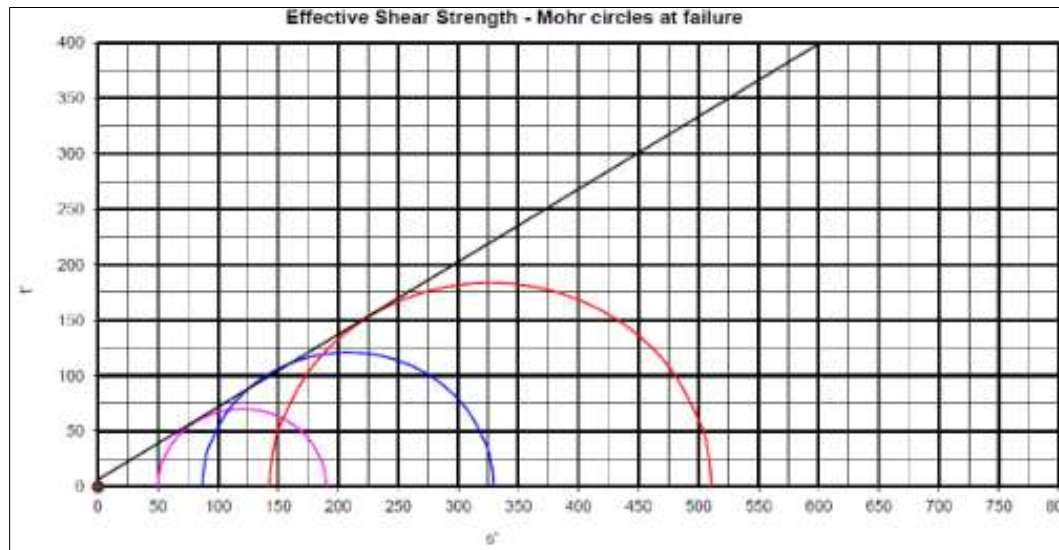


**Figure 4. 22:** Mohr-Coulomb circles and failure envelope for Sample 1.

<b>Table 4. 15:</b> Summary of results from set of Triaxial tests on Sample 3											
Rate of Strain (%/hour)	0.3	Dry Density (kg/m <sup>3</sup> )	MC (%)	Cell Pressure (kPa)	Deviator stress at failure (kPa)	Axial strain at failure (%)	Membrane correction	Excess pore pressure (kPa)	Effective Principal stress ratio	$\sigma_1'$	$\sigma_3'$
Specimen A		1728	12.3	50	117.3	2.44	1.1	19.6	5.093	146	28.7
Specimen B		1716	13.7	100	208.4	2.15	1.1	48.1	5.172	258.4	50
Specimen C		1768	13.4	200	362.7	2.34	1.1	109.8	4.992	453.6	90.9

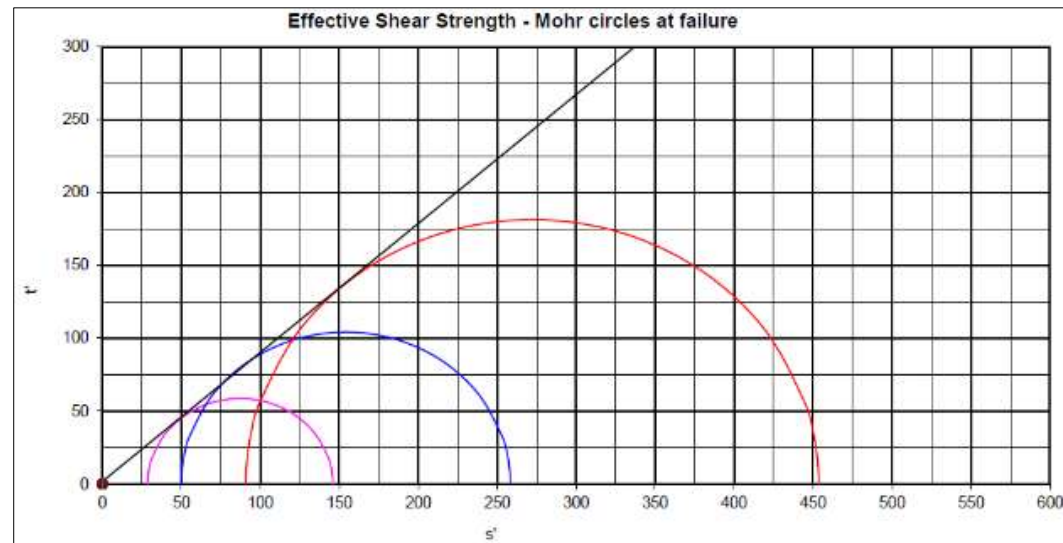


**Figure 4. 23:** Mohr-Coulomb circles and failure envelope for Sample 3.

<b>Table 4. 16:</b> Summary of results from set of Triaxial tests on Sample 4											
Rate of Strain (%/hour)	0.3	Dry Density (kg/m <sup>3</sup> )	MC (%)	Cell Pressure (kPa)	Deviator stress at failure (kPa)	Axial strain at failure (%)	Membrane correction	Excess pore pressure (kPa)	Effective Principal stress ratio	$\sigma_1'$	$\sigma_3'$
Specimen A		1572	9	50	147.4	2.02	1.1	-6.6	3.686	202.2	54.9
Specimen B		1577	8.9	100	263.9	2.16	1.1	-1.1	3.609	365	101.1
Specimen C		1588	8.8	200	466.4	4.04	1.1	8.8	3.395	661.2	194.7

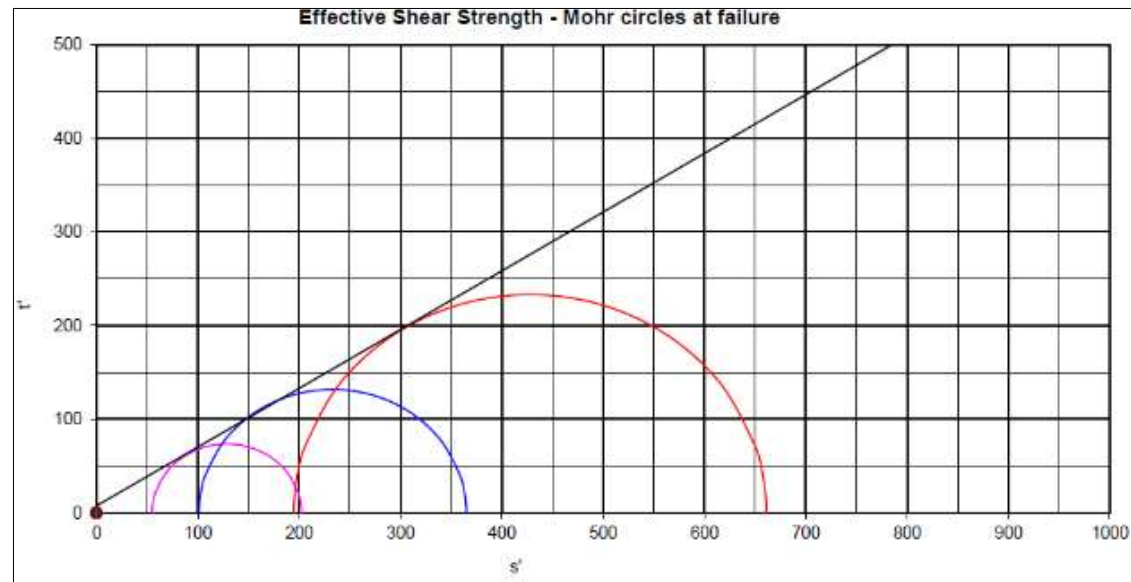


**Figure 4. 24:** Mohr-Coulomb circles and failure envelope for Sample 4.

#### 4.12 Summary of laboratory results for Site A

The soils from Site A, Samples 1 and 2, were both classified as well graded, gravelly SANDS, as per the Unified Soil Classification System (USCS). The *in situ* or natural moisture content (NMC) was 9.5%. Both samples displayed relatively low void ratios ( $e$ ) and porosities ( $n$ ) as a result of the well graded nature of the soils, with smaller particles infilling the voids in the soil mass. The two soils from Site A are considered fairly similar in their soil characteristics and behaviour. Their average Atterberg Limits were  $LL = 31.75\%$ ,  $PL = 19.28\%$ ,  $SL = 34\%$  and  $PI = 12.48\%$ , with zero swelling potential. The topsoil from Site A, Sample 1, yielded an OMC of 8.7% in order to achieve a MDD of  $1816 \text{ Kg/m}^3$ . Sample 2 compaction characteristic was unreliable as the sample was mostly bedrock which was occasionally recovered as soil. Both total and matric pore water suction of the samples decreased as the gravimetric moisture content increased. The SWCC for both samples of soil demonstrated increased suction with a decrease in volumetric water content. The AEV for Sample 1 was determined as approximately 3.9 kPa, whereas the AEV for Sample 2 was not able to be determined. Sample 1 experienced greater permeability under dryer conditions, whereas the permeability of Sample 2 increased significantly under wetter conditions. The DSB results of Sample 1 indicate that the sand is cohesionless. The angle of internal friction is similar under optimum and wet water conditions; however it decreases significantly under dryer conditions. This implies that the introduction of water into this soil is a positive influence on the soil strength properties up to a certain extent. The topsoil (sample 1) on Site A is more prone to failure without sufficient water content, or in dryer conditions. The triaxial test results of Sample 1 at OMC, yielded an effective cohesion of 6.4 kPa and an internal angle of friction of  $33.2^\circ$ , which were used in the slope stability analysis. No triaxial tests were performed on Sample 2.

#### 4.13 Summary of laboratory results for Site B

The soils from Site B, Samples 3 and 4, were both classified as slightly gravelly, fine grained SANDS, as per the Unified Soil Classification System (USCS). The *in situ* or natural moisture content was 27.75 %, with zero swelling potential. Both soils were poorly graded, and gap graded with high contents of only sand size particles and very little to none of other soil sizes. Due to the uniformity and well-rounded nature of the beach sands, the samples from Site B yielded very high void ratios (average of 71.97), with low to no incidence of particle interlocking or void infilling. The Atterberg Limits for Samples 3 and 4 could not be easily or accurately obtained because the samples were failing at all water contents and could not retain any shape, due to the high sand

content and lack of fines. The NMC (27.75 %) of the soils from Site B was already much higher than their calculated LL's (~17%) indicating that the soils were in a potential state of liquefaction when they were first collected from site. The samples from Site B yielded an average OMC of 10% to achieve an average MDD of 1853 Kg/m<sup>3</sup>. The DSB results from Sample 3 indicate that this Berea sand was cohesionless in all water conditions, with no significant change in the angle of internal friction. Sample 4 beach sands were also cohesionless in all water conditions, however the angle of internal friction was observed to decrease significantly upon increasing water content. This implies that the soil becomes more prone to failure upon the introduction of water. The triaxial test results of Sample 3 at OMC, yielded an effective cohesion of 1.7 kPa and an internal angle of friction of 41.5°. The triaxial test results of Sample 4 at OMC, yielded a higher effective cohesion of 7.6 kPa and a lower internal angle of friction of 32.1°.

## CHAPTER FIVE

### SLOPE STABILITY ANALYSES

---

#### 5.1 Introduction

The measurements and parameters obtained from each site during fieldwork, were used to model the 2 sites to scale, using RocScience© Slide2© software. Material properties (table 5.1), as determined from laboratory testing, or published data where necessary, were input to provide more accurate models of the site and *in-situ* conditions. Laboratory tests were conducted under varying moisture conditions, with the aim of analysing the soil variability and subsequent slope reaction with a change in moisture content. Conditions assessed were “dry” with a moisture content below the optimum, “optimum” at optimum moisture content (OMC) and “wet”, with moisture content above the optimum. The table below summarises the materials on site, the parameters input, and the methods used to obtain them.

<b>Table 5. 1:</b> Summary of materials and material properties				
	Sample No.	Material Description	Material property	Source
Site A	1	Residual Diamictite	1) Unit weight ( $\gamma$ ) 2) Total Cohesion ( $C_T$ ) 3) Effective Cohesion ( $C'$ )	1) Published values (BS 8002:1994) 2) Results of Direct Shearbox tests
	2	Diamictite rock	4) Total Angle of Internal Friction ( $\sigma_T$ )	3) Results of Triaxial Tests
Site B	3	Berea sand	5) Effective Angle of Internal Friction ( $\sigma'$ )	4) Results of Direct Shearbox tests
	4	Beach sand		5) Results of Triaxial Tests

The effective shear strength parameters ( $c'$  and  $\phi'$ ) obtained from triaxial testing are considered to be reliable and accurate. These were conducted at the soils optimum condition (OMC and MDD) as determined by Soilco Laboratory. For the sake of this research project and to compare slope stability between varying moisture conditions, the shear parameters at the “dry” and “wet”

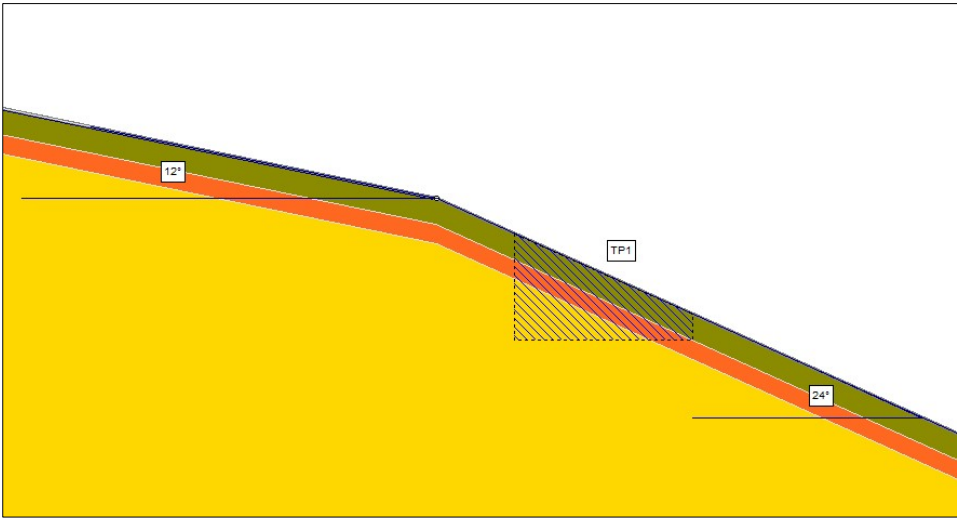
conditions were needed. These were obtained from the direct shearbox tests, the results of which are considered to be incorrect (cohesion was found to be zero throughout) and unreliable (section 4.10). The research shows that the shear strength of soils decreases with increasing water contents. As soils reach optimum conditions i.e., OMC and MDD, the angle of internal friction ( $\phi_f$ ) decreases and cohesion ( $c$ ) increases, however, upon increasing water contents further or saturating the soil, there is a decrease in the soil cohesion and little to no effect on the soils internal friction (Cokca *et al*, 2004; Huang *et al*, 2012). Based on this, the shear strength parameters in the “dry” and “wet” conditions were assumed, through extrapolation of the triaxial results at optimum and using the results of direct shear box tests as a guideline where possible.

For Site A samples, due to a discrepancy between the researchers optimum water condition and that obtained by the external soils laboratory, there were no available shear strength parameters for water contents less than optimum (8.7%). However, as with the other water conditions, these shear strength parameters were assumed. In all cases, cohesion for the “dry” condition was assumed to be 1 and for the “wet” condition it was assumed to be 0.  $\Phi_f$  was based on the values obtained during direct shear box testing and adjusted where necessary to be larger in the “dry” condition than the optimum condition, and close to the same value as the optimum, during “wet” conditions. The parameters used for slope stability analysis in RocScience software, are summarised in the table below.

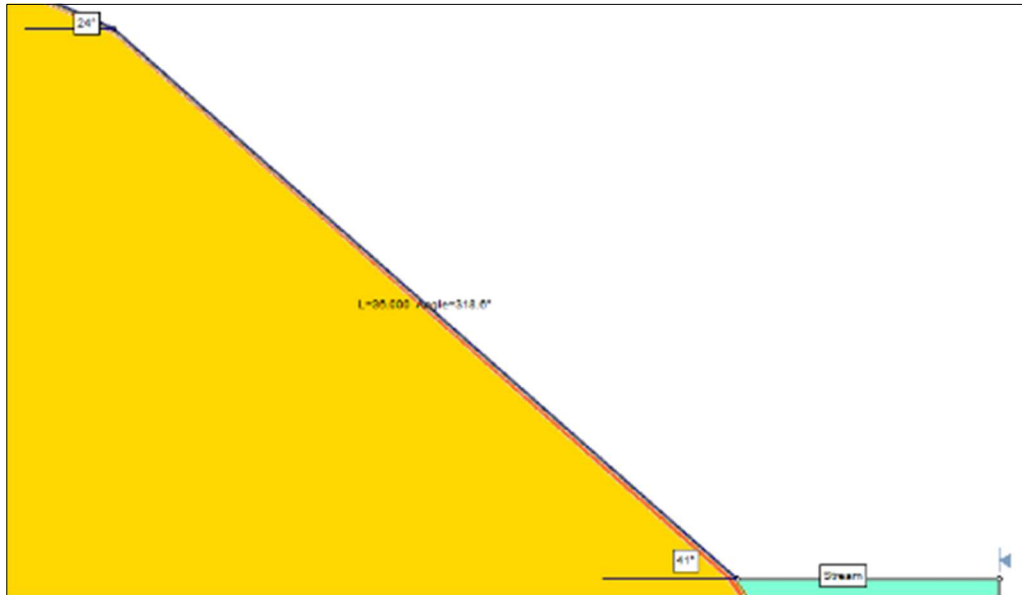
<b>Table 5. 2:</b> Soil properties and shear strength parameters used during slope stability analysis, under varying moisture conditions								
			<b>Dry – &lt; 8.7%</b>		<b>Optimum – 8.7%</b>		<b>Wet – 12%</b>	
		$\gamma$ (kN/m <sup>3</sup> )	$C_T$	$\Phi_T$	$C'$	$\Phi'$	$C_T$	$\Phi_T$
<b>Site A</b>	Sample 1	20	1	37.58	6.4	33.2	0	33
	Sample 2	21	-	-	-	-	-	-
<b>Site B</b>	Sample 3	18.5	<b>Dry - 9 %</b>		<b>Optimum – 12%</b>		<b>Wet – 14%</b>	
			$C_T$	$\Phi_T$	$C'$	$C_T$	$\Phi_T$	$C'$
			1	42	1.7	41.5	0	41
	Sample 4	Unsaturated – 16.5 Saturated - 20	<b>Dry – 8 %</b>		<b>Optimum – 8.3%</b>		<b>Wet – 12%</b>	
			$C_T$	$\Phi_T$	$C'$	$C_T$	$\Phi_T$	$C'$
			1	38.64	7.6	32.1	0	33

RocScience Slide offers multiple conventional methods as options to calculate slope stability. In this analysis Janbu Simplified and Bishops Simplified were selected, both of which are defined as methods of slices. The failure surfaces of sliding in slopes predominantly takes the form of a circular arc. The semi-circle formed in this way is then split into slices and the safety of each slice is calculated. The Bishop simplified method is a circular method that uses total **moment** equilibrium around the centre of rotation, and forces are calculated in a vertical direction instead of normal to the arc. The Janbu simplified method is a non-circular method that considers total **force** equilibrium, in a direction horizontal to the arc (Bishop, 1955; Azimi, 2016). An “overall” probabilistic analysis considering spatial variability of the three major parameters, was also conducted on each slope condition, using the Monte Carlo simulation (MCS), as detailed in Section 2.3.

Figure 5.1a, b and figure 5.2 shows the models of Sites A and B respectively, as drawn on RocScience Slide. The model for Site A had to be split into two because of the large scale of the site. The material boundaries, slope lengths and angles and the positions of the test pits dug on site are shown as well.



a.



b.

**Figure 5. 1a and b:** Showing close up model of Site A as drawn on RocScience Slide; a) uppermost, left hand side of the model close to the road, b) bottommost right hand side of model close to the stream.

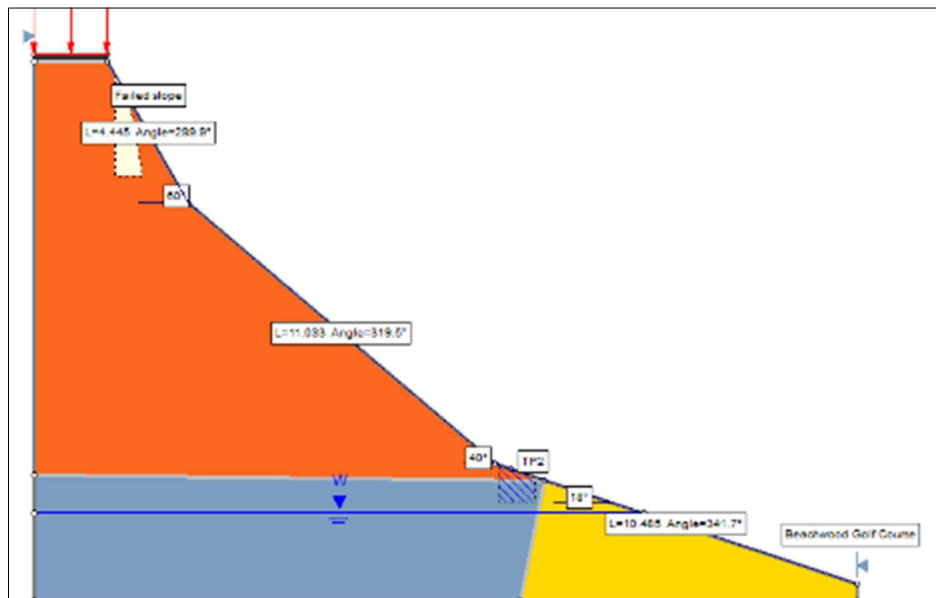


**Figure 5. 2:** Showing close up model of Site B as drawn on Rocscience Slide.

Images of each slope stability computation or “run” at each moisture content, are provided in the sections below. The results of each slope stability analysis are discussed in detail thereafter. In general, only failure surfaces with factors of safety (FOS) less than ( $<1$ ) are shown, except in cases where the slope is considered stable, and the majority of slip circles are those greater than 1 ( $>1$ ). The slip circle or failure surface of the most “consequence” upon failure was also selected for each run, for comparison purposes. The associated FOS and probabilities of failure (POF) are tabularised in table 5.3 thereafter.

## 5.2 Site A Slope Stability Analysis

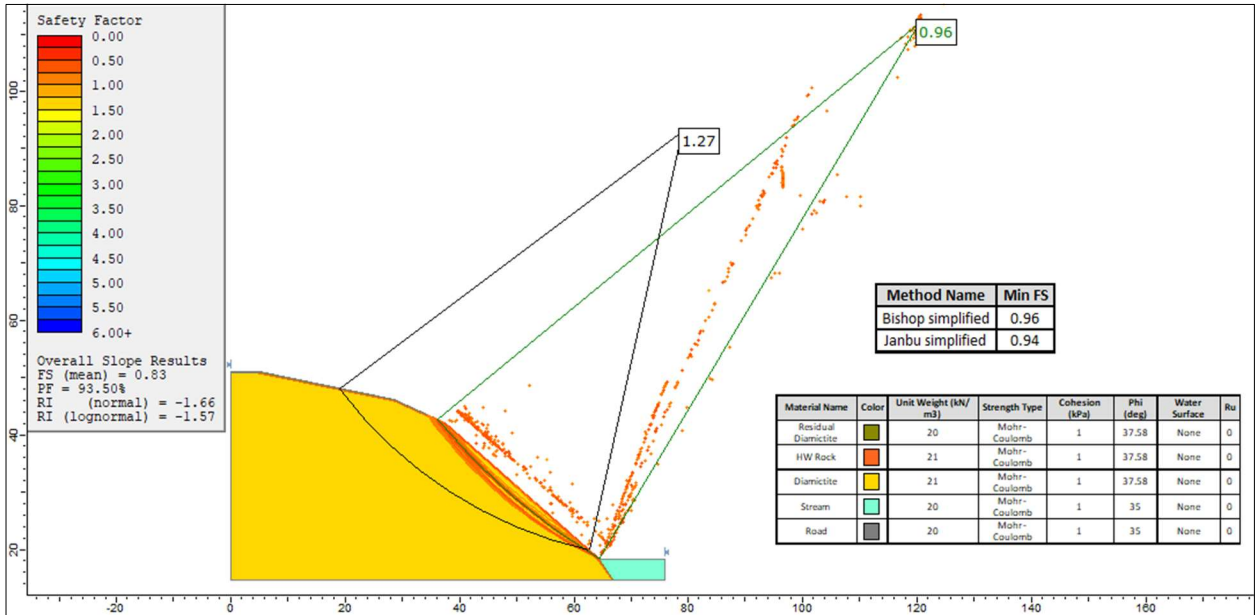
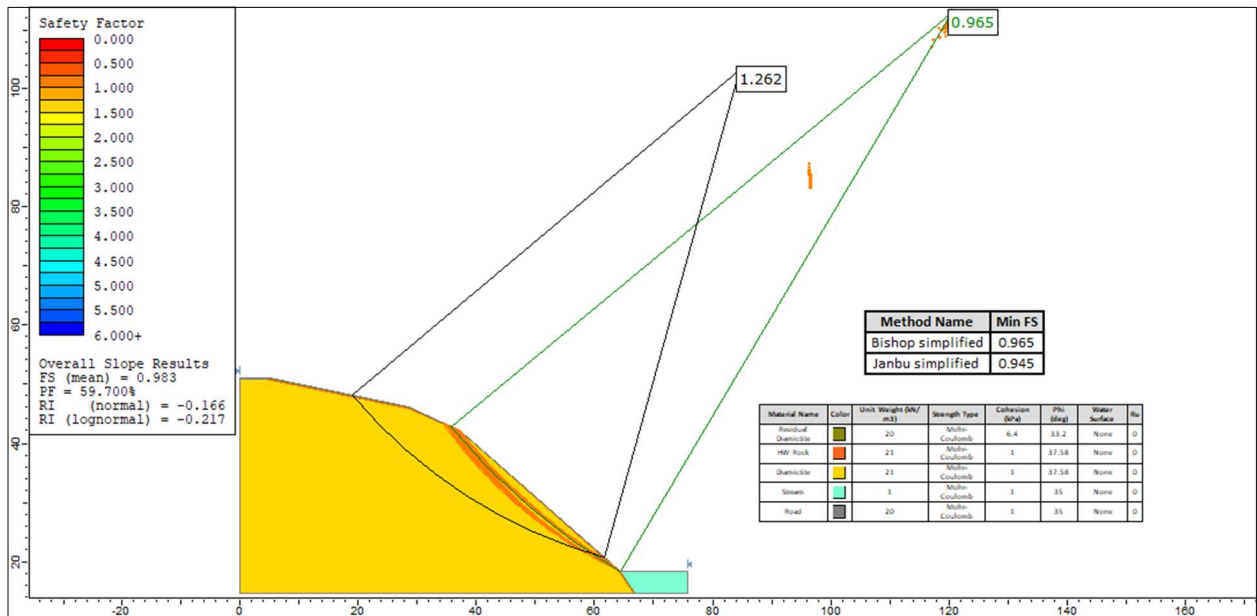


Figure 5. 3: Slope stability analysis of site A in “dry” water conditions (< 8.7 %)

The deterministic analysis for Site A in “dry” conditions (Figure 5.3) yielded a global minimum FOS for the entire slope of 0.96. This failure surface and all others less than 1, occur on the bottommost and steepest part of the slope in all subsequent water conditions. The most unstable part of the slope on Site A is therefore this portion. It should be noted that these are relatively shallow failures possibly as a result of erosion. Because they do not undercut the mass area beneath the slope, they are considered superficial failures of little consequence. A slip circle of the greatest “consequence” upon failure was selected, starting from the middle of the uppermost part of the slope where any future construction will most likely occur. This failure surface has a FOS of 1.27, which is considered stable (>1). The probabilistic analysis however, calculated an overall slope stability with a mean FOS of 0.83 (<1) and a 94% probability of failure. This slope is therefore considered unstable in dryer conditions when there is a lack of water within the soil mass.



**Figure 5. 4:** Slope stability analysis of site A in “optimum” water conditions (8.7 %)

The slope stability analysis for “optimum” water conditions of Site A are provided in Figure 5.4 above. The deterministic analysis for this water condition yielded the same approximate results as those for the “dry” condition. Even the selected slip circle of consequence is approximately the same. However, the probabilistic analysis exhibited an overall or mean FOS of 0.98 (~1) with a 60% probability of failure. This FOS may even be considered as equal to 1, which implies an overall “safe” slope. In general, Site A in “optimum” water conditions is much more stable than in dry conditions. It is important to note that the “optimum” water condition percentage was very close to the soil’s natural moisture content (9.5%). This indicates that the stability analysis provided in Figure 5.4 can be considered as *in-situ*.

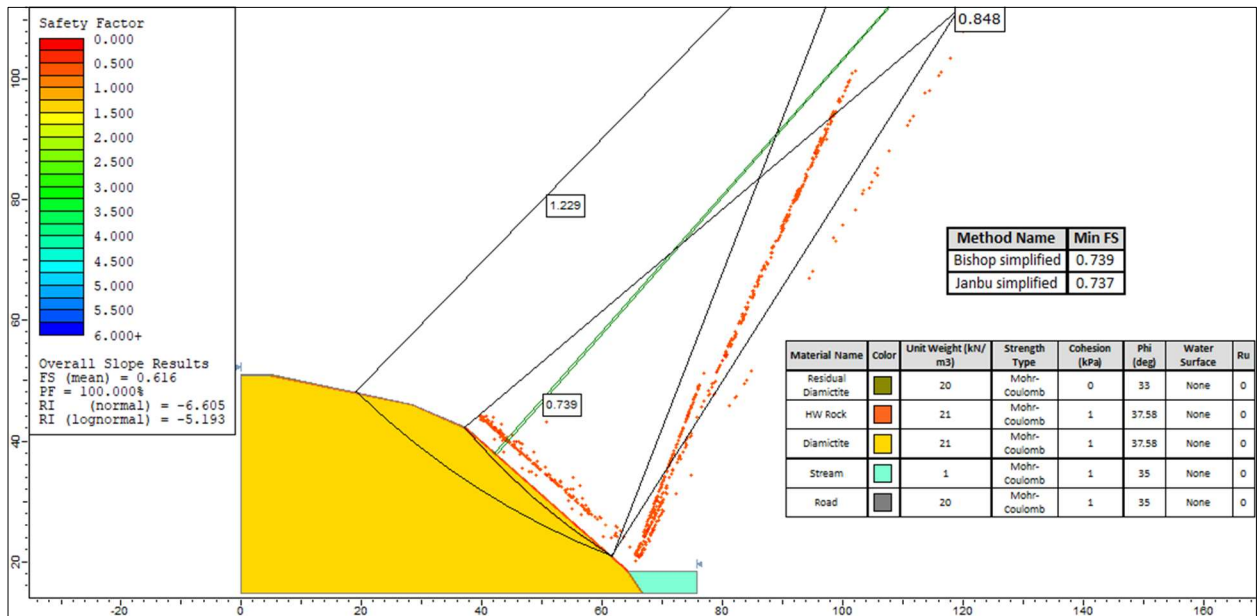


**Figure 5. 5:** Slope stability analysis of site A in “wet” water conditions (12%)

As is evident in figure 5.5 above, the stability of the slope has deteriorated on multiple fronts, under “wet” conditions. Firstly, the deterministic analysis yielded a global minimum of 0.739, which is much lower than the previous water conditions. Although this slip circle is very small, on the surface of the slope and of no consequence, this is still an indication of slope deterioration. The selected slip circle of consequence further up the slope is still the same, however the overall/mean FOS of the entire slope has decreased significantly to 0.616 with a 100% probability of failure. Site A in “wet” water conditions is clearly unstable and unsafe.

Histogram graphs of the FOS of the slope under varying water conditions were created as a further graphic to display the slopes stability. They are provided in the images below (Figures 5.6a, b and c), side by side in order to make the best comparison. The histograms clearly indicate that the slope stability of Site A increases with the addition of some water till optimum conditions are reached, but then decreases drastically as water content increases further. The frequency of failure (indicated by the highlighted data in red, FOS < 1) is high in the dry condition with the majority of slip circles being <1, lower in the optimum condition where only half the slip circles are < 1, and very high in the wet condition with all slip circles being <1.

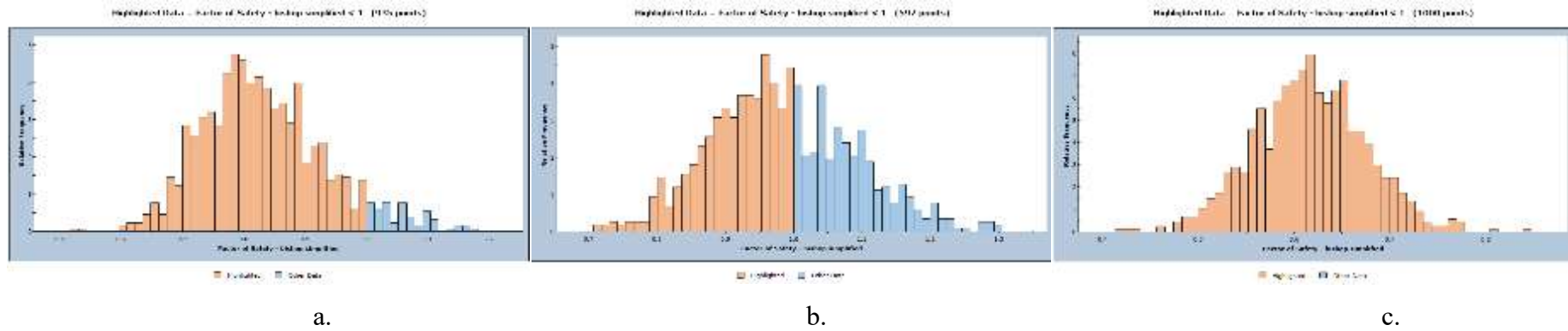


**Figure 5. 6a, b and c:** Histogram/bar graphs of Site A showing FOS for the slope of Site A in a) dry water conditions, b) optimum water conditions and c) wet conditions.

### 5.2.1 Site A FEA Groundwater Seepage Analysis and subsequent slope stability analysis

A groundwater seepage analysis was conducted for Site A at OMC, based on the results of the soil suction testing. The results from this test provided an Air entry value (AEV) for Sample 1, which was used as a parameter for the Finite Element Analysis (FEA). The groundwater seepage analysis is provided in figure 5.7 below, followed by the slope stability analysis of the same scenario (Figure 5.8). The elevation for the start point of groundwater seepage was assumed at halfway beneath the slope, as this was not a factor that was ascertained during the site investigation. The permeability ( $k$ ) of samples 1 and 2 were found from the results of consolidation testing (Section 4.9) and they were required for this analysis. All parameters used for the groundwater seepage analysis are summarised in Table 5.3 below.

Sample No.	$C_T/C'$	$\sigma_T/\sigma'$	AEV (kPa)	$k$
1	6.4	33.2	3.9	$5,07 \times 10^{-13}$
2	1	37.58	-	$4,36 \times 10^{-13}$

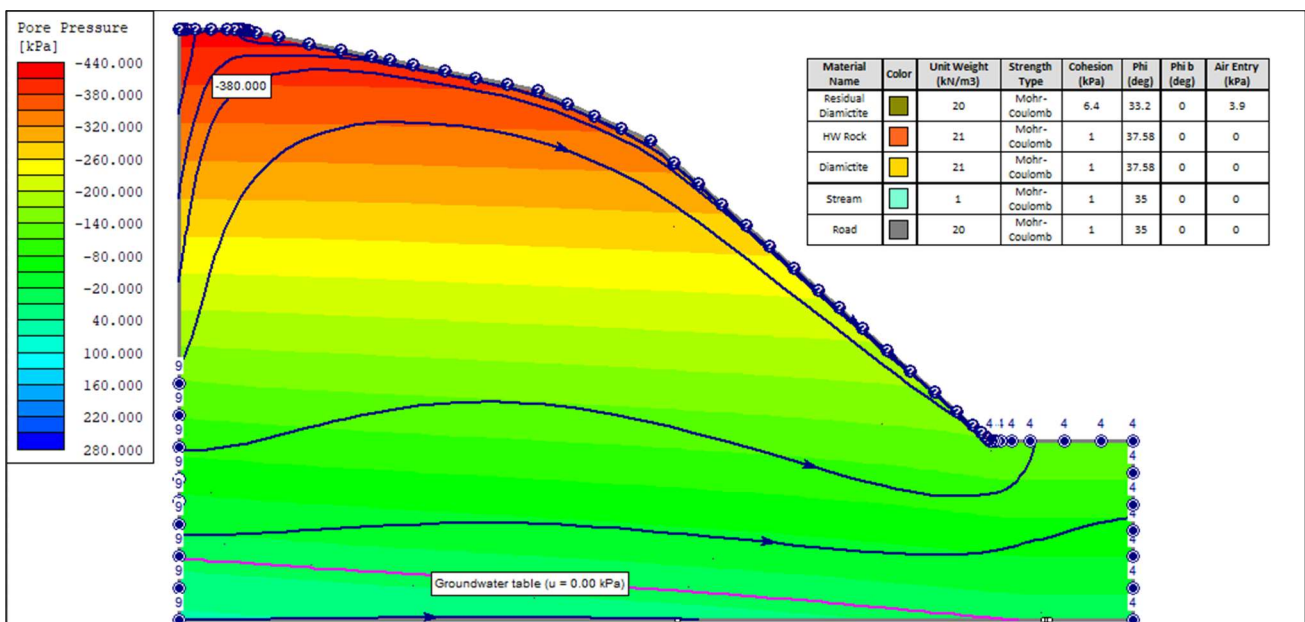


**Figure 5. 7:** FEA and Groundwater Seepage Analysis of Site A in Optimum conditions

The FEA-Groundwater Seepage Analysis provided in figure 5.7, shows that the groundwater table presents at approximately 40 metres beneath the surface of the site. Although this is very deep, the

effects of the groundwater table such as pore pressure, matric suction and uplift pressure are felt throughout the slope, with some flow lines even extending to the surface of Site A. The pore pressure near the surface is approximately – 400kPa. This negative pore water pressure is due to the effects of matric suction as a result of capillary rise, in those unsaturated zones above the groundwater table. Hydrostatic uplift pressure can be calculated by the following equation:

$$\text{Uplift pressure} = \mu \times \gamma_w \tag{22}$$

Where  $\mu$  is the pore water pressure and  $\gamma_w$  is the unit weight of water which is 9.81 kN/m<sup>3</sup>.

Using equation 22, the uplift pressure at the surface of the site is 3924 kPa. This is a relatively low value indicating that any future structure on the surface of the site will almost definitely have an overburden pressure greater than the uplift pressure present within the slope mass. In this way, the site is not considered to be at major risk of experiencing hydraulic failure (EN 1997-1, 2004).

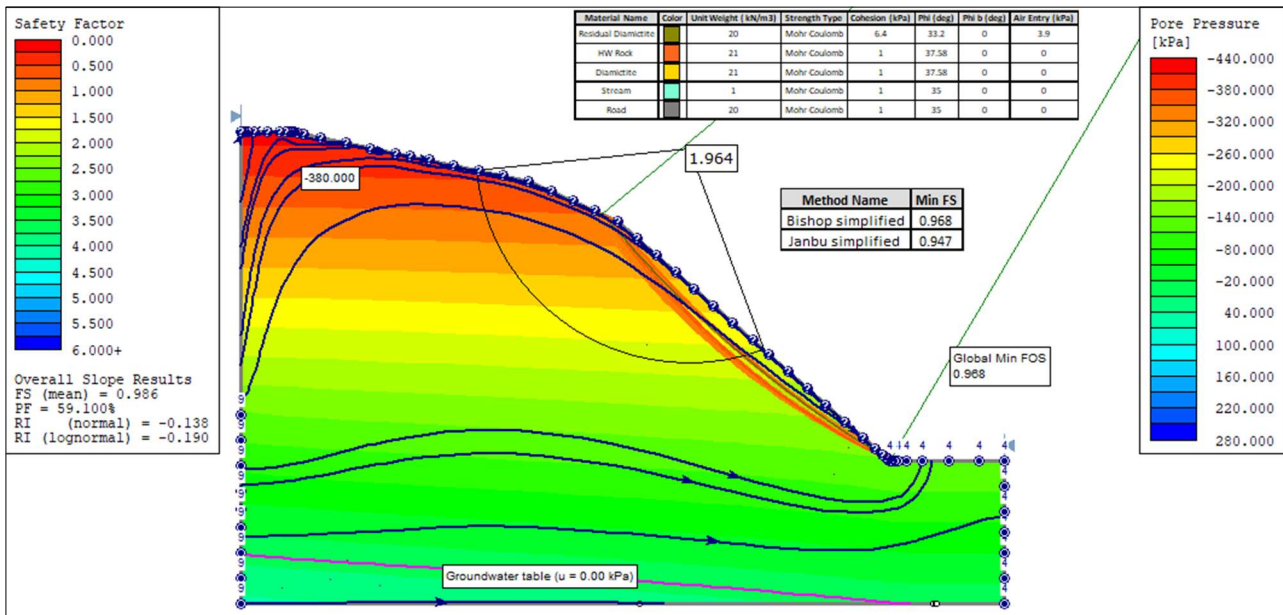


**Figure 5.8:** Slope stability analysis of Site A (OMC) with matric suction parameters

The slope stability analysis shown in figure 5.8 above yielded a global minimum FOS of 0.968. This is approximately equal to 1 (FOS = 1) indicating a relatively safe slope. As is the case in all presented scenarios for Site A, the most unstable part of the slope is this steepest portion. All failures here can be considered superficial and not of great consequence. The slope stability of Site A under optimum conditions was compared with matric suction (figure 5.8) and without matric suction (Figure 5.4). It was observed that the slope stability of Site A improved very slightly from a FOS of 0.983 without an AEV, to 0.968 with an AEV. The effects of matric suction are very small due to the small AEV, and this change in FOS results could be considered negligible. However, it is still indicative of slope

stability improvement due to the positive effects of matric suction, which further agrees with the literature presented in Chapter 2 of this study.

### 5.3 Site B Slope Stability Analysis

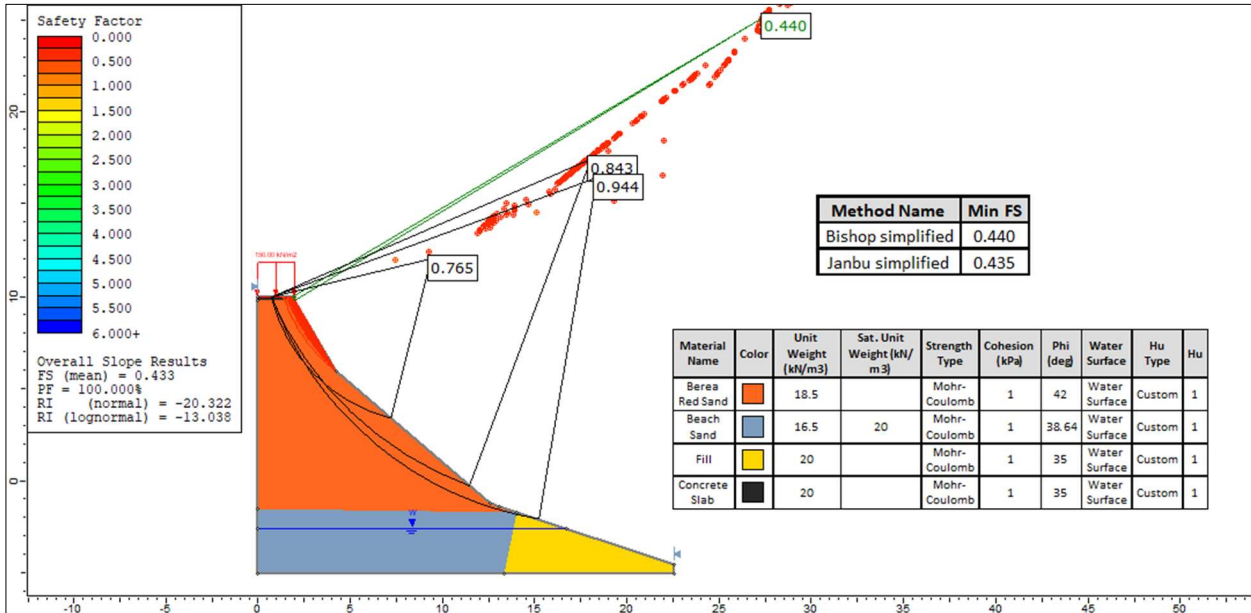


**Figure 5. 9:** Slope stability analysis of site B in “dry” water conditions (~8.5 %).

In the “dry” water condition as provided in Figure 5.7 above, the global minimum FOS is 0.440. There are multiple failure arcs (<1). Three slip circles of consequence were selected, all stemming from the midpoint of the overlying structure, and all exhibiting failure. The probabilistic analysis exhibited an overall or mean FOS of 0.433 with a 100% probability of failure. As such in the “dry” condition, this slope is unsafe and unstable.

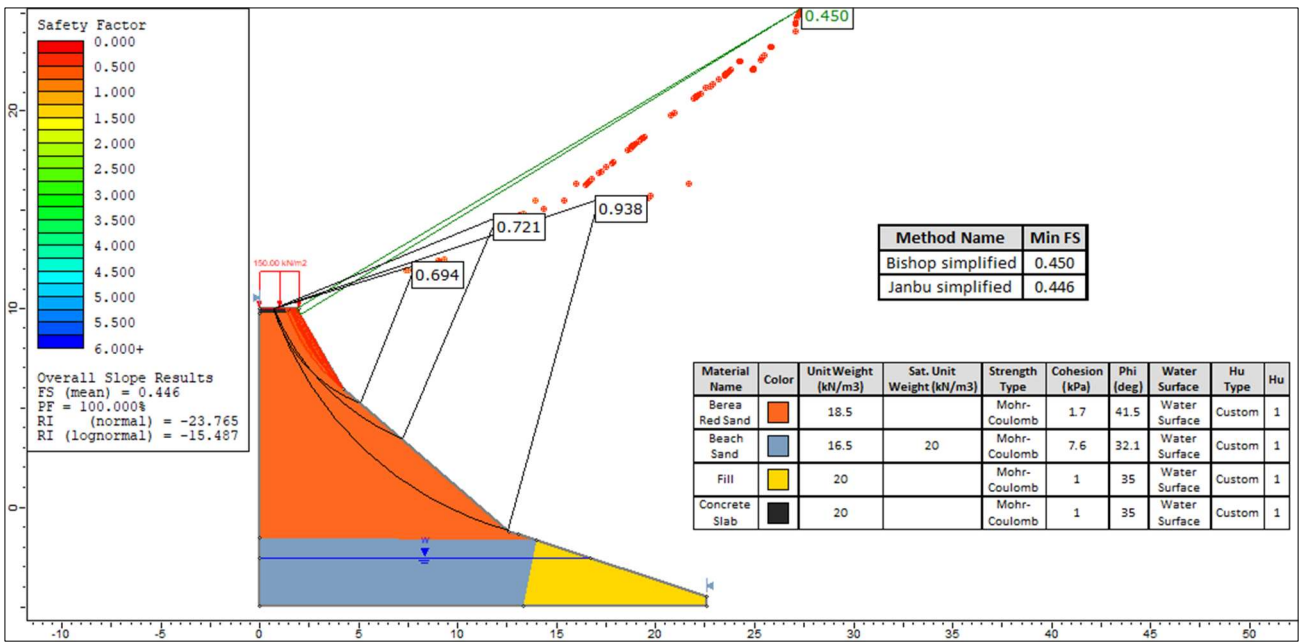


**Figure 5. 10:** Slope stability analysis of site B in “optimum” water conditions (~ 10%)

In “optimum” water conditions (Figure 5.8), the slope displays the same stability behaviour as before, with the same approximate global minimum and abundant failure surfaces less than 1. For comparison purposes, the same approximate slip circles of consequence were selected, all of which exhibit FOS’ < 1. The overall FOS of the slope, as calculated from the probabilistic analysis, improved very slightly from 0.43 in the dry condition to 0.45 in the “optimum” condition, with 100% probability of failure. The change in the FOS result can be considered negligible. The addition of water into the soil mass to reach “optimum” conditions has had little to no effect on the soil behaviour. It is important to mention again what was observed during laboratory testing – the soils are too uniform and do not retain water easily as they severely lack the fines that are necessary to bind water in the soil.

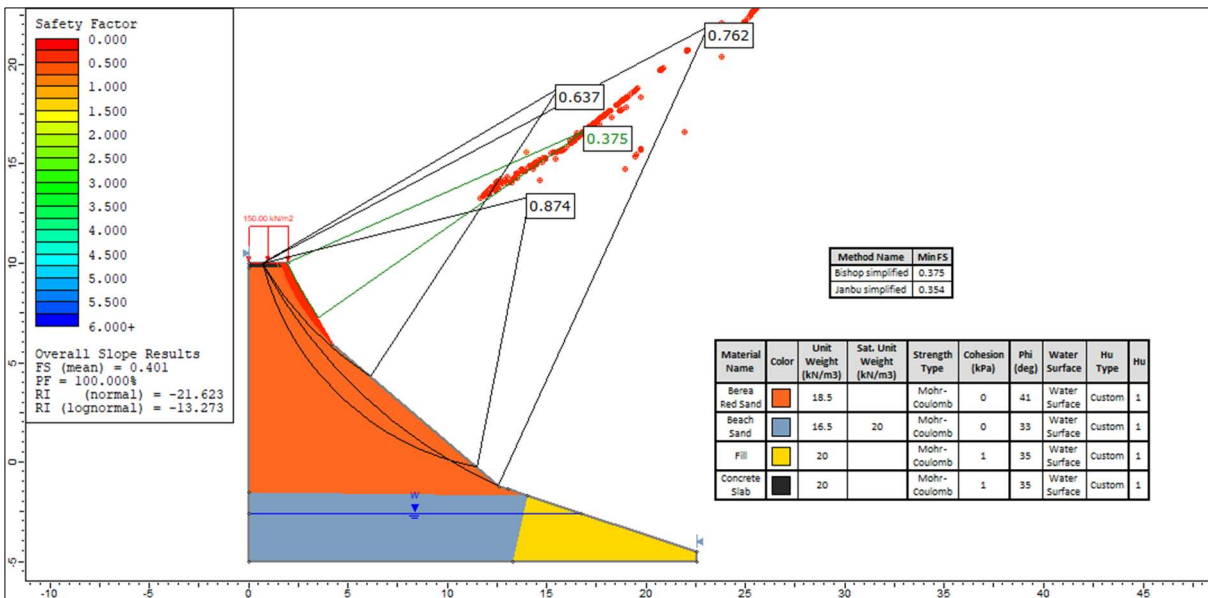
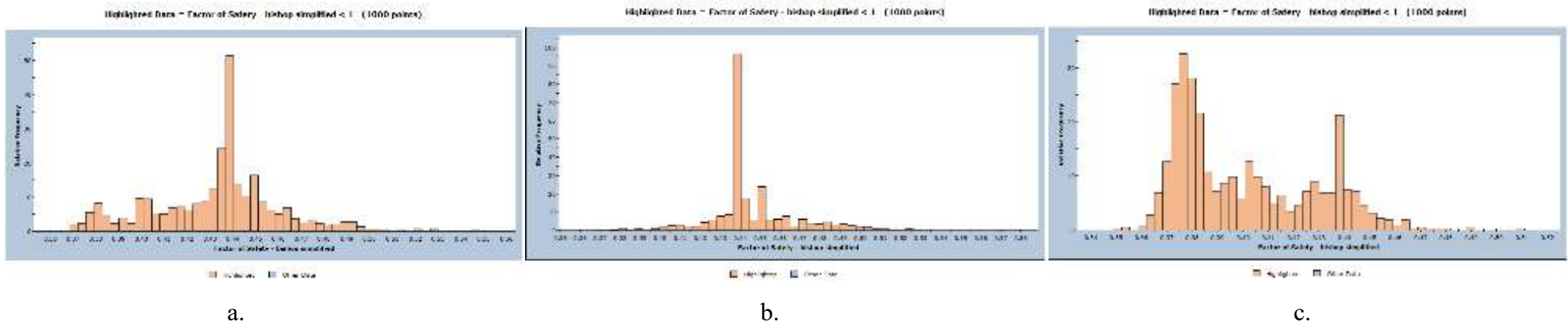


**Figure 5. 11:** Slope stability analysis of site B in “wet” water conditions (~ 13%).

Figure 5.9 shows the slope stability of Site B in the “wet” condition. Upon the introduction of excess water into the slope, the slope stability is observed to deteriorate greatly with a global minimum of 0.375 and many more failure surfaces presenting. The overall/mean FOS has decreased to 0.40 with 100% probability of failure. It is important to note that the NMC of the soils on site were already much greater than this “wet” condition, at 27.75 %, implying just how unstable the slope on Site A was *in situ*.

The histogram graphs of the FOS’ of Site B under varying water conditions are provided in figure 5.10a, b and c. In the dry condition, there is an abundance of slip circles with a FOS of 0.4. This spike remains in the “optimum” condition; however, it can be observed that the number of failure surfaces of other FOS values decreases slightly. In the “wet” condition, there is an observed increase in the amount of slip circles that are < 1, implying a greater potential for failure to occur. It is evident in all water conditions that the soil mass making up the slope of Site B is unstable and unsafe.



## 5.4 Summary of slope stability analyses

The results from the slope stability analyses conducted of each site, under varying water conditions, are summarised in the Table below.

<b>Table 5. 3:</b> Results of Factor of safety (deterministic) and “overall” probabilistic slope stability analyses considering spatial variability, for Site A and B						
	<b>Dry</b>		<b>Optimum</b>		<b>Wet</b>	
	$\overline{FOS}$	POF (%)	$\overline{FOS}$	POF (%)	$\overline{FOS}$	POF (%)
<b>Site A</b>	0.83	93.50	0.983	59.7	0.616	100
<b>Site B</b>	0.433	100	0.446	100	0.401	100

Site A is generally unstable in the dry condition, becoming almost stable in optimum conditions and highly unstable with much slope deterioration, in the wet condition. The optimum water condition can be considered *in situ*, as it was closest to the sites NMC. The worst failures (<1) occur at the bottommost, steep part of the site, near the stream. The area of greatest consequence on the topmost part of the site near the road, is considered stable and unaffected in all conditions. Analysis of the histograms clearly indicate that the slope stability of Site A increases with the addition of some water till optimum conditions are reached, but then decreases drastically as water content increases further. A FEA- groundwater seepage analysis was conducted for Site A at optimum conditions. In summary, Site A is not considered to be at major risk of experiencing hydraulic failure, with an uplift pressure seemingly lower than any future overburden pressure. The slope stability of Site A at OMC was compared with consideration of matric suction, showing a slight improvement in the FOS due to the positive effects of matric suction, as posed in the literature review of this study.

Site B is unstable and unsafe in all water conditions with 100% POF throughout. The addition of water into the soil mass to reach “optimum” conditions has had little to no effect on the soil behaviour as the soils are too uniform and lack the fines necessary to bind water in the soil. Severe slope deterioration was observed in the wet condition with many more failure surfaces present than in the other two conditions. The NMC of the soils on site was already two times greater than this “wet” condition, implying just how unstable the slope on Site A was *in situ*.

## CHAPTER SIX

### DISCUSSION

---

#### 6.1 Introduction

The results from the experimentals conducted in this research study (fieldwork and laboratory testing) combined with the slope stability analyses, were thoroughly assessed to provide the following discussions, recommendations, and conclusions of each site. The various water conditions that were considered for the sites must be kept in mind throughout and are summarised in the table below.

<b>Table 6. 1:</b> Summary of various water conditions assessed for both sites				
	<b>~NMC %</b>	<b>Dry %</b>	<b>Optimum %</b>	<b>Wet %</b>
<b>Site A</b>	9.5	< 8.7	8.7	12
<b>Site B</b>	27.75	~ 8.5	~ 10	~ 13

#### 6.2 Discussion on Site A slope stability

As was observed in the slope stability analysis, the slope is unstable under “dry” conditions, with a high probability of failure. The slope becomes stable, with a Factor of Safety (FOS) of approximately 1 and a relatively low POF, at “optimum” water content. It was starkly evident that the FOS decreased drastically, and the POF increased drastically when the water content of the slope increased further. The following observations are made:

1. Seeing as the slope is unstable when conditions are “dry”, and becomes stable at OMC, this indicates that the introduction of some water into the soil mass positively affects the slope stability. This may be attributed to the action of matric suction that occurs under partial saturation, and which adds a significant strength contribution to the soil (Indraratna *et al*, 2015). The positive effects of matric suction on the stability of the slope on Site A was proven in Section 5.2.1 of this research project (Figure 5.8). Zhou *et al* (2020) also

proved the beneficial effects that water pressure provides as back pressure, to further stabilise the slope.

2. The stability of the slope decreased drastically under increased water content in the “wet” condition. This occurs due to the following reasons:

- An increase in water content causes a significant increase in the mass of the material on a slope, making it more prone to failure due to gravity (Earle, 2019).
- The matric suction that previously contributed to the slope’s stability under OMC, can easily be lost upon further saturation and entry of water into the pores (Indraratna *et al*, 2015).
- The study conducted by Zhou *et al* (2020) proved how the stability of a slope decreased with continuous infiltration or introduction of water, caused by the increase in pore pressure. The build-up of enough pore water pressure may trigger reduction in the shear strength resistance of the material, such as a loss of cohesion resulting in slope failure (Weiler *et al.*, 2006).
- The residual soil beneath the slope is a thin layer that can mostly be considered negligible, except in the steeper areas. Therefore, the bulk of the slope’s stability stems from the underlying bedrock. In the case of a rock slope such as this one, the physical and chemical effects of pore water pressure can cause a decrease in the compressive strength of the rock when confining stress is reduced (Chaulya and Prasad, 2016).

### **6.3 Discussion on Site B slope stability**

The results of the slope stability analyses indicate that the slope of Site B is unstable in all varying water conditions. It is important to remember that the slope has already experienced both surficial and massive failure and the natural moisture content of the soils on site are already much greater than the 3 water conditions assessed in this study (refer to Table 6.1). As such, this outcome is expected. Although this slope is unstable in every condition, with 100% probability of failure throughout, it was observed that the “wet” condition resulted in many more slip circles with FOS < 1. This implies that there is a greater potential for failure as water content increases. This is most likely due to the following reasons:

1. The soils in this slope have proven to be treacherous to work with and entirely unsuitable for engineering or construction purposes. They are cohesionless, poorly graded and too well sorted comprising an abundance of only one grain size i.e., fine to medium sand. This lack of fines, clay and silt, is problematic as there are no particles present to bind water to the soil through electro-molecular and electrochemical forces (Vondráčková *et al*, 2016) or even through matric suction (Indraratna *et al*, 2015). Figure 6.1 below indicates the soils reaction during the application of force. Water was not taken up by the soil, but it was pushed out instead and is seen pooling at the bottom of the compaction apparatus.



**Figure 6. 1:** Showing the soil reaction to pressure under compaction, with emphasis on the driven-out water at the base of the proctor mould.

2. The soils also exhibited the potential to “liquefy” with the introduction of enough water. Increased pore water pressure results in the soil particles losing whatever little contact they have with each other. The soil loses its strength and begins to behave more like a liquid than a solid, in a process called "liquefaction." (Khan, M.A. *et al*, 2016). Cohesionless soils undergo liquefaction as a result of multiple factors including void ratio, relative density, cyclic stresses, effective stresses and particle shape and particle size distribution (Seed and Lee 1966; Chakraborty and Das, 2018). Uniformly graded, rounded fine sands are found to be most susceptible to liquefaction (Poulos *et al*.1985). Soils containing less than 10%

finer (as is the case here) are also more prone to experience liquefaction. In loose, fine grained sands such as these, the larger void ratio is responsible for developing higher pore water pressures. An increase in percentage of fines would ensure that more of the voids become filled. A decrease in void ratio and subsequent decrease in pore water pressure directly mitigates the event of liquefaction (Khan, M.A. *et al*, 2016).

3. The increase in water in the “wet” condition results in more potential for slope failure due to the following reasons (taken from research presented in this study’s literature review in Chapter 2, page 8):
  - Groundwater interaction adversely affects soil properties and stability by altering cohesion and frictional parameters. A decrease in cohesion and friction results in a decrease in effective normal stress and thereby an overall reduction in shear strength of the soil (Chaulya and Prasad, 2016).
  - An increase in water infiltration results in the air voids in soil becoming replaced with water instead. This causes a loss of soil suction and a significant reduction in strength. (Indraratna *et al*, 2015)
  - An increase in seepage velocity may occur due to the steepness of the slope at the crest (approximately 60°). An increase in slope steepness results in an increase in the hydraulic gradient and seepage flow of the slope, leading to a decrease in slope stability (Indraratna *et al*, 2015).
4. It was also observed during laboratory testing that the sands underlying the site cannot tolerate any stress and are prone to crumbling under even slight pressure. This occurs in loose sands during the application of rapid loading, as individual soil particles are forced into the voids in the soil mass in an attempt to form a denser configuration (Khan, M.A. *et al*, 2016).

## CHAPTER SEVEN

### CONCLUSION AND RECOMMENDATIONS

---

#### 7.1 Conclusions

Slope instability is a major problem in the study area of Durban, KwaZulu-Natal. Slope failures occur largely due to soil variability in a slope and associated geological threats, the most significant being that of groundwater seepage and infiltration. This research aimed at analysing and comparing the stability of two slopes under different water conditions in the form of Factors of Safety and Probabilities of Failure using RocScience© software. The interactions between slope configuration, shear strength resistance and pore-water pressure were all taken into consideration. As anticipated based on the findings of the literature review, the results of this research project demonstrated both the positive effects of pore water in the form of matric suction (during partial saturation), as well as the ultimate negative effects of pore water (under further saturation) on the soil's properties, making them all the more variable and hazardous to the stability of the slopes under investigation. Site A displayed a slight increase in stability under partial saturation, due to the positive effects provided by the action of matric suction. However, both sites displayed increased potential for failure, with the introduction of increasing water contents into the slopes. Deterministically, the Factors of Safety (FOS) increased from the dry to the optimum condition and then decreased drastically from the optimum to wet condition. Probabilistically, the probability of failure (POF) decreased significantly when the slope condition was at "optimum" water content (OMC). Upon further saturation, when the OMC was exceeded, the POF increased again significantly. This was qualified further by the obvious increase in the amount of failure/slip circles present when water conditions were at their greatest. Based on these findings, water content is observed to be a great factor affecting a soils variability, its properties and strength. As such, there is a need to consider and further characterise soil variability in problematic areas so as to mitigate slope failure at a later stage. The results and conclusions of this research prove the importance of investigating a soils variability and the subsequent slope reaction under varying moisture conditions.

## **7.2 Recommendations**

Based on the results obtained from this research project and the discussion provided with reference to the literature review, the following practical recommendations are made for each site / slope.

### **7.2.1 Site A recommendations**

In the area of instability, the residual soil layer thins out even further than at the investigated portion of the slope (0.1 metres), and the potential failure is most likely attributed to the slope geometry and steepness, rather than the soils variability. The soils natural moisture content (NMC) is very close to the “optimum” condition, which was observed to be practically safe. This was also the case on site, with no major failure or instability occurring.

Any structures or dwellings will most likely be constructed on the uppermost part of the site, near the road, where there are no failures imminent i.e., all FOS > 1. Thus, no major mitigation measures are currently necessary to avoid slope failure. However, it would be important to incorporate adequate drainage to allow excess water to drain out of the slope, so as to avoid water conditions reaching those that will result in failure. Every effort should be made to maintain vegetation cover on the lower parts of the slope for erosion control and to anchor the soil against surficial failures.

### **7.2.2 Site B recommendations**

Site B is considered unstable in all water conditions and has already experienced failure. The soils are considered dangerous and not suitable for any construction or load-bearing purpose. Cut and fill of these dangerous soils to replace them with more suitable soils is very rarely an option, as it is not cost effective in any way. The best recommendation would be to add external reinforcement in the form of stepped gabion walls. Gabion wall retaining structures are considered one of the most cost-effective and efficient solutions for the stabilization of natural soil slopes. (Toprak *et al*, 2016)

The specifications for construction of Gabion retaining walls are laid out in ASTM A975 (2011). Gabion boxes of various sizes are made up of wire mesh that has been double twisted mechanically and interconnected to form square or cylindrical shapes. The general properties of gabion wire

mesh are provided in figure 6.2 below. The filling material should consist of naturally occurring hard stones that are resistant to weathering, insoluble and of high specific gravity (Al Helo *et al*, 2016).

Due to the proven devastating effects of water interaction with the soils on Site B, it is crucial to keep water out of the slope mass through the use of horizontal drainage channels. Gabion walls provide efficiency of drainage as a multi-purpose and are generally the preferred option (Toprak *et al*, 2016).

Raw Material	Gabion Wire Mesh General Properties		
Technical Properties	Unit	Descriptions	Tolerance
Mesh	mm	50x70, 60x80, 80x100, 100x120	
Wire Thickness (Max)	mm	2-5 mm	0,05
Amount of Covering	gr/m <sup>2</sup>	30-300	5
Tensile Strength	N/mm <sup>2</sup>	350-2000	2

**Figure 6. 2:** General properties of gabion wire mesh (Uray Ve and Tan, 2015; Toprak *et al*, 2016)

Another option to remediate the slope would be to reinforce the soil mass by “blending” it with other materials, such as cement or lime. Research has proven that the addition of just 1% of these substances provides great stabilisation effects to a soil (Mohamed and Paleologos, 2018). These mixes will contain fines and other particle sizes that will help to broaden the grain size distribution of the poorly graded, uniform *in situ* soil.

At a later visit to Site B in November 2020, it was observed that remediation of the slope was already underway. This involved the construction of gabion walls, as recommended here. Images of the slope rehabilitation are provided in the figures below.



**Figure 6. 3a and b:** Showing construction of Gabion walls as rehabilitation of the failed slope and mitigation of further slope failure on Site B.

## REFERENCES

- Abd, I.A., Fattah, M.Y. and Mekkiyah, H. (2020). Relationship between the matric suction and the shear strength in unsaturated soils. *Case Studies in Construction Materials*, 13, p. e00441
- Abramson, L., Lee, T., Boyce, G. and Sharma, S. (2002). *Handbook of Slope Stability and Stabilization Methods*. 2nd ed. Wiley, New York.
- Agus, S. S., and Schanz, T. (2006). *Drying, Wetting, and Suction Characteristic Curve of Bentonite-sand Mixture*. In: Proceeding 4<sup>th</sup> International Conference on unsaturated soil, Arizona, USA, p.1405–1414.
- Al Helo, M.Z., Al-Massri, M.S., Abu-Assi, H.H., Hammouda, M.J. and Joma, I.T. Dawood, O. (Supervisor). (2016). Experimental study of structural behavior of mesh-box Gabion. University of Palestine. Graduation project is submitted to the Civil Engineering Department in partial fulfilment of the requirements for the degree of B.Sc. in Civil Engineering
- Aneke, F. I., Mostafa, M. H. and Moubarak, A. (2019). Resilient modulus and microstructure of unsaturated expansive subgrade stabilized with activated fly ash. *International Journal of Geotechnical Engineering*, DOI: 10.1080/19386362.2019.1656919. Available from: <https://doi.org/10.1080/19386362.2019.1656919>
- Arasan, S., Akbulut, S. and Hasiloglu, A.S. (2011). Effect of particle size and shape on the grain-size distribution using image analysis. *International Journal of Civil and Structural Engineering*, 1(4), p. 968-985.
- ASTM. (2003). *ASTM D5298-03, Standard test method for measurement of soil potential (suction) using filter paper*, ASTM International, West Conshohocken, PA. Available from: [www.astm.org](http://www.astm.org)
- ASTM. (2011). *Standard practice for classification of soils for engineering purposes (unified soil classification system)*. ASTM D2487, West Conshohocken, PA.
- ASTM Int. (2017). *ASTM D6913 / D6913M-17, Standard test methods for particle-size distribution (gradation) of soils using sieve analysis*. Available from: [www.astm.org](http://www.astm.org)

ASTM. (2014). *ASTM D854-14, Standard test methods for specific gravity of soil solids by water pycnometer*, ASTM International, West Conshohocken, PA. Available from: [www.astm.org](http://www.astm.org)

Azimi, S.R. (2016). Soil slope stability techniques: a comprehensive analysis. Doctoral Dissertation (Civil Engineering), Curtin University. Available from: <https://www.researchgate.net/publication/318816471>

Baba, K., Bahi, L., Ouadif, L. and Akhsas, A. (2012). Slope stability evaluations by limit equilibrium and finite element methods applied to a railway in the Moroccan Rif. *Open Journal of Civil Engineering*, 2(1). Available from: [https://www.scirp.org/html/5-1880014\\_17817.htm](https://www.scirp.org/html/5-1880014_17817.htm)

Barounis, N. and Philpot, J. (2017). *Estimation of in-situ water content, void ratio, dry unit weight and porosity using CPT for saturated sands*. 20th NZGS Symposium, New Zealand Available from: [https://www.nzgs.org/library/nzgs20\\_barounis/](https://www.nzgs.org/library/nzgs20_barounis/)

Beckedahl, H.R., Hanvey, P.M. and Dardis, G.F. (1988). Geomorphology of the Esikhaleni mass complex, Transkei, South Africa: preliminary observations. In: Dardis, G.F. and Moon, B.P. (Eds): *Geomorphological Studies in Southern Africa*, Balkema, Rotterdam, p. 457-471.

Bell, F.G. and Maud, R.R. (1996). Examples of landslides associated with the Natal Group and Pietermaritzburg Formation in the greater Durban area of Natal, South Africa. *Bulletin of the International Association of Engineering Geology*, 53, p. 11–20.  
Available from: <https://doi.org/10.1007/BF02594936>

Bicalho, K.V., Correia, A.G., Ferreira, S., Fleureau, J.M. and Marinho, F.A.M. (2007). *Filter Paper Method of Soil Suction Measurement*. XIII Panamerican Conference on Soil Mechanics and Geotechnical Engineering.

Bishop, A. W. (1955). The use of the slip circle in the stability analysis of slopes. *Geotechnique*, 5(1), p. 7–17.

Brand, E.W., Premchitt, J., and Phillipson, H.B. (1984). *Relationship between rainfall and landslides in Hong Kong*. Proc. IV Int. Symp. on Landslides, Toronto, Canada.

British Standards Institution, BS 8002:1994 - *Code of practice for earth retaining structures*. Available from: <https://www.abg-geosynthetics.com/soil-properties-unit-weight.html>

Brown, T.H., Cunningham, C., Findley, D.J. and Schroeder, B. (2015). *Highway engineering*. Butterworth-Heinemann. Available from: <https://www.sciencedirect.com/topics/engineering/atterberg-limit>

Cawthra, H.C., Uken, R. and Ovechkina, M.N. (2012). New insights into the geological evolution of the Durban Bluff and adjacent Blood Reef, South Africa. *South African Journal of Geology*, 115(3), p 291-308. Available from: <https://www.researchgate.net/publication/263794353>

Chakraborty, P. and Das, A. (2018). *Effect of soil grain size on liquefaction strength of sandy soil*. Indian Geotechnical Conference. Indian Institute of Science, 13-15.

Chandler, R. J., Crilley, M. S. and Montgomery-Smith, G. (1992). A low-cost method of assessing clay desiccation for low-rise buildings. *Proceedings of the Institution of Civil Engineers- Civil Engineering*, 92(2), p 82 - 89.

Chaulya S.K. and Prasad, G.M. (2016). *Sensing and monitoring technologies for mines and hazardous areas: Chapter 1 - Slope failure mechanism and monitoring techniques*. Elsevier. Pp 1-86. Available from: <http://www.sciencedirect.com/science/article/pii/B978012803194000015>

Chen, X., Wu, Y. K., Yu, Y., Liu, J. K., Xu, X. F., and Ren, J. (2014). A two-grid search scheme for large-scale 3-D finite element analyses of slope stability. *Computers and Geotechnics*, 62, p. 203–215.

Cheng, Y.M. and Lau, C.K. (2008). *Slope stability analysis and stabilization. new methods and insight*. CRC Press, London.

Chiliza, S.G. and Richardson, S. (2008). Landslide incidence in the Limpopo Province, South Africa. In: *Proceedings of the First World Landslide Forum*, United Nations University, Tokyo, Japan, p 100–103.

Cho, S. E. and Lee, S. R. (2001). Instability of unsaturated soil slopes due to infiltration. *Computers and Geotechnics*, 28(3), p 185-208. Available from: <https://www.sciencedirect.com/science/article/abs/pii/S0266352X00000276>

Choi, S. O. and Chung, S. (2004). Stability analysis of jointed rock slopes using the Barton–Bandis constitutive model in UDEC. *International Journal of Rock Mechanics and Mining Sciences*, 41(3), p 469-469.

Chok, Y.H. (2009). Modelling the effects of soil variability and vegetation on the stability of natural slopes. The University of Adelaide, School of Civil, Environmental and Mining Engineering. Available from: <https://www.researchgate.net/publication/267389202>

Chowdhury, R. N. and Xu, D. W. (1994). Slope system reliability with general slip surfaces. *Soils and Foundations*, 34(3), p. 99-105. Available from: [https://doi.org/10.3208/sandf1972.34.3\\_99](https://doi.org/10.3208/sandf1972.34.3_99)

Chowdhury, R., Flentje, P., Miner, A and Mazengarb, C. (2010). Periodic and continuous landslide monitoring to assess landslide frequency – selected Australian examples. *University of Wollongong, Research Online*. Available from: <https://ro.uow.edu.au/engpapers/553>

Clayton, R. A. (1989). Investigation of stabilized berea red soil with emphasis on tensile and cyclic triaxial tests. M.Sc. , University of Cape Town.

Clough, R. W. and Woodward, R. J. (1967). Analysis of embankment stresses and deformations. *Journal of the Soil Mechanics and Foundation Division, ASCE*, 93 (SM4), p. 529-549.

Cokca, E., Erol, O. and Armangil, F. (2004). Effects of compaction moisture content on the shear strength of an unsaturated clay. *Geotechnical and Geological Engineering*, 22, 285. Available from: <https://doi.org/10.1023/B:GEGE.0000018349.40866.3e>

Council for Geoscience. (2008). Available from: <http://www.geoscience.org.za>

Crilly, M.S. and Chandler, R.J. (1993). *A method of determining the state of desiccation in clay soils*. BRE Information Paper IP 4/93 Garston, Construction Research Communications Ltd.

Dai, A., Trenberth, K. E. and Karl, T. R. (1999). Effects of clouds, soil moisture, precipitation, and water vapor on diurnal temperature range. *Journal of Climate*, 12, p. 2451–2473.

Das, B.M. (2009). *Principles of geotechnical engineering*, 7<sup>th</sup> Ed. Cengage Learning, Stanford, USA, p 530-531.

Duncan, J. M. (1996). State of the art: Limit equilibrium and finite-element analysis of slopes. *Journal of Geotechnical and Geoenvironmental Engineering*, 122(7), p. 577-596.

Duncan, J.M. and Wright, S.G. (2005). *Soil strength and slope stability*. Wiley,

Duncan, J. M. and Dunlop, P. (1969). Slopes in stiff- fissured clays and shales. *Journal of the Soil Mechanics and Foundations Division*, 95(2), p. 467-492.

Earle, S. (2019). Physical Geology – 2nd Ed. In: *Chapter 15 - Factors that control slope stability*. Victoria, B.C.: BC campus. Available from:

<https://opentextbc.ca/physicalgeology2ed/>.

Engineering Council of South Africa (ECSA). (2017). *The Failure of concrete retaining block (crb) walls in South Africa*. Practice note arising from the contravention of the ECSA rules of conduct for registered persons. Practice Note No. 2017/01.

Elkateb, T., Chalaturnyk, R., and Robertson, P.K. (2002). An over- view of soil heterogeneity: quantification and implications on geotechnical field problems. *Canadian Geotechnical Journal*, 40, p. 1–15.

El-Ramly, H., Morgenstern, N. R. and Cruden, D. M. (2002). Probabilistic slope stability analysis for practice. *Canadian Geotechnical Journal*, 39(3), p. 665–683.

EN, 1997-1. (2004). *Eurocode 7: Geotechnical design - Part 1: General rules*. Authority: The European Union Per Regulation 305/2011, Directive 98/34/EC, Directive 2004/18/EC. Available from: [https://www.ngm2016.com/uploads/2/1/7/9/21790806/eurocode\\_7\\_-\\_geotechnical\\_designen.1997.1.2004.pdf](https://www.ngm2016.com/uploads/2/1/7/9/21790806/eurocode_7_-_geotechnical_designen.1997.1.2004.pdf)

Fellenius, W. (1936). *Calculation of stability of earth dams*. Transactions, 2nd Congress Large Dams, Washington, DC, p. 445–462.

Fenton, G. A. (1999). Random field modeling of CPT data. *Journal of Geotechnical and Geoenvironmental Engineering*, 125(6), p. 486–498.

Fenton, G.A. and Griffiths, D.V. (2008). *Risk Assessment in geotechnical engineering*. John Wiley and Sons, Inc.

Floodlist. (2019). South Africa – Deadly floods and landslides hit KZN and Eastern Cape. Available from: <http://floodlist.com/africa/south-africa-floods-kzn-eastern-cape-april-2019>

Fredlund, D.G., Morgenstern, N.R. and Widger, R.A. (1978). The shear strength of unsaturated soils. *Canadian Geotechnical Journal*, 15(3), p. 313-321.

Fredlund, D.G. and Rahardjo, H. (1993). *Soil mechanics for unsaturated soils*. Wiley, Toronto.

Fredlund, D.G. and Xing, A. (1994). Equations for the soil-water characteristic curve. *Canadian Geotechnical Journal*, 31, p. 521-532

Garland, G.G. and Olivier, M.J. (1993). Predicting landslides from rainfall in a humid, sub-tropical region. *Geomorphology*, 8, p. 165-173. Available from: <http://www.sciencedirect.com/science/article/pii/0169555X9390035Z>

Garland, G.G. (1978) An embankment landslide in Berea Red Sands, Durban, South African Geographical Journal, 60:1, 63-70, DOI: [10.1080/03736245.1978.10559591](https://doi.org/10.1080/03736245.1978.10559591)

Gasmo, J. M., Rahardjo, H. and Leong, E. (2000). Infiltration effects on stability of a residual soil slope. *Computers and Geotechnics*, 26(2), p. 145-165.

Gibbs, H.J. and Coffey, C.T. (1969). *Techniques for Pore Pressure Measurements and Shear Testing of Soil*. International Society for Soil Mechanics and Geotechnical Engineering. Available from: <https://www.issmge.org/publications/online-library>

Gofar, N., Lee, M. L. and Asof, M. (2006). Transient seepage and slope stability analysis for rainfall-induced landslide: a case study. *Malaysian Journal of Civil Engineering*, 18(1), p. 1–13.

Griffiths, D.V. and Lane, P.A. (1999). Slope stability analysis by finite elements. *Geotechnique*, 49(3), p. 387 – 403.

Griffiths, D.V. and Fenton, G.A. (2004). Probabilistic stability analysis by finite elements. *Journal of Geotechnical and Geoenvironmental Engineering*, 130(5), 507-518.

Hammouri, N.A., Husein Malkawi, A.I. and Yamin, M.M.A. (2008). Stability analysis of slopes using the finite element method and limiting equilibrium approach. *Bulletin of Engineering Geology and the Environment*, 67(4), p. 471-478.

Head, K. H. (2006). *Manual of soil laboratory testing, Vol 1. 3rd Ed.* Whittles Publishing, Scotland, UK.

Head, K. H. (1994). *Manual of soil laboratory testing, Vol 2. 2<sup>nd</sup> Ed.* John Wiley and Sons, NY – Toronto.

Hicks, M. A. (2005). Risk and variability in geotechnical engineering. *Geotechnique*, 55(1), p 1–2.

Hicks, M. A. and Spencer, W. A. (2010). Influence of heterogeneity on the reliability and failure of a long 3D slope. *Computers and Geotechnics*, 37(7-8), p. 948–955.

Hight, D.W. and Leroueil, S. (2003). Characterisation of soils for engineering practice. Tan, T.S., Phoon, K.K., Hight, D.W. and Leroueil, S. (Eds.), *Characterisation and engineering properties of natural soils; Proceedings of the first International Workshop on Characterisation and Engineering Properties of Natural Soils*. Swets and Zeitlinger, Singapore, December 2-4, 2002

Holtz, R.D. (2001). Construction materials: soil and natural materials. *Encyclopedia of Materials: Science and Technology*, p. 1559-1563. Available from: <https://www.sciencedirect.com/science/article/pii/B0080431526002783>

Hong, W., Jung, Y., Kang, S. and Lee, J. (2016). Estimation of soil-water characteristic curves in multiple-cycles using membrane and TDR System. *Materials*, 9(12), p. 1019. doi:10.3390/ma9121019. Available from: [www.mdpi.com/journal/materials](http://www.mdpi.com/journal/materials).

Huang, K., Wan, J., Chen, G. and Zeng, Y. (2012). Testing study of relationship between water content and shear strength of unsaturated soils. *Rock and Soil Mechanics*, 33(9), 1-7.

Huang, J., Lyamin, A. V., Griffiths, D. V., Krabbenhoft, K., and Sloan, S. W. (2013). Quantitative risk assessment of landslide by limit analysis and random fields. *Computers and Geotechnics*, 53, p.60–67.

Huber, M. (2013). *Soil variability and its consequences in geotechnical engineering*. Institut für Geotechnik Universität Stuttgart, Germany.

Indraratna, B., Chu, J. and Rujikiatkamjorn, C. (Eds.). (2015). Ground improvement case histories: *Chapter 21 - environmentally friendly slope stabilization using a soil nail and root system in Canada*. Butterworth-Heinemann. Available from: <http://www.sciencedirect.com/science/article/pii/B9780081001912099937>

Janbu, N. (1968). *Slope stability computation*. Soil Mechanics and Foundation Engineering Report, Trondheim.

Johnson, K. A. and Sitar, N. (1990). Hydrologic conditons leading to debris-flow initiation. *Canadian Geotechnical Journal*, 27(6), p. 789-801.

Johnson, M.R., Anhaeusser, C.R. and Thomas, R.J. (2006). *The geology of South Africa*. Geological Society of South Africa (GSSA). Johannesburg.

Kaliakin, V.N. (2017). *Soil Mechanics. Calculations, Principles, and Methods*. Butterworth-Heinemann. Chapter 2 and 10, p 51-92; 421-424. Available from: <https://www.sciencedirect.com/topics/engineering/atterberg-limit>

Kainthola1, A., Verma, D., Thareja, R. and Singh, T. N. (2013). A review on numerical slope stability analysis. *International Journal of Science, Engineering and Technology Research (IJSETR)*, 2(6), p.

Kellet, J., Caravani, A. and Pichon, F. (2014). *Financing disaster risk reduction: towards a coherent and comprehensive approach*. Research reports and studies, July 2014. Available from: <https://www.odi.org/publications/8347>

Khan, M.A., Khan, M.Z. and Khan, M.B. (2016). Effect of fines on liquefaction resistance in fine sand and silty sand. *International Journal of Engineering Research and Applications*, 6(10), p. 102-106. Available from: [www.ijera.com](http://www.ijera.com)

Krahn, J. (2004). Stability modeling with SLOPE/W. *An engineering methodology*, 1st edn. Revision 1, GEO-SLOPE/W International Ltd. Available from: <http://www.geoslope.com>

Kumsar, H., Aydan, Ö. and Ulusay, R. (2000). Dynamic and static stability assessment of rock slopes against wedge failures. *Rock Mechanics and Rock Engineering*, 33, p. 31-51.

Lacasse, S. and Nadim, F. (1996). Uncertainties in characterizing soil properties. In: Shackelford C.D., Nelson P. P. and Roth M. J. S. (Eds). *Uncertainty in the geologic environment: from theory to practice*. ASCE. New York, USA.

Li, L. and Chu, X. (2015). Risk assessment of slope failure by representative slip surfaces and response surface function. *KSCE Journal of Civil Engineering*, 20(5), p 1783–1792.

Li, Y.J., Hicks, M.A. and Nuttall, J.D. (2015a). Comparative analyses of slope reliability in 3D. *Journal of Engineering Geology*, 196, p. 12-23. Available from: <https://www.sciencedirect.com/science/article/pii/S0013795215002070>

Li, D. Q., Xiao, T., Cao, Z. J., Zhou, C. B., and Zhang, L. M. (2015b). Enhancement of random finite element method in reliability analysis and risk assessment of soil slopes using subset simulation. *Landslides*, 13(2), p. 293–303.

Li, L., Chu, X. and Ji, J. (Ed). (2019a). Failure mechanism and factor of safety for spatially variable undrained soil slope. *Advances in Civil Engineering*, Article ID 8575439. Available from: <https://doi.org/10.1155/2019/8575439>

Li, Y., Qian, C. and Liu, K. (2019b). Sampling efficiency in spatially varying soils for slope stability assessment. *Advances in Civil Engineering*, Article ID 8267601. Available from: <https://doi.org/10.1155/2019/8267601>

Li, K. S. and Lumb, P. (1987). Probabilistic design of slopes. *Canadian Geotechnical Journal*, 24 (4). Available from: <https://doi.org/10.1139/t87-068>

Lim, T. T., Rahardjo, H., Chang, M. and Fredlund, D. D. (1996). Effect of rainfall on matric suctions in a residual soil slope. *Canadian Geotechnical Journal*, 33(4), p. 618-628.

Lowe, J. and Karafiath, L. (1960). *Stability of earth dams upon drawdown*. In: Proceedings of the first Panamerican Conference on Soil Mechanics and Foundation Engineering, Mexico City, vol 2, p 537–552.

Noor, M. J. Md., Hadi, B. A. and Hafez, M. A. (2009). *Modeling of shallow slope failure using curved-surface envelope extended Mohr-Coulomb model*. 4th Asia Pacific Conference on Unsaturated Soils, Newcastle, Australia. Available from: <https://iopscience.iop.org/article/10.1088/1757-899X/513/1/012013/pdf>

Malkawi, A. I. H., Hassan, W. F. and Abdulla, F. A. (2000). Uncertainty and reliability analysis applied to slope stability. *Structural Safety*, 22(2), p. 161-187. Available from: [https://doi.org/10.1016/S0167-4730\(00\)00006-0](https://doi.org/10.1016/S0167-4730(00)00006-0)

Matsui, T. and San, K. (1992). Finite element slope stability analysis by shear strength reduction technique. *Soils and Foundations*, 32(1), p. 59-70.

Maud, R.R. (1985). Instability of road embankment on N3 freeway, Rickivy, Pietermaritzburg. In: Brink, A.B.A. (Ed), *Engineering Geology of Southern Africa*, 4, Post-Gondwana deposits, p. 165-166.

Maurenbrecher, P.M. (1973). Instability of a road embankment at Rickivy, Pietermaritzburg. *Civil Engineering=Siviele Ingenieurswese*, (8), 218-224.

Maurenbrecher, P. M. and Booth, A. R. (1975). Some slope stability problems in soils derived from the Ecca shales of Natal, South Africa. *Engineering Geology*, 9(2), p. 99–121.

Mohamed, A.O. and Paleologos, E. K. (2018). Stability and safety of engineered barrier systems for waste containment. In: *Fundamentals of Geoenvironmental Engineering*. Elsevier.

Morgenstern, N. R. and Price, V. E. (1965). The analysis of the stability of general slip surfaces. *Geotechnique*, 15(1), p. 79–93.

Mostyn, G. R. and Li, K. S. (1993). Probabilistic slope stability— State of play. In: Li, K. S. and Lo, S.-C. R. (Eds.) *Probabilistic Methods in Geotechnical Engineering*. Balkema, Rotterdam, The Netherlands, p. 89–110.

Mostyn, G. R., and Soo, S. (1992). The effect of autocorrelation on the probability of failure of slopes. *Proceeding of the 6th Australia, New Zealand Conference on Geomechanics: Geotechnical Risk*, p. 542–546.

Ng, C. W. W. and Shi, Q. (1998). Influence of rainfall intensity and duration on slope stability in unsaturated soils. *Quarterly Journal of Engineering Geology and Hydrogeology*, 31(2), p. 105-113.

Ng, C. W. W., Wang, B. and Tung, Y. K. (2001). Three-dimensional numerical investigations of groundwater responses in an unsaturated slope subjected to various rainfall patterns. *Canadian Geotechnical Journal*. Available from: <https://doi.org/10.1139/t01-057>.

Nie, X., Zhang, J., Huang, H., Liu, Z. and Lacasse, S. Schweckendiek, V.T. *et al.* (Eds). (2015). *Scale of Fluctuation for Geotechnical Probabilistic Analysis*. Available from: <https://www.researchgate.net>

Niroumand, H., Kassim, K.A., Ghafooripour, A., Nazir, R. and Far, S.Y.Z. (2012). Investigation of slope failures in soil mechanics. *Electronic Journal of Geotechnical Engineering*, 17, p 2703-2709. Available at: <https://www.researchgate.net/publication/256326626>

Obregon, C. and Mitri, H. (2019). Probabilistic approach for open pit bench slope stability analysis – A mine case study. *International Journal of Mining Science and Technology*. Available from: [www.elsevier.com/locate/ijmst](http://www.elsevier.com/locate/ijmst)

Okamura, M. and Yure, M. (2001). Movement processes of the Kage Landslide in the Mikabu Greenstone Belt, central Shikoku, Japan. *The Japan Landslide Society*, 37 (4), p. 74-81. Available from: [https://doi.org/10.3313/jls1964.37.4\\_74](https://doi.org/10.3313/jls1964.37.4_74)

Othman, M. A. (1989). Highway cut slope instability problems in West Malaysia. Ph.D., Department of Geography, University of Bristol, United Kingdom.

Paige-Green, P. (1989). The influence of geotechnical properties on the performance of gravel wearing course materials. Ph.D., Faculty of Science, University of Pretoria.

Paige-Green, P. and Croukamp, L. (2004). A revised landslide susceptibility map of Southern Africa. *Geoscience Africa*, p 508.

Peterson, J. L. (1999). Probability analysis of slope stability. M.Sc. Dissertations, and Problem Reports. 990. Available from: <https://researchrepository.wvu.edu/etd/990>

Phoon, K. K. and Kulhawy, F. H. (1999). Characterization of geotechnical variability. *Canadian Geotechnical Journal*, 36(4), p. 612–624.

Poulos, S.J., Castro, G., and France, W. (1985). Liquefaction evaluation procedure. *Journal of Geotechnical Engineering Division.*, ASCE, 111(6), p. 772-792.

Pradhan, S.P., Vishal, V. and Singh, T.N. (2011). Slope mass rating for evaluation of health of slope in an open cast mine in Jharia coalfield. *India. Mining Engineers' Journal*, 12(10), p. 36-40.

Punmia, B.C., Kumar Jain, A. and Kumar Jain, A. (2005). *Soil mechanics and foundations*. Laxmi Productions (Pty) Ltd, India.

Rahardjo, H., Li, X.W., Toll, D.G., and Leong, E.C. (2001). The effect of antecedent rainfall on slope stability. *Journal of Geotechnical and Geological Engineering*, Special Issue on “Unsaturated and Collapsible Soils,” ASCE, 19(3–4), p. 371–399.

Rahardjo, H., Hritzuk, K.J., Leong, E.C. and Rezaur, R.B. (2003). Effectiveness of horizontal drains of slope stability. *Journal of Engineering Geology*, 69(3-4), p. 295-308.

Robinson, D.A. and Friedman, S.P. (2002). Observations of the effects of particle shape and particle size distribution on avalanching of granular media. *Physica A*, 311, p 97-110. Available from: [www.elsevier.com/locate/physa](http://www.elsevier.com/locate/physa)

RocScience Inc. (2001-2004). *Application of the finite element method to slope stability*. Available from: <http://www.roscience.com>

Salunkhe, D.P., Chvan, G., Bartakke, R.N., and Kothavale, P.R. (2017). An Overview on Methods for Slope Stability Analysis. *International Journal of Engineering Research and Technology (IJERT)*, 6(3). Available from: <http://www.ijert.org>

Sarkar, S., Kanungo, D. P. and Kumar, S. (2012). Rock mass classification and slope stability assessment of road cut slopes in Garhwal Himalaya, India. *Geotechnical and Geological Engineering*, 30(4).

Seed, H.B. and Lee, K.L. (1966). Liquefaction of saturated sands during cyclic loading. *Journal of Soil Mechanics and Foundations Division, ASCE*, 92(6).

Seki, K. (2007). SWRC fit - a nonlinear fitting program with a water retention curve for soils having unimodal and bimodal pore structure. *Hydrology and Earth System Sciences Discussion*, 4, p. 407-437. doi:10.5194/hessd-4-407-2007

Singh, R.G., Botha, G.A., Richards, N.P. and McCarthy, T.S. (2008). Holocene landslides in KwaZulu-Natal, South Africa. *South African Journal of Geology*, 111, p 39-52. Available from: <https://www.researchgate.net/publication/250085461>

Singh, R. G., McCarthy, T. and Botha, G. A. (2009). Landslide Classification, Characterization and Susceptibility Modeling in KwaZulu-Natal. M.Sc., University of the Witwatersrand.

Sivakumar, V., and Wheeler, S. (2000). Influence of compaction procedure on the mechanical behaviour of an unsaturated compacted clay. Part 1: Wetting and isotropic compression. *Geotechnique*, 50(4), p. 59–368. doi:10.1680/geot.2000.50.4.359.

Snitbhan, N. and Chen, W.F. (1978). Elastic-plastic deformation analysis of soil slopes. *Computers and Structures*, 9(6), p. 567 – 577.

Spencer, E. (1967). A method of analysis of the stability of embankments assuming parallel inter-slice forces. *Geotechnique*, 17(1), p. 11–26.

Standard Test Methods. (1986). *Method A6. The determination of the grain size distribution in soils by means of a hydrometer*. Pretoria, South Africa.

Toprak, B., Sevim, O. and Kalkan, I. (2016). Gabion walls and their use. *International Journal of Advances in Mechanical and Civil Engineering*, 3(4), p. 56-58.

Tsaparas, I., Rahardjo, H., Toll, D. and Leong, E.C. (2003). Infiltration characteristics of two instrumented residual soil slopes. *Canadian Geotechnical Journal*, 40(5), p. 1012–1032.

Tschuchnigg, F., Schweiger, H., Sloan, S., Lyamin, A., and Raissakis, I. (2015). Comparison of finite-element limit analysis and strength reduction techniques. *Geotechnique*, 65(4), p. 249–257.

Uray Ve, E. and Tan, O. (2015). *Gabion type restraining structures*. Broadcasts of Chamber of Civil Engineers Turkey (TMMOB), pp 19-29, TMH- 485, 2015/2.

U.S. Army Corps of Engineers. (1997). *Engineering and design: introduction to probability and reliability methods for use in geotechnical engineering*. Department of the Army, Washington, D.C. Engineer Technical Letter 1110-2-547. Available from: <https://apps.dtic.mil/sti/pdfs/ADA403281.pdf>

United States Geological Survey (USGS). (2020). Natural Hazards – How many deaths result from landslides each year? Available from: [https://www.usgs.gov/faqs/how-many-deaths-result-landslides-each-year?qt-news\\_science\\_products=0#qt-news\\_science\\_products](https://www.usgs.gov/faqs/how-many-deaths-result-landslides-each-year?qt-news_science_products=0#qt-news_science_products)

Uzielli, M., Lacasse, S., Nadim, F. and Phoon, K.K. (2006). *Soil Variability Analysis for Geotechnical Practice*. Available from: DOI: [10.1201/NOE0415426916.ch3](https://doi.org/10.1201/NOE0415426916.ch3)

Vanmarcke, E. H. (1977). Probabilistic modelling of soil properties. *Journal of Geotechnical and Geoenvironmental Engineering*, ASCE, 103(11), p. 1227-1246.

Vanmarcke, E. H. (1983). *Random fields: analysis and synthesis*. MIT Press, Cambridge, MA, USA.

Vondráčková, T., Kmec, J., Čejka, J., Bartuška, L. and Stopka, O. (2016). *Evaluation of the Parameters Affecting the Cohesion of Fine Grained Soil*. World Multidisciplinary Earth Sciences Symposium (WMESS 2016) IOP Conf. Series: Earth and Environmental Science 44

Wang, C., Tannant, D.D. and Lilly, P.A. (2003). *Numerical analysis of the stability of heavily jointed rock slopes using PFC2D*. *International Journal Rock Mechanics and Mining Sciences*, 40, p. 415 – 424.

Webb, D.L. (1983). Slope failure on shale of the Pietermaritzburg Shale Formation, Mayat Place, Durban. In: Brink, A.B.A. *Engineering geology of Southern Africa: Volume 3. The Karoo Sequence*. Building Publications, Pretoria, p. 107–111.

Wei, W. B., Cheng, Y. M., and Li, L. (2009). Three-dimensional slope failure analysis by the strength reduction and limit equilibrium methods. *Computers and Geotechnics*, 36(1), p. 70–80.

Weiler, M., McDonnell, J., Van Meerveld, I. and Uchida, T. (2006). Subsurface Stormflow. *Encyclopedia of Hydrological Sciences*.

Wieczorek, G.F. (1984). Preparing a detailed landslide-inventory map for hazard evaluation and reduction. *Environmental and Engineering Geoscience*, xxi(3), p. 337-342. Available from: <https://doi.org/10.2113/gseegeosci.xxi.3.337>

Wong, F. S. (1984). Uncertainties in FE modeling of slope stability. *Computers & Structures*, 19 (5–6), p. 777-791.

Yang, Y., Xing, H., Yang, X. and Zhou, J. (2016). Determining the critical slip surface of three-dimensional soil slopes from the stress fields solved using the finite element method. *Mathematical Problems in Engineering*, Article ID 7895615 Available from: <http://dx.doi.org/10.1155/2016/7895615>

Zaki, A. (1999). *Slope stability analysis overview*. University of Toronto

Zhang, X., Vincent, L. A., Hogg, W. D. and Niitsoo, A. (2000). Temperature and precipitation trends in Canada during the 20th Century. *Atmosphere-Ocean*, 38(3), p. 395-429.

Zheng, H., Liu, D. F. and Li, C. G. (2005). Slope stability analysis based on elasto-plastic finite element method. *International Journal for Numerical Methods in Engineering*, 64(14), p. 1871–1888.

Zhou, Y., Qi, S., Fan, G., Chen, M. and Zhou, J. (2020). Topographic effects on three dimensional slope stability for fluctuating water conditions using numerical analysis. *MDPI Journal: Water*. 12(2). Available from: [www.mdpi.com/journal/water](http://www.mdpi.com/journal/water)

Zhu, J., Zaman, M. M. and Anderson, S. A. (1998). Modelling of shearing behaviour of a residual soil with recurrent neural network. *International Journal for Numerical and Analytical Methods in Geomechanics*, 22(8), p. 671-687.

Zienkiewicz, O. C. (1971). *The finite element method in engineering science*. McGraw-Hill, New York.